



Copyright Undertaking

This thesis is protected by copyright, with all rights reserved.

By reading and using the thesis, the reader understands and agrees to the following terms:

1. The reader will abide by the rules and legal ordinances governing copyright regarding the use of the thesis.
2. The reader will use the thesis for the purpose of research or private study only and not for distribution or further reproduction or any other purpose.
3. The reader agrees to indemnify and hold the University harmless from and against any loss, damage, cost, liability or expenses arising from copyright infringement or unauthorized usage.

IMPORTANT

If you have reasons to believe that any materials in this thesis are deemed not suitable to be distributed in this form, or a copyright owner having difficulty with the material being included in our database, please contact lbsys@polyu.edu.hk providing details. The Library will look into your claim and consider taking remedial action upon receipt of the written requests.

**AN IMPROVED MODAL STRAIN ENERGY METHOD
FOR BRIDGE DAMAGE IDENTIFICATION**

PARVIZ MORADI POUR

PhD

The Hong Kong Polytechnic University

**This programme is jointly offered by The Hong Kong
Polytechnic University and The Queensland University of
Technology**

2018

THE HONG KONG POLYTECHNIC UNIVERSITY
DEPARTMENT OF CIVIL AND ENVIRONMENTAL ENGINEERING
THE QUEENSLAND UNIVERSITY OF TECHNOLOGY
SCHOOL OF CIVIL AND ENVIRONMENTAL ENGINEERING

**AN IMPROVED MODAL STRAIN ENERGY METHOD
FOR BRIDGE DAMAGE IDENTIFICATION**

PARVIZ MORADI POUR

**A thesis submitted in partial fulfilment of the requirements for the
degree of Doctor of Philosophy**

July 2017

To my beloved family

ABSTRACT

Increasing the importance of infrastructures demands an effective and timely structural health monitoring (SHM) systems. Structural damage detection using modal strain energy (MSE) is one of the efficient and reliable SHM techniques. However, some existing MSE methods have been validated only for special types of the structures such as beams or steel truss bridges or have had an unsatisfactory performance. This circumstance demands either improving the available methods or proposing new approaches. The current study focuses on improving a two-stage MSE-based damage detection method to accurately detect and quantify the damage in bridges. Primarily, it is attempted to more accurately establish an equation for the MSE stored in each element of the structure before and after the damage. This can be achieved by mathematically considering the actual damaged stiffness matrix into the traditional MSE equation as an unknown parameter. Establishing a more exact amount of MSE change during the damage leads to attaining a more sensitive matrix which assists realizing the damage more accurately at an early stage of forming with higher reliability. It is also tried to generalize the improved method to be applicable for any bridge. The improved MSE method for detecting the structural damage has two consequent stages, stage one, locating the damage, and stage two, quantifying the damage. The crucial key for identifying the location of damage in the structure is to calculate the elemental MSE change of the structure before and after the damage. Therefore, an elemental MSE-based indicator is used to show the ratio of the MSE change for each element. The elements with the higher amount of MSE change ratio

are the most likely elements to be damaged and are nominated for further investigation in the second stage. Sensitivity matrix is used to quantify the damage which is a matrix derived from MSE change with respect to extent of the damage as an unknown independent variable. To validate the improved method, numerical studies are performed on some structures including, a fixed-end beam, a three-story frame, a steel truss bridge and a concrete bridge frame model. Consequently, experimental verifications are conducted on a simply supported beam, a cantilever beam and a three-story steel frame model. To examine the application of the improved method to a real model also, it is applied to the 4-DOF three-story structure of Los Alamos National Laboratory (LANL). In most of the numerical verifications, different scenarios including single and multiple damages, affected by up to seven percent noise are considered. Finally, to observe the applicability of the improved method in reality, it is applied to the I-40 Bridge in New Mexico; the USA using the available data. The results indicate that the improved method is able to detect any single or multiple damage at any element or node of the structure at most of the cases studied. In numerical case studies, the improved method is precisely able to detect and quantify the damage with minimal error. However, in experimental case studies, real structure and bridge, there are few errors because of some sources such as the difference between physical structure and FEM model, material properties modelling, incomplete and limited measurements, data processing, software and unknown factors and uncertainties. According to the findings of this dissertation the improved method is proper for health monitoring of complex bridges and well identifies the damage in the most cases and being more accurate and efficient than its predecessors in terms of well recognition of the location of the damage and identifying its extent. The findings of this study can confidently contribute to academic studies and bridge industry to realize

the genuine condition and behaviour of complex bridges during the damage to minimize the loss of lives and property by identifying the unforeseen structural damages.

LIST OF PUBLICATIONS

Journal Articles:

Moradipour, P., Chan, T. H. T. and Gallage, C. (2015). “An improved modal strain energy method for structural damage detection, 2D simulation.” *Structural Engineering and Mechanics*, 54(1), 105-119.

Moradipour, P., Chan, T. H. and Gallage, C. (2017). “Benchmark studies for bridge health monitoring using an improved modal strain energy method.” *Procedia Engineering*, 188, 194-200.

Conference Papers:

Moradipour, P., Chan, T. H. T. and Gallage, C. (2013). “Health monitoring of short- and medium-span bridges using an improved modal strain energy method.” In *Proceedings of the 5th International Workshop on Civil Structural Health Monitoring*, Ube, Yamaguchi, Japan, 24-26 Oct., edited by Miyamoto, A., Hakola, I., Yabe, A. and Emoto, H., 166-181: International Society for Structural Health Monitoring of Intelligent Infrastructure.

Moradipour, P., Chan, T. H. T. and Gallage, C. (2015). “An experimental study on structural damage detection using an improved modal strain energy method.” *Proceedings of Engineering Mechanics Institute (EMI) 2015 HK*, Hong Kong, 7-9 Jan.,

edited by Chau, K. T. and Leung, A.: American Society of Civil Engineering (ASCE),
The Hong Kong Polytechnic University.

ACKNOWLEDGEMENTS

I would like to express my sincere gratefulness to my chief supervisor, Professor Y.Q. Ni, for giving me this great opportunity, his patience, helpful comments, invaluable guidance, continuous encouragement and supports to help me fulfil my research work successfully.

The special thank also extended to my chief supervisor at Queensland University of Technology, Professor Tommy H.T Chan for his encouragement, kind concern, useful advice and comments and supports.

Sincere thanks go to my associate supervisor, Dr Chaminda Gallage, for his motivation, advice and suggestions on my work.

I should thank Banyo Pilot Plant Precinct and Engineering Precinct of QUT, CEBE staff, HPC unit, librarians, IT Help, RSC and QUT HDR support Team, SHM Research Group at QUT of QUT and HKPU structural dynamic lab staff, RO, FO, IT and Library of HKPU. I also gratefully acknowledge the Financial supports provided by the QUT, The Queensland University of Technology Postgraduate Research Award (QUTPRA), the QUT Science and Engineering Scholarship and Science and Engineering Faculty Top Up Scholarship, and the Research Studentship of the Hong Kong Polytechnic University (PolyU).

I gratefully thank all my friends, for their encouragement and support especially Dr.

Craig Cowled at QUT and Mr Chen Ran and Mr Pinghe Ni at HKPU.

The last, but not least, thank my beloved wife for her patience, kindness, and valuable support and my family for their great supports, encouragement, and care.

CONTENTS

CERTIFICATE OF ORIGINALITY	i
ABSTRACT	ii
LIST OF PUBLICATIONS	v
ACKNOWLEDGEMENTS.....	vii
LIST OF FIGURES	xiv
LIST OF TABLES	xix
LIST OF SYMBOLS.....	xxii
LIST OF ABBREVIATIONS	xxvi
CHAPTER 1 INTRODUCTION	1
1.1 Structural damage.....	1
1.2 Failure in bridges around the world	2
1.3 Bridge management and Bridge failure in Australia and New Zealand	5
1.4 Non-destructive testing	7
1.5 Structural health monitoring (SHM)	7
1.6 Research problems	9
1.7 Aims and objectives	10
1.8 Significance.....	12
1.9 Scope of the research	13
1.10 Thesis outline	13
CHAPTER 2 LITERATURE REVIEW	15
2.1 Parametric based VBDD methods	15
2.1.1 Natural frequency variation-based methods.....	16
2.1.2 Mode shape variation-based methods	18
2.1.3 Modal strain energy-based method	23
2.2 Frequency response function method.....	28
2.3 Mathematical and statistical tools for damage detection	29
2.3.1 Genetic algorithm-based method	29

2.3.2 Artificial neural network-based method.....	30
2.3.3 Wavelet transforms techniques.....	32
2.4 Concluding remarks	33
2.5 Research gaps.....	34
CHAPTER 3 METHODOLOGY AND RESEARCH PLAN OF THE IMPROVED MODAL STRAIN ENERGY METHOD	36
3.1 Introduction.....	37
3.2 Formulating the two-stage MSE method	39
3.2.1 Establishment of the MSE change and sensitivity matrix to damage	39
3.2.2 Stage one – Identifying the location of damage.....	41
3.2.3 Stage two – Quantifying the damage	41
3.2.4 Damage detection with noise polluted data	42
3.3 Verifications	43
3.3.1 Numerical simulations	43
3.3.2 Experimental studies	46
3.3.3 Applying to a real model and a real bridge	49
3.4 Conclusion	51
CHAPTER 4 THEORY OF STUDY AND MATHEMATICAL IMPROVEMENT OF THE MODAL STRAIN ENERGY METHOD.....	53
4.1 Theory of study	54
4.2 Traditional MSE method.....	55
4.2.1 Direct Modal Strain Energy Correlation	59
4.3 The improved MSE method	60
4.3.1 Improved modal strain energy change	61
4.3.2 Improved sensitivity matrix	64
4.3.3 Locating the damage	65
4.3.4 Quantifying the damage	66
4.3.5 Required modes shapes and natural frequencies.....	76
4.3.6 Noise effect	77

4.4 Concluding remarks	78
CHAPTER 5 COMPARATIVE STUDIES	79
5.1 The numerical fixed-end beam model.....	79
5.2 Study of the accuracy and convergence of the improved MSE method	80
5.2.1 Single damage	81
5.2.2 Multiple damage.....	84
5.2.3 Results and discussions	87
5.3 Conclusion	88
CHAPTER 6 NUMERICAL SIMULATIONS	89
6.1 Introduction.....	89
6.2 Guideline for practical application of the improved method	90
6.3 Case study 1: A fixed-end steel beam	92
6.3.1 Results of case study 1	93
6.3.2 Discussion on case study 1.....	101
6.4 Case study 2: A three-story steel frame.....	104
6.4.1 Results of case study 2	105
6.4.2 Discussion on case study 2.....	110
6.5 Case study 3: A 2D steel truss structure.....	111
6.5.1 Results of case study 3	112
6.5.2 Discussion on case study 3.....	117
6.6 Case study 4: A concrete bridge frame.....	118
6.6.1 Results of case study 4	119
6.6.2 Discussion on case study 4.....	124
6.7 Quantifying the minimum damage magnitude.....	124
6.7.1 Discussion on quantifying the small damages	129
6.8 Conclusion	130
CHAPTER 7 EXPERIMENTAL VERIFICATIONS	132
7.1 Introduction.....	132
7.1.1 Data processing	134
7.2 Case study 1 (Specimen 1): A simply-support steel beam	135

7.2.1 Damage cases made	137
7.2.2 Results of case study 1	137
7.2.3 FEM analysis.....	142
7.2.4 MAC value comparison	143
7.2.5 Discussion on case study 1.....	144
7.3 Case study 2 (Specimen 2): A cantilever beam model.....	145
7.3.1 Damage case created	147
7.3.2 Results of case study 2	147
7.3.3 FEM analysis.....	151
7.3.4 MAC value comparison	152
7.3.5 Discussion on case study 2.....	153
7.4 Case study 3 (Specimen 3): A three-story steel frame model	154
7.4.1 Damage cases created	157
7.4.2 Results of case study 3	158
7.4.3 FEM analysis.....	167
7.4.4 MAC value comparison	169
7.4.5 Discussion on case study 3.....	170
7.5 Conclusion	171

CHAPTER 8 APPLICATION OF THE IMPROVED MODAL STRAIN ENERGY METHOD TO LOS ALAMOS NATIONAL LABORATORY MODEL AND A REAL BRIDGE 173

8.1 Case study 1: LANL 4-DOF Three-story Model	174
8.1.1 Results of different damage states.....	176
8.1.2 Discussion	180
8.2 Case study 2: I-40 Bridge, New Mexico, USA.....	182
8.2.1 Instrumentation	184
8.2.2 Damage cases created	185
8.2.3 Mode shape comparison.....	186
8.2.4 Application of the improved MSE method	190
8.2.5 Results and discussion	191

8.2.6 MAC value comparison	197
8.3 Conclusion	200
CHAPTER 9 CONCLUSION AND FUTURE STUDIES	203
9.1 Conclusions	205
9.2 Significance and contributions	207
9.3 Recommendations for Further Researches	209
REFERENCES.....	211

LIST OF FIGURES

Figure 1.1 Collapse in I-35W Bridge in the US, Aug., 2007	4
Figure 1.2 Collapse in De la Concorde Overpass Bridge in Quebec, Canada Sept., 2006.....	5
Figure 3.1 The overall methodology of the research	38
Figure 3.2 The FEM model of the fixed-supported beam.....	44
Figure 3.3 The FEM model of the three-story steel frame.....	44
Figure 3.4 The FEM model of the steel truss model.....	45
Figure 3.5 The FEM model of the concrete bridge frame.....	46
Figure 3.6 The FEM model of the cantilever beam model (dimensions are in mm).....	48
Figure 3.7 The FEM model of the steel simply-support beam	48
Figure 3.8 The FEM model of the three-story steel frame laboratory model	49
Figure 3.9 The Los Alamos National Laboratory 4-DOF three-story structure.	50
Figure 3.10 I-40 Bridge, New Mexico, USA	51
Figure 5.1 The FEM of the fixed-supported beam.....	80
Figure 5.2 The MSECR of the elements, single damage (element 5 with a stiffness loss of 10%)	81
Figure 5.3 Damage extent of element 5 quantified with mode 1 in both MSEC and MSECimp methods	82
Figure 5.4 Damage extent of element 4 quantified with mode 1 in both MSEC and MSECimp methods	82
Figure 5.5 Damage extent of element 6 quantified with mode 1 in both MSEC and MSECimp methods	83
Figure 5.6 MSECR of the elements, multiple damage, (elements 4 and 9 with a stiffness loss of 10 and 15%, respectively)	84
Figure 5.7 Damage extent of element 4 quantified with mode 1 in both MSEC and MSECimp methods	85
Figure 5.8 Damage extent of element 8 quantified with mode 1 in both MSEC and MSECimp methods	85
Figure 5.9 Damage extent of element 9 quantified with mode 1 in both MSEC and MSECimp methods	86
Figure 6.1 The FEM model of the steel fixed-supported beam	93
Figure 6.2 The MSECR of the elements, single damage, scenario 1 (element 7 with a stiffness loss of 5%)	95
Figure 6.3 The extent of the damage, single damage, scenario 1 (element 7 with a stiffness loss of 5%)	97

Figure 6.4 The MSECR of the elements, multiple damage, scenario 2 (elements 4 and 10 with stiffness loss of 5 and 10%, respectively)	97
Figure 6.5 The extent of the damage, multiple damage, scenario 2 (elements 4 and 10 with stiffness loss of 5 and 10%, respectively)	99
Figure 6.6 The MSECR of the elements, multiple damage, scenario 3 (elements 3, 6 and 11 with stiffness loss of 5, 3 and 8%, respectively)	99
Figure 6.7 The extent of the damage, multiple damage, scenario 3 (elements 3, 6 and 11 with stiffness loss of 5,3 and 8%, respectively)	101
Figure 6.8 FEM of the three-story steel frame	104
Figure 6.9 The MSECR of the elements, single damage, scenario 1 (element 7 with stiffness loss of 8%)	106
Figure 6.10 The extent of the damage, single damage, scenario 1 (element 7 with stiffness loss of 8%)	107
Figure 6.11 MSECR of the elements, multiple damage, scenario 2 (elements 4 and 8 with stiffness loss of 5 and 8%, respectively)	108
Figure 6.12 The extent of the damage, multiple damage, scenario 2 (elements 4 and 8 with stiffness loss of 5 and 8%, respectively)	110
Figure 6.13 The FEM model of the steel truss model.....	112
Figure 6.14 The MSECR of the elements, single damage, scenario 1 (element 5 with stiffness loss of 3%)	113
Figure 6.15 The extent of the damage, single damage, scenario 1 (element 5 with stiffness loss of 3%)	114
Figure 6.16 The MSECR of the elements, multiple damage, scenario 2 (elements 16 and 19 with stiffness loss of 5 and 12%, respectively).....	115
Figure 6.17 The extent of the damage, multiple damage, scenario 2 (elements 16 and 19 with stiffness loss of 5 and 12%, respectively)	116
Figure 6.18 The FEM model of the concrete bridge frame.....	118
Figure 6.19 The MSECR of the elements, single damage, scenario 1 (element 3 with stiffness loss of 6%)	120
Figure 6.20 The extent of the damage, single damage, scenario 1 (element 3 with stiffness loss of 6%)	122
Figure 6.21 The MSECR of the elements, multiple damage, scenario 2 (elements 3 and 6 with stiffness loss of 6 and 4%, respectively).....	122
Figure 6.22 The extent of the damage, multiple damage, scenario 2 (elements 3 and 6 with stiffness loss of 6 and 4%, respectively)	123
Figure 6.23 The MSECR of the elements, single damage, scenario 1 (element 7 with stiffness loss of 1%)	125
Figure 6.24 The extent of the damage, single damage, scenario 1 (element 7 with stiffness loss of 1%)	127
Figure 6.25 The MSECR of the elements, multiple damage, scenario 2 (elements 3, 6 and 11 with stiffness loss of 0.5, 1 and 0.75%, respectively)	127
Figure 6.26 The extent of the damage, multiple damage, scenario 2 (elements 3,6 and 11 with stiffness loss of 0.5, 1 and 0.75%, respectively)	129

Figure 7.1 Physical model of the simply-support beam sample	136
Figure 7.2 The FEM model of the simply-support beam.....	136
Figure 7.3 Experimental elemental MSECR, single damage scenario (element 7 with added mass of 1 kg)	138
Figure 7.4 Experimental damage extents, single damage scenario (element 7 with added mass of 1 kg)	139
Figure 7.5 Numerical elemental MSECR, single damage scenario (elements 7 with added mass of 1 kg)	141
Figure 7.6 Numerical extent of the damage, single damage scenario (element 7 with added mass of 1 kg)	142
Figure 7.7 The first six numerical mode shapes of undamaged - sample 1	143
Figure 7.8 The cantilever beam model.....	146
Figure 7.9 The FEM model of the cantilever beam model (dimensions are in mm)	146
Figure 7.10 The cantilever beam model (dimensions are in mm).....	147
Figure 7.11 Numerical MSECR of the elements, single damage scenario (element 1 with stiffness loss of 40%)	148
Figure 7.12 Numerical extent of the damage, single damage scenario (element 1 with stiffness loss of 40%)	149
Figure 7.13 Experimental MSECR of the elements, single damage scenario (element 1 with stiffness loss of 40%)	150
Figure 7.14 Experimental extents of the damage, single damage scenario (element 1 with stiffness loss of 40%)	150
Figure 7.15 The first six numerical mode shapes of undamaged sample 1	152
Figure 7.16 Physical model of the three-story steel frame.....	155
Figure 7.17 FEM model of the three-story steel frame model.....	155
Figure 7.18 Typical time series data acquired from Channel 4, case1	156
Figure 7.19 Typical sensor placement.....	157
Figure 7.20 The Experimental elemental MSECR, Multiple damage, Case 1 (elements 5 and 6 with stiffness loss of 20% in each)	159
Figure 7.21 Experimental damage extent, Multiple damage, Case 1, Set 1 (elements 5 and 6 with stiffness loss of 20% in each)	160
Figure 7.22 Experimental damage extent, Multiple damage, Case 1, Set 2 (elements 5 and 6 with stiffness loss of 20% in each)	160
Figure 7.23 Numerical elemental MSECR, Multiple damage, Case 1 (elements 5 and 6 with stiffness loss of 20% in each)	161
Figure 7.24 Numerical damage extent, Multiple damage, Case 1, Set 1 (elements 5 and 6 with stiffness loss of 20% in each)	161
Figure 7.25 Numerical damage extent, Multiple damage, Case 1, Set 2 (elements 5 and 6 with stiffness loss of 20% in each)	162
Figure 7.26 Experimental elemental MSECR, Multiple damage, Case 2 (elements 5, 6, 11 and 12 with stiffness loss of 20% in each).....	162
Figure 7.27 Experimental damage extent, Multiple damage, Case 2, Set 1 (elements 5, 6, 11 and 12 with stiffness loss of 20% in each).....	163

Figure 7.28 Experimental damage extent, Multiple damage, Case 2, Set 1 (elements 5, 6, 11 and 12 with stiffness loss of 20% in each).....	163
Figure 7.29 Numerical elemental MSECR, Multiple damage, Case 2 (elements 5, 6, 11 and 12 with stiffness loss of 20% in each)	164
Figure 7.30 Numerical damage extent, Multiple damage, Case 2 (elements 5, 6, 11 and 12 with stiffness loss of 20% in each)	164
Figure 7.31 Experimental elemental MSECR, Multiple damage, Case 3 (elements 5, 6 and 14 with stiffness loss of 20, 20 and 99%, respectively)	165
Figure 7.32 Experimental damage extent, Multiple damage, Case 3 (elements 5, 6 and 14 with stiffness loss of 20, 20 and 99%, respectively)	165
Figure 7.33 Numerical elemental MSECR, Multiple damage, Case 3 (elements 5, 6 and 14 with stiffness loss of 20, 20 and 99%, respectively)	166
Figure 7.34 Numerical damage extent, Multiple damage, Case 3 (elements 5, 6 and 14 with stiffness loss of 20, 20 and 99%, respectively)	166
Figure 7.35 The first six numerical mode shapes of undamaged sample 3	168
Figure 8.1 The LANL 4-DOF three-story structure	175
Figure 8.2 Basic dimensions of the LANL three-story structure	175
Figure 8.3 The FEM model of the LANL three-story structure	176
Figure 8.4 Damage state 1, mass on the 1st floor	177
Figure 8.5 Damage state 2, mass at the base.....	178
Figure 8.6 Damage state 17, Column: 1BD – 50% stiffness reduction	178
Figure 8.7 Damage state 18, Column: 1AD + 1BD – 50% stiffness reduction.....	178
Figure 8.8 Damage state 21, Column: 3BD – 50% stiffness reduction	179
Figure 8.9 Damage state 22, Column: 3AD + 3BD – 50% stiffness reduction.....	179
Figure 8.10 Damage state 23, Column: 2AD + 2BD – 50% stiffness reduction	179
Figure 8.11 Damage state 24, Column: 2BD – 50% stiffness reduction.....	180
Figure 8.12 I-40 Bridges over the Rio Grande River in Albuquerque, New Mexico (Farrar <i>et al.</i> , 1999)	182
Figure 8.13 Typical cross section geometry of the bridge (Farrar <i>et al.</i> , 1994)	183
Figure 8.14 Bridge substructure (Farrar, 1994).....	183
Figure 8.15 Instrumentation and DoF numbering.....	184
Figure 8.16 The four damage cases created in the I-40 plate girder	186
Figure 8.17 Comparison of numerical and experimental mode shape - Mode 1	187
Figure 8.18 Comparison of numerical and experimental mode shape – Mode 2	187
Figure 8.19 Comparison of numerical and experimental mode shape – Mode 3	188
Figure 8.20 Comparison of numerical and experimental mode shape – Mode 4	188

Figure 8.21 Comparison of numerical and experimental mode shape – Mode 5	189
Figure 8.22 Comparison of numerical and experimental mode shape – Mode 6	189
Figure 8.23 MSECR vs element number of I-40 Bridge, Case 1.....	191
Figure 8.24 Damage extent vs element number of I-40 Bridge, Case 1	192
Figure 8.25 MSECR vs element number of I-40 Bridge, Case 2.....	193
Figure 8.26 Damage extent vs element number of I-40 Bridge, Case 2	193
Figure 8.27 MSECR vs element number of I-40 Bridge, Case 3.....	194
Figure 8.28 Damage extent vs element number of I-40 Bridge, Case 3, set 1.	194
Figure 8.29 Damage extent vs element number of I-40 Bridge, Case 3, set 2.	195
Figure 8.30 MSECR vs element number of I-40 Bridge, Case 4.....	196
Figure 8.31 Damage extent vs element number of I-40 Bridge, Case 4	196

LIST OF TABLES

Table 1.1 List of bridge failures around the world during the years 2016 and 2017.....	3
Table 1.2 List of the most recent bridge failures in Australia and New Zealand.	6
Table 5.1 Material properties and geometric information – numerical case study	80
Table 5.2 Comparison of damage extents quantified using MSEC and MSECimp methods - single damage.....	83
Table 5.3 Comparison of damage extents quantified using MSEC and MSECimp methods - multiple damage.....	86
Table 6.1 Material properties and geometric information – numerical case study 1.....	92
Table 6.2 Damage extent of selected element at each iteration, single damage, scenario 1 (element 7 with a stiffness loss of 5%).....	96
Table 6.3 Damage extent of selected element at each iteration, multiple damage, scenario 2 (elements 4 and 10 with stiffness loss of 5 and 10%, respectively)	98
Table 6.4 Damage extent of selected element at each iteration, multiple damage, scenario 3 (elements 3, 6 and 11 with stiffness loss of 5,3 and 8%, respectively)	100
Table 6.5 The percentage of error of damage extent for selected elements with different noise level, scenario 3 (elements 3, 6 and 11 with stiffness loss of 5,3 and 8%, respectively)	103
Table 6.6 Material properties and geometric information – numerical case study 2.....	104
Table 6.7 Damage extent of selected element at each iteration, single damage, scenario 1 (element 7 with stiffness loss of 8%).....	107
Table 6.8 Damage extent of selected element at each iteration, multiple damage, scenario 2 (elements 4 and 8 with stiffness loss of 5 and 8%, respectively)	109
Table 6.9 Material properties and geometric information – numerical case study 3.....	111
Table 6.10 Damage extent of selected element at each iteration, single damage, scenario 1 (element 5 with stiffness loss of 3%).....	114
Table 6.11 Damage extent of selected element at each iteration, multiple damage, scenario 2 (elements 16 and 19 with stiffness loss of 5 and 12%, respectively)	116

Table 6.12 Material properties and geometric information – numerical case study 4	118
Table 6.13 Damage extent of selected element at each iteration, single damage, scenario 1 (element 3 with stiffness loss of 6%).....	121
Table 6.14 Damage extent of selected element at each iteration, multiple damage, scenario 2 (elements 3 and 6 with stiffness loss of 6 and 4%, respectively)	123
Table 6.15 Damage extent of selected element at each iteration, single damage, scenario 1 (element 7 with stiffness loss of 1%).....	126
Table 6.16 Damage extent of selected element at each iteration, multiple damage, scenario 2 (elements 3,6 and 11 with stiffness loss of 0.5, 1 and 0.75%, respectively).....	128
Table 6.17 The percentage of error of damage extent for selected elements with different noise level, scenario 2 (elements 3,6 and 11 with stiffness loss of 0.5, 1 and 0.75%, respectively)	130
Table 7.1 Material properties and geometric information – experimental case study 1	136
Table 7.2 Natural frequency of the structure in different cases, single damage (element 7 with added mass of 1 kg)	140
Table 7.3 MAC values for comparison mode shapes identified from FEM compared with mode shapes acquired from experiments, single damage, case study 1	144
Table 7.4 Material properties and geometric information – experimental case study 2	146
Table 7.5 MAC values for comparison mode shapes identified from FEM compared with mode shapes acquired from experiments, single damage, case study 2	153
Table 7.6 Material properties and geometric information – experimental case study 3	154
Table 7.7 Sensitivity of accelerometer sensors	156
Table 7.8 MAC values for comparison mode shapes identified from FEM compared with mode shapes acquired from experiments, single damage, case 1, case study 3	169
Table 7.9 MAC values for comparison mode shapes identified from FEM compared with mode shapes acquired from experiments, multiple damage, case 2, case study 3	169
Table 7.10 MAC values for comparison mode shapes identified from FEM compared with mode shapes acquired from experiments, multiple damage, case 3, case study 3	170
Table 8.1 List of damage states	177
Table 8.2 MAC values for comparison mode shapes identified from FEM compared with mode shapes acquired from experiments-Case C0	197
Table 8.3 MAC values for mode shapes identified from FEM compared with mode shapes acquired from experiments-Case C1	198

Table 8.4 MAC values for mode shapes identified from FEM compared with Mode Shapes acquired from Experiments-Case C2	198
Table 8.5 MAC values for Mode Shapes Identified from FEM Compared with Mode Shapes acquired from Experiments-Case C3	198
Table 8.6 MAC values for Mode Shapes Identified from FEM Compared with Mode Shapes acquired from Experiments-Case C4	199

LIST OF SYMBOLS

The main symbols used in this thesis are listed below:

Chapter 2

- v'' Mode shape derivation
- M Bending moment
- EI Stiffness
- i Mode shape number
- j Node number
- h The distance between the nodes (length of the element)
- Φ Modal matrix
- Λ Diagonal eigenvalue matrix
- ω Modal frequency
- m Number of measured mode shapes
- MSE_r MSE at r th mode shape
- K Stiffness matrix
- Φ_r The r th mode shape matrix

Chapter 3

- $MSE_{i,j}^d$ MSE at mode i and element j of damaged case
- ϕ_i^d Mode shape at mode i of damaged case
- K_j^d Stiffness of element j of damaged case
- K Global stiffness of the structure of undamaged case
- α Damage extent (fractional reduction of elemental stiffness matrix)
- MSE_{ij} MSE of element j at mode i before the damage

$MSE_{i,j}^d$ MSE of element j at mode i after the damage

Chapter 4

$\{\phi_i\}$ Mode shapes at mode i of undamaged case

$\{\phi_i^d\}$ Mode shapes at mode i of damaged case

$[K_j]$ The undamaged stiffness at element j

$\{\Delta\phi_i\}$ Change in mode shapes due to damage

c_{ir} A scalar factor

md Number of analytical modes

λ_i^d Eigenvalues (frequencies) at mode i of the damaged case

λ_i Eigenvalues (frequencies) at mode i of the undamaged case

m Element number

L Number of elements

α The damage extent

n Total number of analytical modes

ΔS_k Change in rotational stiffness at the k th joint

$\frac{\partial[K_j]}{\partial[S_k]}$ sensitivity of the j th elemental stiffness matrix with respect to a change in the rotational stiffness in the k th joint

α_k Fractional change in the k th rotational stiffness

$\delta MSE_j^{(k)}$ The MSE change of element j at mode k subjected to a known damage case

$[K_m^d]$ Stiffness matrix of damaged case of element m

$[K_m]$ Stiffness matrix of undamaged case of element m

$[\Delta K]$ Change in stiffness due to damage

ΔMSE_{ij}^{imp} Change in MSE at element j and mode i for the improved MSE method

r Number of analytical modes under consideration

$S_{i,j}^{MSE}$ Sensitivity matrix at element j and mode i in terms of MSE

$S_{i,j}^{\phi,s}$	Sensitivity matrix at element j and mode i in terms of mode-shape-stiffness
β_{st}	Sensitivity coefficient of MSEC to damage
s	A selected element for computation of the MSEC
t	A suspect damaged element
$\bar{\varphi}_{ij}$	Noise polluted modes shape of the j th mode at i th DOF
φ_{ij}	The mode shape components of the j th mode at i th DOF
γ_i^{φ}	Random numbers with the mean of zero and a variance of one
ρ^{φ}	Noise level (per cent)
$\varphi_{\max,j}$	The largest component of the j th mode shape

Chapter 5

l	Length of each element
L	Total length of the model
E	Modulus of elasticity
A	Cross-sectional area
I	Second moment of area
ρ	Mass density

MSECimp MSEC index of the improved MSE method

Chapter 7

f	Natural frequency (Hz)
-----	------------------------

$MAC(\phi_{1i}, \phi_{2i})$ MAC value of the i th mode shape of the modal matrices 1 and 2

A_b	Beam cross-sectional area
A_c	Column cross-sectional area
I_b	Beam second moment of area
I_c	Column second moment of area

Chapter 8

$y_{s,l}(t)$	Normalized time history data measured at location s and direction l
--------------	---

- $y_l(t)$ Raw time history data measured
- j Number of data points of the signal
- $y_{sn,l}(t)$ Standardized time history data at location s and direction l
- μ The mean of data
- σ Standard deviation of the data

LIST OF ABBREVIATIONS

ANN	Artificial Neural Network
BHM	Bridge Health Monitoring
BP	Back Propagation
CMSE	Cross Modal Strain Energy
DI	Damage Indicator
DLV	Damage Locating Vector
DoF	Degree-of-Freedom
DMSEC	Direct Model Strain Energy Correlation
EMAC	Energy-Based Modal Assurance Criteria
FFT	Fast Fourier Transform
FE	Finite Element
FEM	Finite Element Method
FRF	Frequency Response Function
FRFCM	Frequency Response Function Change Method
FNN	Fuzzy Neural Network
GA	Genetic Algorithm
IABMAS	International Association For Bridge Maintenance And Safety
IMSE	Iterative Modal Strain Energy
MAC	Modal Assurance Criteria
MF	Modal Flexibility
MFC	Modal Flexibility Changes
MSE	Modal Strain Energy
MSEBI	Modal Strain Energy Based Index
MSECR	Modal Strain Energy Change Ratio
MSEC	Modal Strain Energy Correlation

MSC	Mode Shape Curvature
ML-GA	Multi-Layer Genetic Algorithm
MDLAC	Multiple Damage Localization Assurance Criterion
PCA	Principal Component Analysis
PNN	Probabilistic Neural Network
QUT	Queensland University of Technology
SCCM	Spectral Centre Correction Method
SDIM	Stubbs Damage Index Method
SHM	Structural Health Monitoring
HKPU	The Hong Kong Polytechnic University
3-D	Three Dimensional
NDT	Traditional Non-Destructive Tests
VBDD	Vibration Based Damage Detection
WSS	Wireless Sensing System

CHAPTER 1

INTRODUCTION

1.1 Structural damage

Degradation and deterioration of the infrastructure because of corrosion, fatigue, erosion and wear processes (Gopalakrishnan *et al.*, 2011), during the service life contributes to damage in the structures which is defined as bearing capacity reduction (Chen and Ni, 2018). In other words, damage is inducing any changes to material and/or geometric properties of the boundary conditions and connectivity of the system that negatively influences the performance of the system (Farrar and Worden, 2012). Some types of damage are cracks, corrosion and concrete spalls that reduce the stiffness of structure.

To ensure the health of the structures, there is a need to monitor the structure for the damage during the service life. One of the most common and inexpensive way is visual inspection (Choi *et al.*, 2005). However, for complex structures, visual inspection is not adequate to recognize the damage in the structures, firstly, it is unreliable. Secondly, it is not applicable for any structure or any favorite location of the structure because some parts may not be accessible for visual inspection. Besides, some types of damages are not visible to be visually inspected. Furthermore, by visual inspection the extent of damage cannot be quantified.

1.2 Failure in bridges around the world

From 2000 till 2017, about 96 bridges have been collapsed around the world. The list of most recent ones in 2016 and 2017 including name, location, date of collapse and casualties are listed in Table 1.1 (Wikipedia, 2017).

Table 1.1 List of bridge failures around the world during the years 2016 and 2017

No	Bridge name	Location	Country	Date of collapse	Casualties
1	Nipigon River Bridge	Ontario	Canada	10 January 2016	-
2	Vivekananda Flyover Bridge	Kolkata	India	31 March 2016	27 killed, 80+ injured
3	Railway bridge	Tolten River	Chile	19 August 2016	-
4	Nzi River Bridge	near Dimbokro	Ivory Coast	6 September 2016	-
5	Yellow 'Love' Bridge	Klungkung Regency	Indonesia	16 October 2016	9 killed, 30 injured
6	Lecco overpass	Province of Lecco	Italy	28 October 2016	1 killed, 5 injured
7	Camerano overpass	Province of Ancona	Italy	9 March 2017	2 killed, 3 injured
8	Pfeiffer Canyon Bridge	Pfeiffer Big Sur State Park, Big Sur, California	United States	11 March 2017	-
9	I-85N Atlanta	Atlanta	United States	30 March 2017	-
10	Sanvordem River Bridge	Curchorem, Goa	India	18 May 2017	2 killed, 30 missing
11	Sigiri Bridge	Nzoia River, Budalangi, Busia County	Kenya	26 June 2017	3 injured
12	Bridge No 'B1187 - 1978' on N3 at intersection with M2	Johannesburg	South Africa	9 August 2017	6 injured
13	Ramat Elhanan Pedestrian Crossing on Highway 4	Bnei Brak	Israel	14 August 2017	1 killed

For instance, the I-35W Mississippi River Bridge (known as Bridge 9340) was collapsed on August 1, 2007 and led to killing 13 people and injuring 145 as shown in Figure 1.1. It was an eight-lane, steel truss arch bridge carrying 140,000 vehicles daily.

According to the National Transportation Safety Board (NTSB) report (Board, 2008), the cause of the collapse of the I-35W Bridge, was a design error by the firm (Sverdrup & Parcel and Associates, Inc.), causing the gusset plates having insufficient load capacity. Additionally, combination of additional weight on the bridge at the time of event, the traffic and concentrated construction loads were contributed to the unexpected collapse of the bridge.

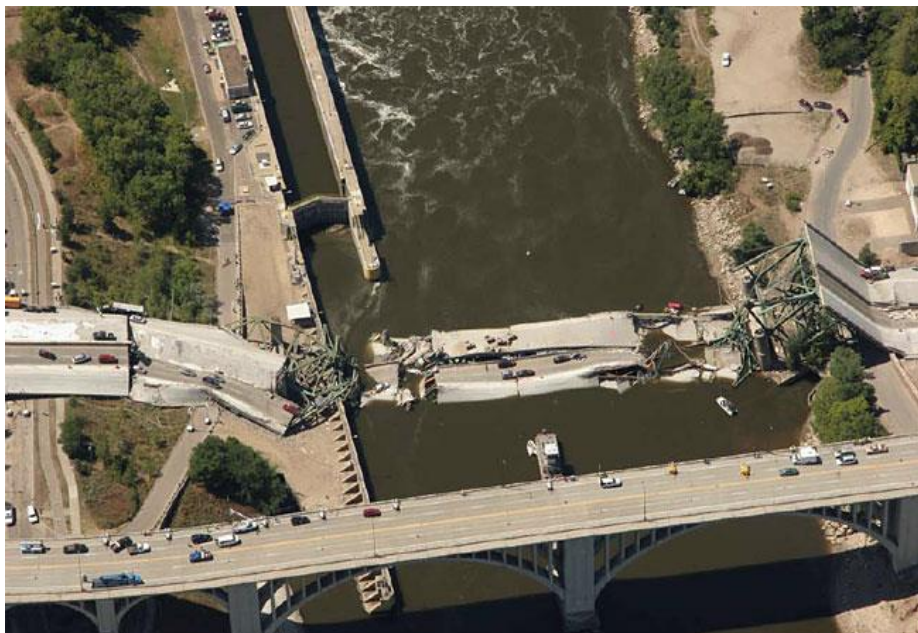


Figure 1.1 Collapse in I-35W Bridge in the US, Aug., 2007

Another sample of the disastrous bridge collapse is the Highway 19 overpass at Laval (De la Concorde Overpass) at a bridge over Quebec Autoroute 19 near Montreal, Quebec, Canada, that was happened on September 30, 2006, killing five people and injuring six others as shown in Figure 1.2. The main reason of the overpasses collapsed accepted by the commissioners of the Quebec Government was shear failure in southeast abutment because of the following problems;

- The designed steel reinforcement was concentrated in one layer, although it was according to the design code at the time of design.
- Putting reinforcement in an improper location during the construction.
- Inferior quality of the abutment concrete resulting in poor freeze-thaw behaviour.

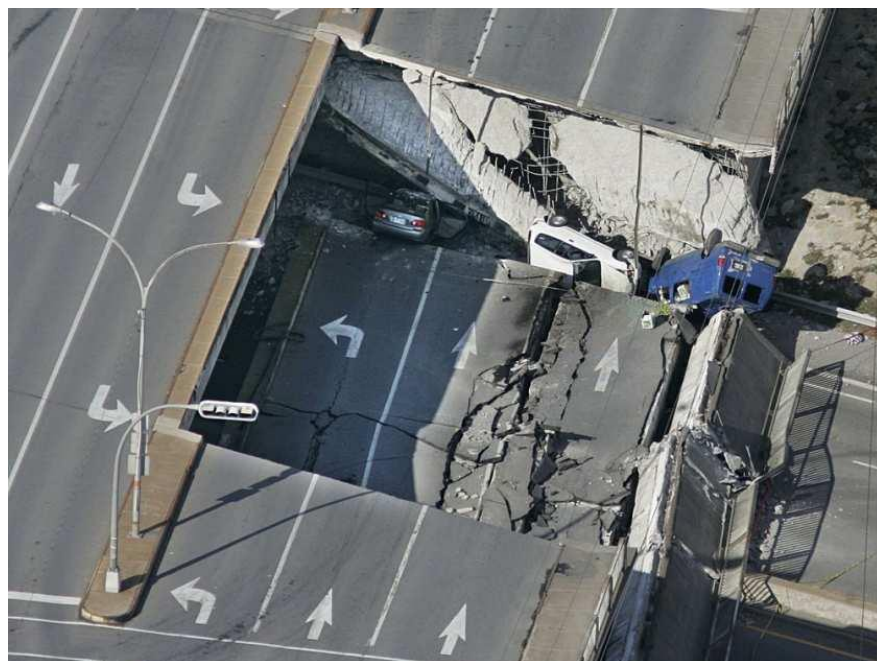


Figure 1.2 Collapse in De la Concorde Overpass Bridge in Quebec, Canada Sept., 2006

1.3 Bridge management and Bridge failure in Australia and New Zealand

There are around 33500 and 17000 road bridges in Australia and New Zealand, respectively, in public ownership, which are managed by over 800 establishments. Austroads that is a responsible association dealing with improvement of the transport

in Australia and New Zealand, often estimates the maintenance and replacement costs of road bridges in Australia and New Zealand, as well. According to AP-R252/04, the overall estimation of road bridge replacement cost in Australia and New Zealand was about A\$20b at June 2002. However, the maintenance expenditure was estimated around A\$100m and NZ\$15m in Australia and New Zealand in 2002/03, respectively (Dowling and Rummey, 2004).

The list of the most recent damaged bridges in Australia and New Zealand are shown in Table 1.2 (Wikipedia, 2017). The bridge failures happened in Australia are very recent occurring in the last decade. While the last bridge failure in New Zealand happened in 1953, which is known as the New Zealand's most horrible train disaster.

Table 1.2 List of the most recent bridge failures in Australia and New Zealand

No	Bridge name	Location	Country	Date of Collapse	Casualties
1	Gosford Culvert washaway	Gosford, New South Wales	Australia	8 June 2007	5 killed
2	Somerton Bridge	Somerton, New South Wales	Australia	8 December 2008	-
3	Devonshire Street pedestrian bridge	Maitland, New South Wales	Australia	5 March 2009	4 injured
4	Gungahlin Drive Extension bridge	Canberra, Australian Capital Territory	Australia	14 August 2010	15 injured
5	Whangaehu River Rail Bridge	Tangiwai	New Zealand	24 December 1953	151 killed

1.4 Non-destructive testing

Another way for monitoring the health of the structures is non-destructive testing (NDT) methods. NDT stands for a variety range of methods for analysis of the material and component properties of a system inducing no damage in the system. The terms nondestructive examination or nondestructive evaluation (NDE) and nondestructive inspection (NDI) are also shows the same implication of NDT technology. NDT is used in several disciplines especially in civil engineering for structural damage detection. The most common NDT methods are radiographic, eddy-current, liquid penetrant, magnetic-particle, ultrasonic, and visual testing. Each of these methods are also subdivided to many other techniques and each of them is proper only for a special application and may not be applicable for other purposes. Therefore, the most important step in using NDT methods is selecting a proper method well-suited with the expected application. However, the traditional NDT methods are useful neither for global damage detection of the large complicated structures nor for quantifying the extent of the damage (Engineering, 1998).

1.5 Structural health monitoring (SHM)

The SHM is a new emerging technology that provides continuous or periodic information on the structure condition to predict its remaining life (Gopalakrishnan *et al.*, 2011). One aspect of the SHM is to evaluate the possible damage in structures using analytical tools (Chan and Thambiratnam, 2011). Damage detection and characterization scheme is a process that is achieved using the SHM techniques. The

SHM delivers a variety of vibration-based damage detection (VBDD) methods that the most common ones are as follows.

- Natural frequency variation based Methods
- Direct mode shape based method
- Mode shape curvature based method
- Dynamically measured flexibility based method
- Modal strain energy based method
- Frequency response function method
- Genetic algorithm based method
- Artificial neural network based method
- Wavelet transforms techniques

Unlike the primary and traditional NDT methods, new SHM techniques not only are practical for complicated structures but also are capable of quantifying the damage in most of the structures. This characteristic of the SHM methods has made them to be increasingly developed.

From the literature reviewed, it is observed that modal strain energy (MSE) has been effectively used for structural damage detection. Yet, the MSE methods have mostly been validated for some types of structure such as beam like structures or steel truss bridges. To more accurately identify the location and severity of structural damage practically, it is essential to enhance/improve the available MSE methods. It leads to provide a more applicable and reliable approach for damage detection and quantification of any bridge. This study aims to improve an MSE scheme to be more

accurate and feasible to detect the minor damages in bridges with having a high number of degree-of-freedom (DoFs). Having such method with high capability, definitely results in decreasing the loss of lives and property by preventing the unexpected structural damages and finally providing the safety of bridges.

Initially, an MSE method is mathematically developed and then numerically applied to some two-dimensional (2-D) structural case studies. The primary numerical verification indicates that the mathematically improved method in this study is more accurate and efficient than the similar method. Consequently, experimental verification is also performed. Finally, a real bridge is studied to evaluate the applicability of the present study for a real bridge.

1.6 Research problems

Occurring the damage in infrastructures, especially in bridges, during their service life is an undeniable phenomenon. Unmonitored structures may expose to unexpected damage and consequently lead to loss of lives and property. Therefore, a proper monitoring is necessary to identify the early structural damage and perform a timely repair to prevent/ minimize the disastrous structural damages.

Although there are many existing VBDD methods available, it is necessary to extend and develop those methods to be more inexpensive, accurate and reliable for health monitoring. According to the literature reviewed, the following issues are still enclosed.

1. There is not enough classified study particularly on different bridges in terms of length, material properties and so on. Different researchers have addressed different problems for some types of bridges, which are very various. Therefore, having a unique method is required in general.
2. The behavior of the structures with having a higher number of DoFs during the damage is unpredictable.
3. Old bridges with different design methods demand different structural damage techniques.
4. Measuring the rotational DoFs and all mode shapes of a structure is very expensive and difficult, so it is better to improve the methods that requires incomplete data i.e. the methods that can detect the structural damage using fewer data of mode shapes are more preferable to enhance/ improve.

1.7 Aims and objectives

The primary aim of this study is to develop a sensitivity matrix based MSE method for structural damage detection. Sensitivity matrix is a matrix in terms of MSE differentiation of each element at any mode shape with respect to fractional reduction of that element. The more sensitive matrix, the more accuracy in damage detection. It is also intended to make it applicable for real bridges in terms of physical model and

material properties. To achieve this, a mathematical formulation is improved, to detect the damage more accurately.

The required input data for the improved method includes all mode shapes and natural frequencies of undamaged structure and only the first five mode shapes and natural frequencies of damaged structure. Therefore, in the numerical case study, the finite element (FE) analysis data of entire model/structure and induced damaged model/structure will be used by applying the improved formulations to validate its proficiency.

The aims of this research are achieved through the following objectives.

1. Improve an MSE method to precisely and safely locate and quantify the damage in bridges.
2. Verify the improved method numerically and experimentally for some models and structures and compare the results
3. Apply the improved method to real models and bridges.

It is evident that in numerical case studies as many as mode shapes and natural frequencies required for the improved method can be easily derived from the simulated models using available FEM softwares. Therefore, it is predicted that the results of numerical studies be more coincided with reality. However, any incomplete and inaccurate data may affect the results of experimental studies. Although in this study, it is tried to overcome this issue using expansion mode shape; it is an undeniable to

face with some errors in experimental studies. However, overall it is expected to get the more accurate results or at least lesser errors than previous studies.

To achieve these, the following procedure is projected.

1. Improve the MSE equation and sensitivity matrix of an existing MSE method to increase the accuracy and performance of the method.
2. Numerically verify the performance of the improved method for some structural models and compare with other similar approaches.
3. Experimentally assess the fulfillment of the improved method for some laboratory models and compare the results with their numerical simulations.
4. Apply the improved method to a real bridge and compare the results with those of from finite element method (FEM) analysis.

1.8Significance

The outcomes of this research provide a safe and inexpensive SHM method for bridges. This can be simply applied to any real bridge, having incomplete measured data to determine the possible damages. Since, from the improved method, it is expected to detect the damage at the initial stage of formation, consequently, it can contribute to a confidently structural health investigation that decreases the lives and property losses.

1.9 Scope of the research

This study concentrates on the MSE methods as a group of the VBDD methods to detect the damage in bridge structures. Therefore, the research scopes are limited to application of the MSE method to detect the damage in any bridge. Also, the damage type is considered as a fractional reduction in element stiffness or rotational stiffness at the end nodes of the element or incremental in element mass, i.e. the damage is an elemental or nodal damage. It means the structure should be considered as a compound of elements and then identify the damage elements. Therefore, any damage such as crack or loosening the joints that can be scaled or measured as a fraction of reduction of stiffness, rotational stiffness or increase of mass of the elements of the system can be identified by this method. The damage should be measured or expressed as a percent of reduction of stiffness or increment of mass from 0 to 100 percent. Otherwise, any other types of damage that cannot be included in this category cannot be recognized by the proposed method. Hence those types of damage are out of the scope of this study.

1.10 Thesis outline

This thesis consists of nine Chapters organized as follows.

A review of some earlier works done in SHM is presented in Chapter 2. In Chapter 3, overall methodology and research plan of the improved MSE method is presented. In Chapter 4, the theory of study and mathematical development of the improved MSE

method is demonstrated. Chapter 5 deals with performance of the improved method compared to other methods. Chapter 6 numerically evaluates the performance of the improved MSE method. Chapter 7 validates the experimental studies on the improved MSE method. Chapter 8 presents the application of the developed MSE method to an actual model and a bridge. Finally, the thesis is concluded in Chapter 9 with some useful suggestions for the future work of researchers.

CHAPTER 2

LITERATURE REVIEW

This chapter provides an overview of some literature in common and the most recent SHM methods which have been used for identifying the structural damage. In the first part of this chapter, some VBDD methods based on natural frequency, mode shape, and MSE are presented. The second part of this chapter covers the review of some other approaches such as the Genetic algorithm (GA), Frequency Response Function (FRF), and Artificial Neural Network (ANN). The main argument performed in this chapter proposes that the MSE methods are more efficient than other damage detection methods which are based on only mode shape or natural frequency.

This extensive literature reviews the gaps in SHM methods to improve an MSE method for detecting the bridge damage accurately and effectively and decreasing the time and computational cycles.

2.1 Parametric based VBDD methods

The first group of the methods reviewed are some common VBDD methods based on natural frequency, mode shape and MSE parameters as follows.

2.1.1 Natural frequency variation-based methods

Natural frequency is one of the common approaches for detecting the existence of damage in simple structures such as beams and plates. It is based on change in the natural frequency of a structure in the presence of damage.

A natural frequency-based damage detection approach was proposed by Zhong *et al.* (2008) for simply supported beams using the output-only time history. This method was based on auxiliary mass spatial probing which was computed by FEM using the spectral centre correction method (SCCM). Verification of the proposed method was performed through a numerical simulation. The direct natural frequency curve did not exactly locate the location of the crack. However, its derivative graph could display the crack (damage). Although this method is inexpensive and efficient for damage detection of beam-like structures, for practical purposes it is expected that experimental noise corrupts the response data.

Messina *et al.* (1998) validated a multiple-damage detection method entitled Multiple Damage Localization Assurance Criterion (MDLAC) for truss structures. Firstly, two algorithms were verified for the location and size of the damage using a three-beam test structure. Then, the required data including changes in the few natural frequencies of the structure between the damaged and undamaged states were measured for two truss structures. The MDLAC method that was based on the first order of sensitivity matrix was able to detect both location and absolute size of structural damages correctly. Although the second order of the sensitivity matrix was also developed,

the difference between the results observed was insignificant compared to those of MDLAC.

According to Wang *et al.* (2012) who cited Rytter (1993) that damage diagnosis can be categorized into four levels;

Level 1: Identify the existence of damage

Level 2: Recognize the location of damage

Level 3: Discover the severity of the located damage

Level 4: Predict the remaining life of the structure

In general, the natural frequency vibration-based method is cost effective and easy to implement, but it requires highly precise measurement when frequency changes are low. Results can also be affected by environmental impacts which have the same effect on structural frequency (Park *et al.*, 2001). Other disadvantages of this method include the fact that

1. It is unable to detect the damage in symmetrical locations (Lu and Gao, 2005).
2. It can detect a low level of damage assessment, however, it is less effective for higher levels (Hejll, 2004).

3. It is applicable only for structural components or elements such as beams, plates or frames (Gudmundson, 1982).

2.1.2 Mode shape variation-based methods

Despite the difficulty in measuring mode shapes and the necessity for large amounts of measurement data, mode shape variation-based methods are more sensitive in locating the damage compared to natural frequency and damping coefficients (Dutta and Talukdar, 2004, Kim *et al.*, 2006). Also, mode shape with derivative indicators seems to be more precise and accurate than other mode shape techniques (Maeck and De Roeck, 2002, Dutta and Talukdar, 2004). Some of the most common of these methods are described in the following sections.

2.1.2.1 Direct mode shape-based method

The mode shape method is based on measuring the difference between two sets of mode shape data to represent the damage in the structure.

A numerical damage detection approach was proposed by Yuen (1985) for a cantilever beam. The method was performed by determining the change in mode shapes and studying the relationship between the location and size of damage and Eigen parameters.

Kim *et al.* (2006) proposed a method to detect the size and location of damage in beam-like structures using only a few lower mode shapes. Results of numerical simulations showed that this method can solve the mode selection, singularity and

axial force problems, however, it involves a dense measurement of grid and an accurate extraction of mode shapes.

2.1.2.2 Mode shape curvature-based method

Mode shape derivations normally provide more accurate information about the location of vibration change and consequently the damage situation (Dutta and Talukdar, 2004). Pandey *et al.* (1991) numerically applied a curvature mode shape to two beam samples, one cantilever and the other one simply supported. The required displacement mode shapes were derived using FEM. Curvature at any section of the beams was given

$$v'' = \frac{M}{EI} \quad (2.1)$$

The following equation shows using the central difference approximation showed that according to the assumed damages, change in modulus of elasticity could cause the change in mode shape curvatures.

$$v''_{ji} = \frac{v_{(j+1)i} - 2v_{ji} + v_{(j-1)i}}{h^2} \quad (2.2)$$

where i is the mode shape number,

j is the node number and

h is the distance between the nodes (length of the element)

So, the damage was located by observing the absolute change in curvature mode shapes. However, quantifying the damage has not been reported.

Dutta and Talukdar (2004) investigated the application of mode shape curvature on a simply supported and a continuous bridge deck to identify the possible multiple damages. The results demonstrated a greater accuracy of the method at lower modes. Besides, mode shape curvature (MSC) was more accurate than mode shape in respect to damage location. However, the multiple damage evaluation of complex structures using this method requires some necessary treatments such as deriving an enough number of modes and an appropriate mode selection.

Sazonov and Klinkhachorn (2005) proposed a method to optimize the sampling interval for acquisition of the displacement mode shapes. The method minimizes the effect of noise measurement, increases the sensitivity to damage and maximizes the number of sampling points. Numerical verification was performed on a free-free aluminium beam. Damage detection was performed on the curvature and strain energy mode shapes using common methods. The results indicated a good performance of the proposed method for optimizing the sampling points. However, in practice, to determine several sampling points, there is a need to properly estimate the measurement errors which depends on the methodology under consideration and the measuring equipment.

Tomaszewska (2010) proposed an absolute damage index to investigate the influence of statistical errors on structural damage detection. The method was first numerically applied to a simply supported beam and then applied to a real structure, tower of the Vistula Mounting Fortress in Gdansk. It was found that in the damage detection method based on using modal characteristics, the effect of modal characteristics error is significant and should be taken into account. Ignoring the modal characteristics contributes to false results in damage detection. Also, when damage detection is based

on using modal data, directly using a multi damage indicator gives better results than using only a single damage indicator. Furthermore, obtaining the true damage is depended on the extent of both damage and error level. However, the methods need to be numerically and experimentally verified for other indices and other type of structures.

Wang *et al.* (2000) simulated the Tsing Ma Bridge using a 3-D FEM model in ABAQUS to analytically determine a proper modal parameter for damage detection in large-scale suspension bridges. For this purpose, ten damage cases were simulated in the bridge to evaluate the sensitivities of different modal parameters to different types of damage. The damages were induced by either disconnecting the tower, damage of hangers at mid-span or at the deck components at middle of the span or at near supports by reducing the element stiffness. Three modal parameters of natural frequency, mode shape curvature and modal flexibility were used to analytically determine the most sensitive one to the damage. The correlation between mode shapes of measured and calculated from the 3-D FEM was evaluated using MAC values. The results showed that the modal flexibility method studied is more sensitive to damage than other two methods of natural frequency and mode shape curvature. In other words, the natural frequency performed worse than other modal parameters studied. It means using only the natural frequency is an improper method for damage detection in such structures, although the frequency change may probably detect the damage. The modal parameters of mode shape and modal flexibility matrix performed better in detecting the damages at near the supports. However, yet it is difficult to practically apply this approach or extend it to other type of structures.

2.1.2.3 Dynamically measured flexibility-based method

This method is also known as natural flexibility method, which uses the modal flexibility matrix as a modal derivative method. The derived modal flexibility matrix is expressed as follows (Pandey and Biswas, 1994, Pandey and Biswas, 1995),

$$F = \Phi \Lambda^{-1} \Phi^T = \sum_{i=1}^m \frac{1}{\omega_i^2} \phi_i \phi_i^T \quad (2.3)$$

where Φ is the modal matrix,

Λ is the diagonal eigenvalue matrix,

ω is modal frequency,

ϕ_i is the i th mode shape and

m is the number of measured mode shapes

Lu and Gao (2005) improved a flexibility-based damage locating vector (DLV) method to detect the damage in a continuous and long-term monitoring. The results from a numerical simulation of a 14-bay planer truss using the mentioned method demonstrated the capability of this method for detecting damage at both single and multiple damage scenarios.

Shih *et al.* (2011) developed a multi-criteria procedure incorporating modal flexibility (MF) and MSE methods through a dynamic computer model. Then, it was applied to a truss bridge incorporating the two parameters, MF and MSE, besides change in natural frequencies, on both damaged and undamaged structural models. Each one of the deck flexural stiffness and the axial stiffness of truss members was also reduced by 50% to simulate two types of damage severity in the structure. Then, eight damage

cases were considered including, two cases consist of combined deck and truss girder together, two deck and four truss cases separately. The combination of MF and MSE parameters provided an optimum chance to accurately assess the damage.

2.1.3 Modal strain energy-based method

MSE based method employs the MSE variable, which identifies the condition of an element in a structure as a relatively sensitive parameter. The MSE variable for the i th mode of a structure is derived (Stubbs *et al.*, 1992) as.

$$\text{MSE}_i = \frac{1}{2} \phi_i^T K \phi_i \quad (2.4)$$

where K is the stiffness matrix of the structure and

ϕ_i is the i th mode shape matrix

Doebbling *et al.* (1997b) developed an MSE based method for selecting a subset of the identified structural vibration modes to be used in FEM correlation and structural damage detection. The MSE modes measured were then ranked and used in descending order. It was observed that a mode selection strategy based on MSE provided more accurate results than a strategy using MF.

Shi *et al.* (1998) established an MSE based damage indicator (DI) for damage location using the change of MSE in each element. Shi's approach is simple and healthy, capable of detecting single or multiple damages of structures. The sensitivity of the MSE with respect to the damage was also derived as a function of the analytical mode shape change and stiffness matrix. Although in this approach only the incomplete

measured mode shapes and analytical system matrices are used for damage location and quantification, there is a need to more accurately quantify the damage severity. The results show that though the proposed approach is noise sensitive, it can locate single and multiple damages.

Shih *et al.* (2009) blended a multi-criteria procedure incorporating MF and MSE methods that was applied to a plate and a beam structure. The purpose was to identify single and multiple damages via a dynamic computer simulation technique. Nine damage scenarios were considered in each element. It was found that for a single damage, modal flexibility change (MFC) and MSE change provide similar results with no location error. Although for multiple damage scenarios MSE change increased the accuracy of the damage location in the plate, but the simulation of the multiple damage needs more investigation.

Yan *et al.* (2010b) formulated a damage detection method based on elemental MSE sensitivity. Yan's method which was adapted a closed form of elemental MSE sensitivity, was numerically applied to some 2D structures and high efficiency results were noted.

Wang *et al.* (2010) improved a modal strain energy correlation (MSEC) method using a theoretically derived MSE-to-damage sensitivity variable. Although this method was efficient, noise contamination might give false results. Wang's method was further developed and validated for complicated steel truss bridges using a multi-layer genetic algorithm (ML-GA) method which become more efficient and feasible even in presence of noise (Wang *et al.*, 2012, Wang, 2012). Though, this effective method might be verified for other types of bridge structures or buildings.

Wahalathantri *et al.* (2012) validated a damage index based MSE method that could capture damage in terms of quantifying and locating at any of the measured modes. By applying the method to a simply supported and a two-span beam it was observed that it is inexpensive and less time-consuming. Although this method is enough efficient, it is unique for simple beams only.

Seyedpoor (2012) proposed a two-stage modal strain energy-based index (MSEBI) to locate and quantify the structural damage. The numerical results of two samples showed the reliability of the method in damage identification. However, convergence achieves after some iterations which usually demands high computations. Also, the effect of noise for the first case study has not been reported.

Kisa and Arif (2005) developed a numerical model to investigate the vibration analysis in the cracked cantilever composite beams. The model employs FEM and component mode synthesis method which is based on total strain energy of the system. Having the modal data, the method, could identify the location and dimension of the defect (crack) in the beam. However, the method is unique for detecting the crack in cantilever composite beams with a special cross section. Also, it requires more studies for the same type of structure with different boundary conditions.

Asgarian *et al.* (2009) numerically applied an MSE method to a 3D four-story frame of a jacket offshore platform for damage detection. Modal strain energy change ratio (MSECR) and cross modal strain energy (CMSE) were used for locating and quantifying the damage, respectively. Although this method performs well for these structures, it is not capable of detecting the damage in all directions of vertical bracing

of the case study demonstrated. Also, it needs experimental studies to be applicable for these types of structures.

Brehm *et al.* (2010) enhanced a purely mathematical modal assurance criteria (MAC) called energy-based modal assurance criteria (EMAC) in terms of MSE. A numerical model and a benchmark study (cantilever truss) were presented to show the efficiency of the proposed method. The method sufficiently reduces uncertainties about mode shapes, particularly when limited spatial information is available. However, this methodology cannot replace a cautious preparation of modal tests. Srinivas *et al.* (2011) proposed a multi-stage approach to detect structural damage using MSE and GA-based optimization technique. The method was successfully applied to a simply supported beam and a plane truss. Although it has been mentioned that the method can be useful for damage detection in large-scale structures, no case study for this type of structures has been reported.

Yan *et al.* (2010c) combined a CMSE with the niche genetic algorithms (GMs). The method was numerically used to detect the damage of an airfoil with composite materials. However, experimental works have not been reported in order to detect the structural damage in bridges or buildings. Wu and Sun (2011) compared and improved two damage identification methods, which were based on MSE. Numerical studies showed that Shi's MSECR method is more accurate than Stubbs' damage index method (SDIM). Since both methods are noise sensitive and have limited robustness in damage identification, to improve these concerns and also the modal expansion method, more studies are required. Hu *et al.* (2011) presented the surface crack detection in an aluminium circular hollow cylinder using MSE and scanning damage index methods. The experimental results indicated the accuracy of the method.

However, this method still needs to be more simplified for large structures and be applicable for a different type of structures and different size of damages.

Li *et al.* (2013) calculated the sensitivity of elemental MSE of three structures including, a fixed–fixed beam, an automobile frame and a two-bar truss structure using the methods available in the literature and also the new method they proposed. The results of three numerical examples done from different methods were compared together. It was resulted that for large numbers of degrees of freedom (DoFs) and when the number of design variables exceeds the number of individual element stiffness matrices of interest, the proposed method has a good preferability. However, the storage capacity issue needs to be improved more.

Wang (2013) developed an iterative modal strain energy (IMSE) method using frequency measurements to estimate the structural damage severity. Unlike the other MSE methods, this method requires only a few modal frequencies from damaged structure. The result of the experimental data from a clamped-free beam indicated the capability of the method in accurately quantifying the damage extent. Wang *et al.* (2013) developed a CMSE method to estimate the connection stiffness of the semi-rigid joints. The numerical study was successfully performed for a four-story frame structure considering different connection type of beam and column in presence of noise. The outcome of this method can be directly used to create an accurate model for structural damage detection.

Cha and Buyukozturk (2015) proposed a novel damage detection technique using hybrid multi-objective optimization algorithms based on the MSE. In this method, the Young's modulus of the elements was reduced to simulate the damage/s in the

structure. The proposed hybrid multi-objective GAs was used to solve an inverse problem by minimizing the total differences of the MSE of structural elements. The method was applied to three different multistorey steel structures with three different multiple damage scenarios. 5% Gaussian random white noise-contaminated mode shape was also considered. The results indicated that the method was able to detect the multiple damages in the structure. The method also worked with incomplete mode shape data. Although the proposed method can be used for detecting the damage in various three-dimensional (3-D) structures, it has been validated for steel structures only so far. Experimental validation with real measurements is needed to evaluate the efficiency of the proposed method. Furthermore, inducing the damage in other types of structures by reducing the Young's modulus with different material properties is another issue that requires more investigation.

2.2 Frequency response function method

The FRF is an output spectrum measuring system for a structure. It uses the structural dynamic responses in a time-invariant system. Some researches using the FRF methods are as follows.

Furukawa *et al.* (2006) assembled a structural damage detection method to investigate the measuring error due to noise. The proposed method iteratively zoomed in on the damaged elements by excluding the undamaged elements from the damage candidates, step by step. It adapted hypothesis testing with the bootstrap method, which is a data-re-sampling method established by Efron and Tibshirani (1994). Results on a 2D frame

structure showed that the method could improve the accuracy of identification in the presence of a large amount of noise.

Hsu *et al.* (2011) constructed a laboratory integrated frequency response function change method (FRFCM) with a wireless sensing system (WSS) for building damage detection. The FRFCM received ground excitations before and after the structure was damaged. The WSS transformed the data to frequency spectrum using Fast Fourier Transform (FFT) algorithm. The damage could be recognized from the stiffness reduction. Verifications of a 6-story steel frame on the shaking table demonstrated the efficiency of the proposed method in locating and quantifying the damage under a free environmental-effect condition.

2.3 Mathematical and statistical tools for damage detection

The second group of the damage detection techniques are some mathematical and statistical tools presented below.

2.3.1 Genetic algorithm-based method

Another popular method is the GA, which is frequently used for damage detection of structures. The GA method is originated from a mechanism of biological evolution. Since the numbers of candidate elements of a structure exposure to damage are high, GA can diagnose the damaged elements. Many researchers have successfully studied the application of the GA in structural damage identification. Some of these studies are as follows,

Guo and Li (2009) for example, presented a two-stage scheme using the fusion technique and the GA to determine the location and extend the multiple structural damages. The results from a numerical simulation of a cantilever beam demonstrated the preference of the proposed method against natural frequency and mode shape methods.

Wang *et al.* (2012) established an ML-GA method using correlation-based MSE as a variable vector to detect the damage in complicated truss bridges. In the ML-GA method, the suspicious elements to damage were split to several groups. In the first layer, optimization was done for all groups. In the second layer, the groups were merged to larger groups and finally there was only one group including all elements which then by a minor optimization, damage elements were detected.

2.3.2 Artificial neural network-based method

ANN is a system originating from biological neural networks, and applicable in many disciplines, especially in structural damage detection. The ANN technique by networking the input and output patterns is able to nearly predict the damage even in case of being uncertain or incomplete data. Some of these studies are as follows,

Ni *et al.* (2001) proposed a method based on Probabilistic Neural Network (PNN) for detecting the damage in the deck of Suspension Tsing Ma Bridge using only natural frequencies. The study demonstrated that the damage identification accuracy is much higher than that of from the traditional PNN. However, application of the method on other components of the suspension bridge has not been reported.

Jiang *et al.* (2011) simulated a two-stage numerical damage detection method which integrated data fusion and Fuzzy Neural Network (FNN) techniques. In the first stage, structural modal parameters were derived and fed into an FNN system as an input. In the second stage, the FNN output was fed into data fusion. Application of the method on a 7-DoF frame model showed the theoretical feasibility and efficiency of the proposed method.

Bandara *et al.* (2014) formulated a novel technique using FRFs based damage index with ANNs for damage detection of building structures. Damage indices corresponding to different damage locations and severities are introduced as an input variable to develop neural networks. Primarily, Principal Component Analysis (PCA) was used to reduce the number of data feeding into a neural network model. Validation was performed through a 3-story bookshelf structure at Los Alamos National Laboratory, USA. By using Back Propagation (BP) neural network models associated with damage indices, damage location and severity were identified with good accuracy. Results demonstrated the suitability and effectiveness of the proposed method, especially when the numbers of baseline datasets or principal components increase.

Although in most cases, ANN methods are useful but with a large amount of data are usually unstable. Also, training pattern to validate the ANN networks is almost difficult.

2.3.3 Wavelet transforms techniques

Mathematical tool of wavelet transform is one of the popular methods of time-frequency transformation which has been mostly used for structural damage detection.

Some researches on this method are as follows,

Nair *et al.* (2006a) analytically and computationally presented a wavelet coefficient sensitivity of structural responses of a single-story plane frame. It was resulted that the structural response was not sensitive as much as the wavelet coefficient for damage detection. Also, wavelet coefficient sensitivity was not sensitive to a different type of the model such as mass density, damping ratio and so on.

Hu *et al.* (2011) experimentally studied the damage detection of a cantilever aluminium beam using wavelet transform. The study was performed for the beam, subjected to a static displacement to identify the crack at its free end. The results showed that the wavelet transform was effective in identifying the damage region even for the crack depth extends up to around a quarter of the thickness of the beam.

Solís *et al.* (2013) proposed a beam damage detection methodology based on continuous wavelet analyses. The damaged and undamaged mode shapes of the structure were first obtained and then a continuous wavelet transform was applied. Finally, the result for each mode was computed along the structure and according to the variation of the natural frequencies, the wavelet coefficients were ranked. The method was experimentally validated for steel beams. The results showed the sensitivity of the method of capturing the little damages (cracks).

2.4 Concluding remarks

The analysis of the literature on existing VBDD methods identified the followings.

1. Natural frequency methods are used only for lower level damage detection and still have not been validated for structures other than beams, plates and frames. Although measuring the natural frequency does not require heavy sensors, it can be influenced by noise and be less accurate.
2. Direct mode shape methods are easy to identify the vibration parameter and more reliable than natural frequency-based methods. Though, they can be affected by noise contaminations and are expensive because of requiring more sensors, as well. The mode shape curvature methods are based on higher order derivations and more sensitive to damage. Yet, they are usually expensive and require a substantial integrated sensory system and may also show false results.
3. There are few literatures indicating the adequate capability of natural flexibility methods. Also, it needs a distributed sensor system.
4. MSE methods are more precise than previous methods mentioned above using incomplete data. Some of these methods have been even experimentally validated for quantifying and locating the damage in bridges. One of the enormous advantages of these methods is their capability to recognize the damage using the

first few measured mode shapes which normally can be acquired through the experimental tests using few sensors. However, MSE methods can be influenced by noise pollution and sometimes may give false results. Nevertheless, these methods are depending on accuracy of data acquired and processed.

To recap the review of the mathematical and statistical approaches it can be concluded also,

In GA approaches, definition of the size of data cannot be done clearly. ANN methods are usually unstable with a large amount of data and validation of ANNs for trained pattern is also a difficult task. FRF methods are also noise-influenced and require high levels of accurate input data for detection of severe damage/s and may provide some false results. Wavelet transforms are usually accurate in damage detection, although demand a lot of computations.

This overall review of the literature identified that multi-approach methods would provide a better understanding of structural damage identification. In other words, in the modern SHM technology, the multiple-damage scenario of complex structures could best be realized by an approach of an efficient VBDD method in accompanying with any of the GA, ANN or FRF methods.

2.5 Research gaps

From the literature surveyed the following research gaps can be drawn.

1. Many numerical VBDD studies have been validated only for elementary structures such as beam and plate-like structures. So, there is a need to enhance the available methods for other types of the structures, especially real structures or propose new methods to be appropriate for detecting the damage.
2. For the most infrastructure, the higher level of damage diagnosis (Level 3 and 4) is required, especially when small damage occurs at the initial stage of formation. Therefore, proposing a more sensitive and reliable damage index could help provide this.
3. There are few literatures on effective recognition of the damage in the real structures having incomplete or limited data. Hence, an attempt needs to be made to propose/improve a method to be capable of recognizing the damage in such cases.
4. There is a lack of the existing methods to perform well in presence of the environmental noise. So, there is a need to overcome the issue using a proper methodology.

CHAPTER 3

METHODOLOGY AND RESEARCH PLAN OF THE IMPROVED MODAL STRAIN ENERGY METHOD

This chapter draws the overall methodology and research plan of an improved modal strain energy (MSE)-based damage detection method for bridge health monitoring (BHM). The first part of the chapter, section 3.1, discusses the sources of structural damage, footprint of damage in structures and the methods for damage detection considering their importance. Section 3.2 presents the formulation of the two-stage MSE method with respect to establishing the new equations for MSE change and sensitivity matrix to damage, respectively. Besides, it demonstrates the two stages of locating the damage and quantifying the extent of the damage, respectively. Section 3.3 proceeds with numerical and experimental verifications and lastly, applying the proposed method to an actual model and a real bridge. The overall approach is then concluded in the last section, section 3.4.

3.1 Introduction

Infrastructures may experience damage by being influenced from the impact loads of orbital debris, material thermal degradation, structure assembling faults, faulty materials or element connections, and so on (Carrasco *et al.*, 1997). These various environmental forces and actions continuously contribute to accumulating the damage during their service life. Structural damage often causes a loss of stiffness in one or more members of a structure affecting its modal characteristics such as modal frequencies and mode shapes (James Hu *et al.*, 2006, Shi *et al.*, 2000, Law *et al.*, 1998).

VBDD methods have increasingly become an essential field of research in structural damage detection and SHM because of their flexibility of measurement, cost-effective, and non-destructive approach of damages in a global structure (Hu *et al.*, 2011).

VBDD methods consider the fact that the vibration signatures of the structure are functions of the mechanical properties (stiffness, mass and damping) (Osegueda *et al.*, 1997, Osegueda *et al.*, 1999). Many methods have been developed to identify the damage based on these alterations. However, most of them have difficulties to be applied to real complex structures (Shi *et al.*, 1998). Generally, the process of damage identification can be divided into three stages, namely; (1) damage detection, i.e., determining the existence of the damage; (2) damage locating, i.e., determining the location of the damage, if current and (3) damage quantifying, i.e., determining the quantity of the damage (Pandey and Biswas, 1995).

Obviously, development of robust approaches for early damage detection is essential to prevent the occurrence of the possible catastrophic structural failure and structural deterioration beyond repair (Li *et al.*, 2006, Doebling *et al.*, 1997b, Pradeep *et al.*, 2014, Yan *et al.*, 2010a).

This chapter discusses the procedure and research plan of the current study, which is dealt with improving an MSE based method. The overall methodology of this research is drawn in Figure 3.1.

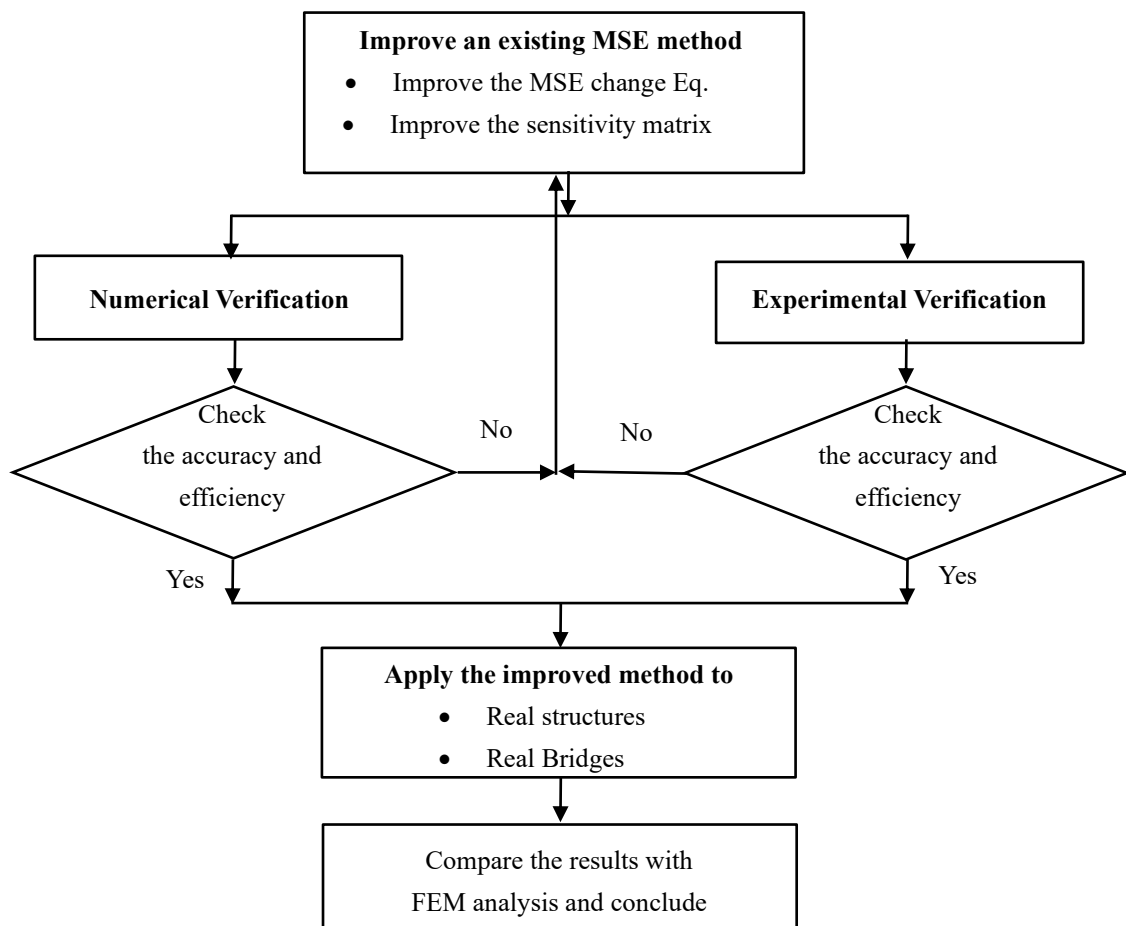


Figure 3.1 The overall methodology of the research

3.2 Formulating the two-stage MSE method

Studies indicate that occurring damage in a structure causes changing the structural dynamic characteristics such as modal parameters, i.e. mode shapes, natural frequencies and damping values. Besides, it also changes the structural parameters, such as mass, damping, stiffness and flexibility matrices (Hwang and Kim, 2004). By drawing inspiration from this fact, the current study focuses on improving an MSE based method for damage detection of bridges to accurately formulate the change of MSE due to a possible damage in the bridge. The mathematical formulations of the MSE method proposed by Shi *et al.* (2000) is improved by extending the theory of study with respect to including the actual structural damaged stiffness matrix into the damaged MSE stored in the structure after the damage. It is also attempted to generalize the improved method to be applicable for any bridge by applying to different bridge models with different material properties and element types.

3.2.1 Establishment of the MSE change and sensitivity matrix to damage

The primary effort is to more accurately establish the difference between MSE stored in the structure before and after the damage. This can be achieved by counting the actual value of the damaged stiffness matrix in MSE equation after the damage through the mathematical formulation (Yan *et al.*, 2010b) as Eq. (3.1).

$$\text{MSE}_{i,j}^d = \frac{1}{2} \{\phi_i^d\}^T [K_j^d] \{\phi_i^d\} \quad (3.1)$$

Where i is the mode shape and j is the element numbers

However, the final equation necessarily should be transformed in terms of undamaged stiffness matrix to be calculable. This can be done considering the theoretical relation between stiffness matrices before and after the damage as Eq. (3.2).

$$[K^d] = [K] + \alpha[K] \quad (-1 < \alpha \leq 0) \quad (3.2)$$

where K^d and K are global stiffness of the structure of damaged and undamaged cases, respectively, and

α is the fractional reduction of elemental stiffness matrix representing the damage extent

Having a more exact value of the change of MSE during the damage allows attaining a more sensitive matrix which assists realizing the damage more accurately at an early stage with higher reliability. The improved MSE method recognizes the structural damage in two consequent stages, stage one, locating the damage and stage two, quantifying the damage as following section. The details of the improved formulations are demonstrated in Chapter 4.

3.2.2 Stage one – Identifying the location of damage

During the damage in a structure, the damaged elements and nodes theoretically receive a higher amount of the MSEC (Shi *et al.*, 2000, Shih *et al.*, 2009). So, the crucial key for identifying the location of the damage in this study is to calculate the MSEC of the structure using the MSE of the elements before and after the damage. Therefore, an elemental MSE-based indicator is used to show the ratio of the MSE change for each element. The elements with higher amounts of MSE change ratio are nominated as the most likely elements to the damage for further investigation in the second stage.

3.2.3 Stage two – Quantifying the damage

Sensitivity matrix is used to quantify the damage which is a matrix derived from MSE change with respect to extent of the damage as an unknown independent variable as Eq. (3.3).

$$\text{Sensitivity matrix} = \frac{\partial \Delta MSE_{ij}}{\partial \alpha_j} = \frac{\partial (MSE_{i,j}^d - MSE_{i,j})}{\partial \alpha_j} \quad (3.3)$$

where MSE_{ij} and $MSE_{i,j}^d$ are the MSE of element j at mode i before and after the damage, respectively, and α_j is the damage extent (percent) at element j

For a structure with n elements, the maximum dimension of sensitivity matrix can be $n \times n$. However, to decrease the computational cycles, it is required to lessen the sensitivity matrix dimension. To do this, some of the most likely elements to the damage are selected from the first stage as the suspected elements. By selecting p suspected elements, the dimension of the sensitivity matrix considerably decreases to $p \times p$.

In this study, it is tried to improve the sensitivity matrix to achieve higher accuracy and sensitivity to minor damages at the initial stage of creation and performing with the existence of some noise in the environment. The method should be able to identify the damage in elements or nodes. For elemental damage the damage is considered as a fractional change of the elemental stiffness matrix while for nodal damage it is considered as a fractional change in the rotational stiffness.

3.2.4 Damage detection with noise polluted data

To simulate the actual condition of the structure, a reasonable percentage of noise is included into the calculations to intensify the data, including mode shapes and natural frequencies of the structure by a usual range of up to 10 percent. The details are presented in Chapter 4.

3.3 Verifications

To evaluate the accuracy and efficiency of the improved method, it is numerically and experimentally validated using some numerical simulations and experimental models. Some damage scenarios including single and multiple damages are simulated in the numerical case studies or created in the laboratory prototypes.

Initially, for each model, all analytical eigenvalues including mode shapes and natural frequencies (Seegerlind and Saunders, 1987) are derived using FEM software packages such as STRAND7, SAP2000, DIAMOND (Doebbling *et al.*, 1997a), and a MATLAB code (Kattan, 2010, Smith and Pournami, 2013). Whereas, for any damaged case, only the first five mode shapes, and natural frequencies are required. Then, the performance of the improved method for each model will be assessed using the couple dataset obtained from the damaged and undamaged cases of that model through a MATLAB code. Lastly, the performance of current study using the data obtained is compared with the existing method.

3.3.1 Numerical simulations

Some numerical models are considered to use for verification of the improved method. The models are various to represent a different type of structures, element type and material properties as follows.

3.3.1.1 Case study 1: A fixed-end steel beam

The numerical simulation is started with a simple structure which is a fixed-end beam consisting of 12 elements and 13 nodes as shown in Figure 3.2. The model is a steel beam with a total length of 7.2 m. The details are given in Chapter 6.

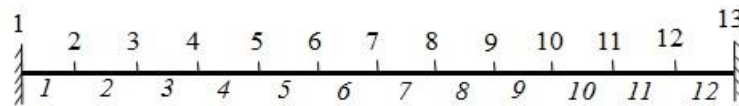


Figure 3.2 The FEM model of the fixed-supported beam

3.3.1.2 Case study 2: A three-story steel frame

The second case study is a three-story steel frame consisting of nine elements and eight nodes as shown in Figure 3.3. The material properties and geometric data will be presented in Chapter 6.

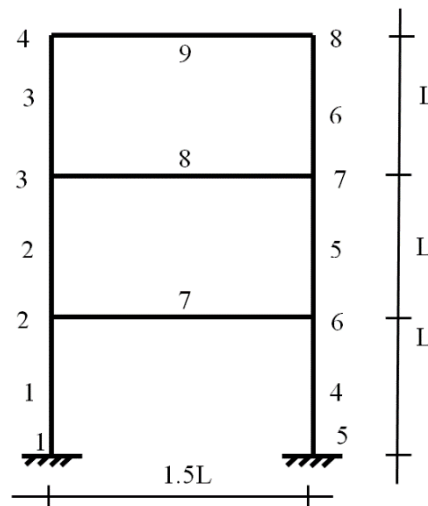


Figure 3.3 The FEM model of the three-story steel frame

Numerical verification of the improved method is further performed by applying to two other structures, a steel truss bridge and a concrete bridge frame representing the framework of the short- and medium-span bridge samples, respectively. These simulations examine the efficiency of the improved method on this category of bridges in terms of dimension and type of the structure. The effect of material properties on performance of the improved method is also observed. These two samples are as follows.

3.3.1.3 Case study 3: A 2D steel truss structure

The third numerical case study is a 2D steel truss structure as shown in Figure 3.4 consisting of 12 nodes and 21 elements. The material properties and geometric data are presented in Chapter 6.

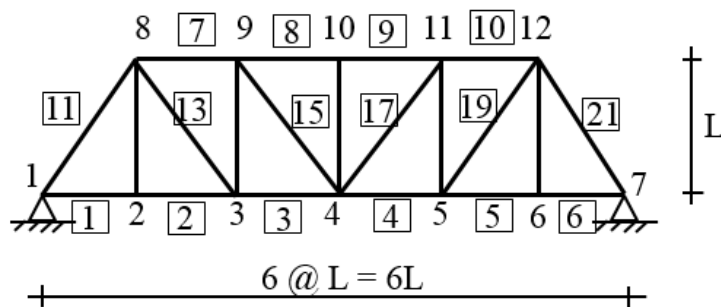


Figure 3.4 The FEM model of the steel truss model

3.3.1.4 Case study 4: A concrete bridge frame

The last case study is a concrete bridge frame as shown in Figure 3.5 consisting of eight nodes and seven elements. The material properties and geometric data are presented in Chapter 6.

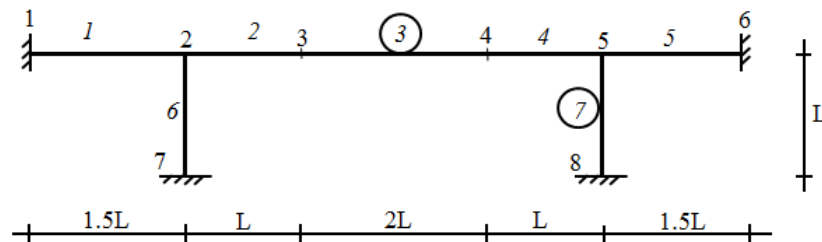


Figure 3.5 The FEM model of the concrete bridge frame

3.3.2 Experimental studies

The laboratory tests are conducted at Banyo Pilot Plant Precinct of the Queensland University of Technology (QUT) and the HKPU to examine the performance of the improved method. Each model is tested at two cases, healthy and damaged. To collect the data, a sensory system is installed at the defined nodes. The model is excited by an impact hammer and the time history data is measured. The natural frequencies and mode shapes are extracted from measured time history data and FRFs (Fu and He, 2001).

Simulation of the damage is performed by either increasing the mass at selected elements or decreasing the cross section of the elements. Similarly, for the

experimental case studies, the performance of the improved method for each model will be evaluated using the couple experimental dataset obtained from the damaged and undamaged cases of each model through a MATLAB code. To accurately acquire the experimental data, each test is repeated several times and averaged to overcome the effect of errors. However, the data are associated with only translational DoFs, since measuring the rotational DoFs, is a difficult and expensive task, although having those DoFs could give a better result and help understand the real behaviour of the structure.

In addition to performing each case twice, damaged and undamaged, the models are also numerically modelled, and all analytical characteristics are derived as the healthy structures. The results will be compared with the experimental ones. The selected models to be studied are as follows.

3.3.2.1 Case study 1: A cantilever beam model

The first experimental model is a cantilever steel beam consisting of eight elements and nine nodes as shown in Figure 3.6. The material properties, geometric data and damage details are presented in Chapter 7.

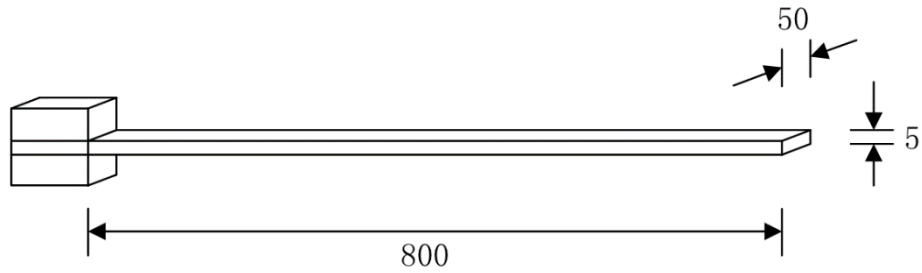


Figure 3.6 The FEM model of the cantilever beam model (dimensions are in mm)

3.3.2.2 Case study 2: A steel simply-support beam

The second experimental case study is a simply-support steel beam consisting of eight elements and nine nodes as shown in Figure 3.7 performing at QUT. The material properties, geometric data and damage details are presented in Chapter 7.

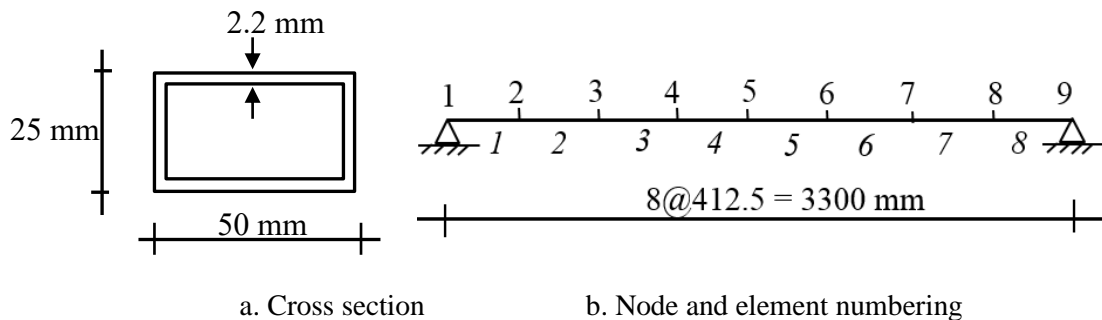


Figure 3.7 The FEM model of the steel simply-support beam

3.3.2.3 Case study 3: A three-story steel frame

The third experimental case study is a three-story steel frame consisting of 15 elements and 14 nodes as shown in Figure 3.8 performing at HKPU. The material properties, geometric data and damage details are presented in Chapter 7.

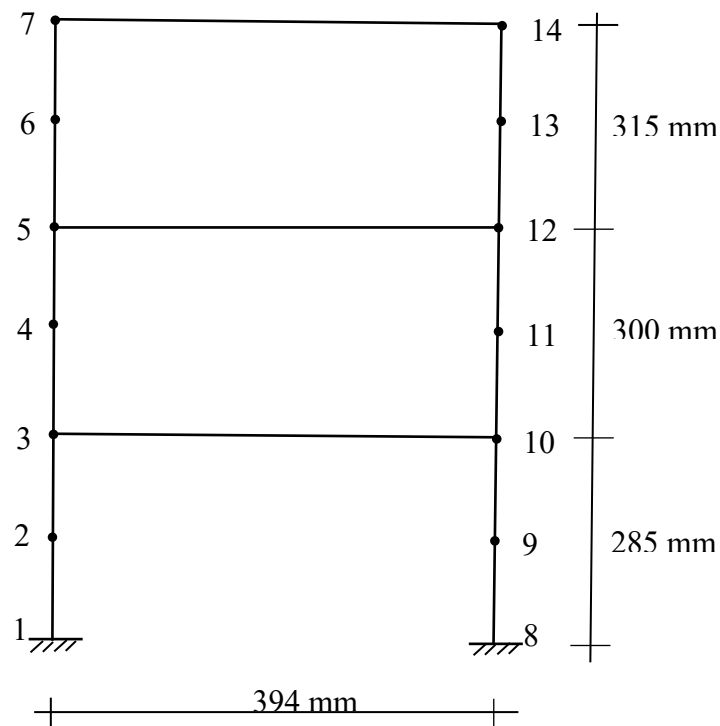


Figure 3.8 The FEM model of the three-story steel frame laboratory model

3.3.3 Applying to a real model and a real bridge

Once the improved method is verified, it is applied to a real structural model and a real bridge to observe its real performance. However, for the real bridge, the available data will be used. Besides, a comparison will be made using the simulation via an FEM model through a MATLAB code and the data given.

3.3.3.1 The Los Alamos National Laboratory 4-DOF three-story structure

The LANL model, which is a three-story frame structure, is used as a real-world structure for applying the improved method as shown in Figure 3.9. The LANL 4-DOF three-story structure is shown in Figure 8.14. The structure consists of aluminium

columns and plates gathered using bolted joints with a rigid Base. There are four columns at each floor located at the corners connected to the aluminium plates. The dimension of column and aluminium plates are $(17.7 \times 2.5 \times 0.6 \text{ cm})$ and $(30.5 \times 30.5 \times 2.5 \text{ cm})$, respectively.

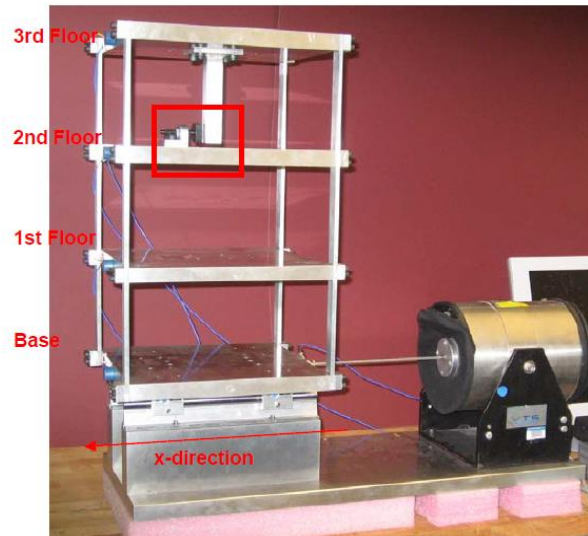


Figure 3.9 The Los Alamos National Laboratory 4-DOF three-story structure

3.3.3.2 I-40 Bridge

The damage identification experiments on I-40 Bridge in New Mexico, USA, has been reported by using data from a series of modal tests of a section of a highway bridge (Farrar *et al.*, 1994, Farrar *et al.*, 2000). Before destruction in 1993, a series of modal tests has been performed on this bridge after closing to traffic. The section of the bridge instrumented for this series of modal tests consisting of three spans with a combined length of about 130 m is shown in Figure 3.10. As a real bridge, the improved MSE

method will be applied to this bridge using available data and compared with the FEM analysis results. The details and results will be presented in Chapter 8.



Figure 3.10 I-40 Bridge, New Mexico, USA

3.4 Conclusion

Because of significance of damage identification in structures especially bridges, the current study focuses on improving an MSE-based damage detection method for BHM. The two-stage method is mathematically established based on the changes in structural modal characteristics affected by occurring damage in the structure. The major contributions of the improved method are improving the MSE change equation and the sensitivity matrix. In the first stage, the location of the damage is identified using the ratio of MSE change in elements of the structure. In the consequent stage, using the sensitivity matrix, the extent of the damage at selected elements among the suspected elements from the first stage is also quantified.

The accuracy and performance of the proposed method is validated via several numerical and experimental studies and lastly, completed by applying to an actual model and a real bridge.

CHAPTER 4

THEORY OF STUDY AND MATHEMATICAL

IMPROVEMENT OF THE MODAL STRAIN ENERGY

METHOD

This chapter elaborates an improved MSE-based damage detection method for bridge damage assessment. First, the theory of MSE study for damage detection is presented in section 4.1. Second, the traditional elemental MSE method and its previous application is described in section 4.2. Section 4.3 demonstrates the comprehensive mathematical improvement of the proposed MSE method by establishing an accurate MSE equation and sensitivity matrix in two consequent stages. Stage one identifies the elemental and nodal damage locations. Accordingly, stage two deals with quantifying those damage extents. Number of mode shapes and natural frequencies required, and effect of noise pollution are also presented. Lastly, section 4.4 draws concluding remarks.

4.1 Theory of study

Researches show, occurring the damage in a structure, regardless of its creating source, results in changing the global dynamic characteristics of the structure such as natural frequencies and mode shapes (Zhou *et al.*, 2002). Theoretically, as these parameters are frequently quantifiable, monitoring their changes over the time is useful to diagnose the damage/s in the structure. For instance, the eigenvectors changes at mode i are as follows.

$$\{\phi_i^d\} = \{\phi_i\} + \{\Delta\phi_i\} \quad (4.1)$$

where $\{\phi_i^d\}$ and $\{\phi_i\}$ are mode shapes of the damaged and undamaged cases at mode i , respectively

However, expanding this perception to real structures requires more deliberations and considerations because of structural complexity and lots of uncertainties associated with time-varying environmental and operational conditions (Kim *et al.*, 2015). For example, significance changes in environment temperature and humidity can similarly affect the structure (Adams and Coppendale, 1976, Salawu, 1997, Purkiss *et al.*, 1994).

The above idea is the basis of VBDD methods. MSE-based methods, as a widely used category of VBDD techniques, in addition of using Eigen parameters, employ the

stiffness of the structure that incorporates the physical properties of the structures into the account, also. According to these methods, the amount of MSE of the healthy structure stored in the j^{th} element at mode i is generally stated as Eq. (4.2).

$$\text{MSE}_{i,j} = \frac{1}{2} \{\phi_i\}^T [K_j] \{\phi_i\} \quad (4.2)$$

where $[K_j]$ is the stiffness of the undamaged case at element j

Using two Eigen datasets of the structure at two subsequent statuses and from changes of the MSE stored in the elements of the structure, the damage in the structure can be recognized through a mathematical procedure. The next sections describe an iterative traditional MSE method and its mathematical improvement, respectively.

4.2 Traditional MSE method

The extent of MSE stored in an element of a structure has been recognized as a reliable index for identifying the structural damage. Shi *et al.* (1998) proposed a structural damage detection method based on MSE change before and after the damage. According to this method, change in structural parameters such as mode shapes, natural frequencies and stiffness are as follows, respectively.

$$\{\phi_i^d\} = \{\phi_i\} + \{\Delta\phi_i\} = \{\phi_i\} + \sum_{r=1}^{md} c_{ir} \{\phi_r\} \quad (4.3)$$

where $c_{ir} = \frac{\{\Phi_r\}^T [\Delta K] \{\Phi_i\}}{\lambda_i - \lambda_r}$ ($i \neq r$),

md is the number of analytical modes, and

$\{\Phi_i^d\}$ and $\{\Phi_i\}$ are mode shapes at mode i of the damaged and undamaged cases, respectively

$$\lambda_i^d = \lambda_i + \Delta\lambda_i \quad (4.4)$$

where λ_i^d and λ_i are eigenvalues (frequencies) at mode i of the damaged and undamaged cases, respectively

Also,

$$[K^d] = [K] + \sum_{m=1}^L [\Delta K_m] = [K] + \sum_{m=1}^L \alpha_m [K_m] \quad (-1 < \alpha_m \leq 0) \quad (4.5)$$

where K^d and K are global stiffness of the structure of damaged and undamaged cases, respectively,

m is element number,

L is number of elements and

α is the damage extent

The extent of MSE stored in the j^{th} element at mode i of the damaged structure is anticipated to be

$$\text{MSE}_{ij}^d = \frac{1}{2} \{\Phi_i^d\}^T [K_j] \{\Phi_i^d\} \quad (4.6)$$

Subtracting Eq. (4.2) from Eq. (4.6), ignoring the coefficient $\frac{1}{2}$ and combining with Eq. (4.3) leads to MSE change at mode i and element j (MSEC_{ij})

$$\text{MSEC}_{ij} = \{\phi_i^d\}^T [K_j] \{\phi_i^d\} - \{\phi_i\}^T [K_j] \{\phi_i\} \quad (4.7)$$

After simplifying

$$\text{MSEC}_{ij} = 2\{\phi_i\}^T [K_j] \left(\sum_{r=1}^n -\frac{\{\phi_r\}^T [\Delta K] \{\phi_i\}}{\lambda_r - \lambda_i} \{\phi_r\} \right) \quad (i \neq r) \quad (4.8)$$

Supposing only one damage happens in member p and substituting Eq. (4.5) into Eq. (4.8) yields

$$\text{MSEC}_{ij} = \sum_{p=1}^L -2\alpha_p \{\phi_i\}^T [K_j] \sum_{r=1}^n \frac{\{\phi_r\}^T [K_p] \{\phi_i\}}{\lambda_r - \lambda_i} \{\phi_r\} \quad (i \neq r) \quad (4.9)$$

To detect the location of damage, one of the following indicators is used.

$$\text{MSECR}_{ij} = \frac{|\text{MSE}_{ij}^d - \text{MSE}_{ij}|}{\text{MSE}_{ij}} \quad (4.10)$$

$$\text{MSECR}_j = \frac{1}{m} \sum_{i=1}^m \frac{\text{MSECR}_{ij}}{\text{MSECR}_{i,\max}} \quad (4.11)$$

where MSECR is the Modal Strain Energy Change Ratio and

MSECR_j is the average of MSECR_{ij} summation for the first m mode shapes normalized with respect to the largest value (MSECR_{i,max}) of each mode

Lastly, after selecting the suspected elements to damage, in order to quantify the damage extent, Eq. (4.9) is expressed in the following form

$$\begin{bmatrix} \text{MSEC}_{i1} \\ \text{MSEC}_{i2} \\ \vdots \\ \text{MSEC}_{ij} \end{bmatrix} = \begin{bmatrix} \beta_{11} & \beta_{12} & \dots & \beta_{1q} \\ \beta_{21} & \beta_{22} & \dots & \beta_{2q} \\ \vdots & \vdots & \ddots & \vdots \\ \beta_{j1} & \beta_{j2} & \dots & \beta_{jq} \end{bmatrix} \begin{bmatrix} \alpha_1 \\ \alpha_2 \\ \vdots \\ \alpha_q \end{bmatrix} \quad (4.12)$$

where $\beta_{Jq} = -2 \sum_{r=1}^n \{\phi_i\}^T [K_J] \frac{\{\phi_r\}^T [K_q] \{\phi_i\}}{\lambda_r - \lambda_i} \phi_r$, ($r \neq i$) and

n is the number of analytical modes

The method can be used to detect the damage at nodes, also. In this case, the damage in the structure is known to be a loss of rotational stiffness at joints. For this purpose, the Eq. (4.5) is converted to

$$[K^d] = [K] + \sum_{j=1}^L [\Delta K_j] = [K] + \sum_{j=1}^L \sum_{l=1}^2 \frac{\partial [K_j]}{\partial [S_l]} [\Delta S_l] \quad [\Delta S_l] = \alpha_l S \quad (4.13)$$

where ΔS_l is change in rotational stiffness at the l th joint,

$\frac{\partial [K_j]}{\partial [S_l]}$ is sensitivity of the j th elemental stiffness matrix with respect to a change

in the rotational stiffness in the l th joint and

α_l is fractional change in the l th rotational stiffness

Similarly, to quantifying the damage at nodes, a new β_{st} can be obtained by substituting β_{st} from Eq. (4.13) into Eq. (4.8)

$$\beta_{st} = -2S \sum_{r=1}^n \{\Phi_i\}^T [K_s] \frac{\{\Phi_r\}^T \frac{\partial [K_t]}{\partial [S_k]} \{\Phi_i\}}{\lambda_r - \lambda_i} \Phi_r, \quad (r \neq i) \quad (4.14)$$

4.2.1 Direct Modal Strain Energy Correlation

Wang *et al.* (2012) used the previous MSEC index and improved an MSE correlation method called direct modal strain energy correlation (DMSEC). The MSE change of element j at mode k subjected to a known damage case theoretically is

$$\delta \text{MSE}_j^{(k)} = \{\Phi_k^0\}^T [K_j^0] \{\Phi_k^0\} - \{\Phi_k^d\}^T [K_j^0] \{\Phi_k^d\} \quad (4.15)$$

The MSE change matrices from theory and measurement for a structure are as follows, respectively.

$$[\delta \text{MSE}] = \begin{bmatrix} \delta \text{MSE}_1^{(1)} & \delta \text{MSE}_2^{(1)} & \dots & \delta \text{MSE}_N^{(1)} \\ \delta \text{MSE}_1^{(2)} & \delta \text{MSE}_2^{(2)} & \dots & \delta \text{MSE}_N^{(2)} \\ \vdots & \vdots & \ddots & \vdots \\ \delta \text{MSE}_1^{(\text{md})} & \delta \text{MSE}_2^{(\text{md})} & \dots & \delta \text{MSE}_N^{(\text{md})} \end{bmatrix} \quad (4.16)$$

and

$$[\Delta \text{MSE}] = \begin{bmatrix} \Delta \text{MSE}_1^{(1)} & \Delta \text{MSE}_2^{(1)} & \dots & \Delta \text{MSE}_N^{(1)} \\ \Delta \text{MSE}_1^{(2)} & \Delta \text{MSE}_2^{(2)} & \dots & \Delta \text{MSE}_N^{(2)} \\ \vdots & \vdots & \ddots & \vdots \\ \Delta \text{MSE}_1^{(\text{md})} & \Delta \text{MSE}_2^{(\text{md})} & \dots & \Delta \text{MSE}_N^{(\text{md})} \end{bmatrix} \quad (4.17)$$

where N is the number of elements and

md is the number of mode shapes

The $vec\{\delta MSE\}$ and $vec\{\Delta MSE\}$ are row-condensed vectors to facilitate the optimization process as follows.

$$\begin{aligned}
 &vec\{\delta MSE\} \\
 &= \left[\sum_{r=1}^{md} \omega_r \{\delta MSE_1^{(r)}\} \quad \sum_{r=1}^{md} \omega_r \{\delta MSE_2^{(r)}\} \quad \cdots \quad \sum_{r=1}^{md} \omega_r \{\delta MSE_N^{(r)}\} \right] \quad (4.18)
 \end{aligned}$$

$$\begin{aligned}
 &vec\{\Delta MSE\} \\
 &= \left[\sum_{r=1}^{md} \omega_r \{\Delta MSE_1^{(r)}\} \quad \sum_{r=1}^{md} \omega_r \{\Delta MSE_2^{(r)}\} \quad \cdots \quad \sum_{r=1}^{md} \omega_r \{\Delta MSE_N^{(r)}\} \right] \quad (4.19)
 \end{aligned}$$

Finally, the optimization objective function used for DMSEC was proposed as

$$\begin{aligned}
 &DMSEC \\
 &= \frac{\left| \{vec\{\Delta MSE\}\}^T \{vec\{\delta MSE\}\} \right|^2}{\left(\{vec\{\Delta MSE\}\}^T \{vec\{\Delta MSE\}\} \right) \left(\{vec\{\delta MSE\}\}^T \{vec\{\delta MSE\}\} \right)} \quad (4.20)
 \end{aligned}$$

4.3 The improved MSE method

In this section, the previous study performed by (Shi *et al.*, 2000) is mathematically improved to increase the sensitivity to damage and accuracy of damage detection, reduce the computational cycle and iteration efforts (Moradipour *et al.*, 2015, Moradipour *et al.*, 2013).

In this method, the extent of elemental or nodal damage is expressed as a fractional reduction of the elemental or rotational stiffness matrix. The current study mainly employs the structural damaged stiffness matrix to establish a more accurate MSE change equation and sensitivity matrix. However, the final equations are transformed to be in terms of undamaged stiffness matrix, which is a known variable.

4.3.1 Improved modal strain energy change

Initially, it is aimed to find an accurate MSE equation and consequently a more precise sensitivity matrix. Assuming element m is damaged with damage extent of α_m , the local stiffness of element m after damage is

$$[K_m^d] = [K_m] + [\Delta K_m] = [K_m] + \alpha_m [K_m] \quad (-1 < \alpha_m \leq 0) \quad (4.21)$$

where $[K_m^d]$ and $[K_m]$ are stiffness matrices of damaged and undamaged cases of element m , respectively and

α_m is the fractional reduction coefficient of m th elemental stiffness matrix

Assuming a structure with L elements that all of them are damaged, extending the Eq. (4.13) for all elements and globally integrating for the entire structure leads to

$$\sum_{m=1}^L [K_m^d] = \sum_{m=1}^L [K_m] + \sum_{m=1}^L [\Delta K_m] = \sum_{m=1}^L [K_m] + \sum_{m=1}^L \alpha_m [K_m] \quad (4.22)$$

Simplifying yields

$$[K^d] = [K] + [\Delta K] = [K] + \sum_{m=1}^L [\Delta K_m] = [K] + \sum_{m=1}^L \alpha_m [K_m] \quad (4.23)$$

where K^d and K are global stiffness of the structure of damaged and undamaged cases, respectively

The MSE stored in the j th element at mode i after damage is

$$\text{MSE}_{i,j}^d = \frac{1}{2} \{\phi_i^d\}^T [K_j^d] \{\phi_i^d\} \quad (4.24)$$

Subtracting Eq. (4.2) from Eq. (4.24) gives the change in MSE

$$\begin{aligned} \Delta \text{MSE}_{ij}^{\text{imp}} &= \text{MSEC}_{ij}^{\text{imp}} = \text{MSE}_{i,j}^d - \text{MSE}_{i,j} \\ &= \frac{1}{2} \{\phi_i^d\}^T [K_j^d] \{\phi_i^d\} - \frac{1}{2} \{\phi_i\}^T [K_j] \{\phi_i\} \end{aligned} \quad (4.25)$$

where “imp” stands for the improved method

Substituting for $\{\phi_i^d\}$ and $[K_j^d]$ in Eq. (4.25) from Eqs. (4.3) and (4.13), respectively.

$$\begin{aligned} \Delta \text{MSE}_{ij}^{\text{imp}} &= \frac{1}{2} \{\phi_i + \Delta \phi_i\}^T ([K_j] + \alpha_j [K_j]) \{\phi_i + \Delta \phi_i\} \\ &\quad - \frac{1}{2} \{\phi_i\}^T [K_j] \{\phi_i\} \end{aligned} \quad (4.26)$$

Simplifying and neglecting the higher order terms leads to

$$\begin{aligned} \Delta \text{MSE}_{ij}^{\text{imp}} &= \frac{1}{2} \alpha_j \{\phi_i\}^T [K_j] \{\phi_i\} \\ &\quad + \frac{1}{2} (1 + \alpha_j) [\{\phi_i\}^T [K_j] \{\Delta \phi_i\} + \{\Delta \phi_i\}^T [K_j] \{\phi_i\}] \end{aligned} \quad (4.27)$$

Substituting for $\{\Delta\phi_i\}$ from Eq. (4.3) into Eq. (4.27) yields

$$\begin{aligned} \Delta\text{MSE}_{ij}^{\text{imp}} &= \frac{1}{2}\alpha_j\{\phi_i\}^T[K_j]\{\phi_i\} + \frac{1}{2}\left(1 + \right. \\ &\alpha_j\left.\left(\{\phi_i\}^T[K_j]\sum_{r=1}^{\text{md}}\frac{\{\phi_r\}^T[\Delta K]\{\phi_i\}}{\lambda_i-\lambda_r}\{\phi_r\} + \right. \right. \\ &\left.\left.\sum_{r=1}^{\text{md}}\frac{\{\phi_r\}^T[\Delta K]\{\phi_i\}}{\lambda_i-\lambda_r}\{\phi_r\}^T[K_j]\{\phi_i\}\right)\right) \quad (i \neq r) \end{aligned} \quad (4.28)$$

where i generally is in the range of 1 to 5 and

r is the number of analytical modes under consideration ($r \leq \text{no. of DOFs}$)

Simplifying

$$\begin{aligned} \Delta\text{MSE}_{ij}^{\text{imp}} &= \frac{1}{2}\alpha_j\{\phi_i\}^T[K_j]\{\phi_i\} + \\ &\frac{1}{2}\{\phi_i\}^T[K_j]\sum_{r=1}^{\text{md}}\frac{\{\phi_r\}^T[\Delta K]\{\phi_i\}}{\lambda_i-\lambda_r}\{\phi_r\} + \\ &\frac{1}{2}\sum_{r=1}^{\text{md}}\frac{\{\phi_r\}^T[\Delta K]\{\phi_i\}}{\lambda_i-\lambda_r}\{\phi_r\}^T[K_j]\{\phi_i\} + \\ &\frac{1}{2}\alpha_j\left(\{\phi_i\}^T[K_j]\sum_{r=1}^{\text{md}}\frac{\{\phi_r\}^T[\Delta K]\{\phi_i\}}{\lambda_i-\lambda_r}\{\phi_r\} + \right. \\ &\left.\sum_{r=1}^{\text{md}}\frac{\{\phi_r\}^T[\Delta K]\{\phi_i\}}{\lambda_i-\lambda_r}\{\phi_r\}^T[K_j]\{\phi_i\}\right) \quad (i \neq r) \end{aligned} \quad (4.29)$$

Substituting for $[\Delta K]$ from Eq. (4.5) into Eq. (4.29) ($[\Delta K] = \sum_{k=1}^p \alpha_k [K_k]$) and simplifying

$$\begin{aligned} \Delta\text{MSE}_{ij}^{\text{imp}} &= \frac{1}{2}\alpha_j\{\phi_i\}^T[K_j]\{\phi_i\} + \\ &\frac{1}{2}\{\phi_i\}^T[K_j]\sum_{k=1}^p \alpha_k \sum_{r=1}^{\text{md}}\frac{\{\phi_r\}^T[K_k]\{\phi_i\}}{\lambda_i-\lambda_r}\{\phi_r\} + \\ &\frac{1}{2}\sum_{k=1}^p \alpha_k \sum_{r=1}^{\text{md}}\frac{\{\phi_r\}^T[K_k]\{\phi_i\}}{\lambda_i-\lambda_r}\{\phi_r\}^T[K_j]\{\phi_i\} + \end{aligned} \quad (4.30)$$

$$\frac{1}{2} \alpha_j \left(\{\phi_i\}^T [K_j] \sum_{k=1}^p \alpha_k \sum_{r=1}^{md} \frac{\{\phi_r\}^T [K_k] \{\phi_i\}}{\lambda_i - \lambda_r} \{\phi_r\} + \sum_{k=1}^p \alpha_k \sum_{r=1}^{md} \frac{\{\phi_r\}^T [K_k] \{\phi_i\}}{\lambda_i - \lambda_r} \{\phi_r\}^T [K_j] \{\phi_i\} \right) \quad (i \neq r)$$

where p is the number of damaged elements of the system

Ignoring the higher order terms leads to the equation of change in the MSE of element j at mode i as follows.

$$\begin{aligned} \Delta \text{MSE}_{ij}^{\text{imp}} &= \frac{1}{2} \alpha_j \{\phi_i\}^T [K_j] \{\phi_i\} \\ &+ \frac{1}{2} \{\phi_i\}^T [K_j] \sum_{k=1}^p \alpha_k \sum_{r=1}^{md} \frac{\{\phi_r\}^T [K_k] \{\phi_i\}}{\lambda_i - \lambda_r} \{\phi_r\} \\ &+ \frac{1}{2} \sum_{k=1}^p \alpha_k \sum_{r=1}^{md} \frac{\{\phi_r\}^T [K_k] \{\phi_i\}}{\lambda_i - \lambda_r} \{\phi_r\}^T [K_j] \{\phi_i\} \end{aligned} \quad (4.31)$$

($i \neq r$)

4.3.2 Improved sensitivity matrix

Partial differentiating Eq. (4.31) with respect to α results in sensitivity matrix at mode i and element j as follow,

$$\begin{aligned} \frac{\partial \text{MSE}_{ij}^{\text{imp}}}{\partial \alpha} &= \frac{1}{2} \{\phi_i\}^T [K_j] \{\phi_i\} \\ &+ \frac{1}{2} \sum_{k=1}^p \sum_{r=1}^n \{\phi_i\}^T [K_j] \frac{\{\phi_r\}^T [K_k] \{\phi_i\}}{\lambda_i - \lambda_r} \{\phi_r\} \\ &+ \frac{1}{2} \sum_{k=1}^p \sum_{r=1}^n \frac{\{\phi_r\}^T [K_k] \{\phi_i\}}{\lambda_i - \lambda_r} \{\phi_r\}^T [K_j] \{\phi_i\} \quad (i \neq r) \end{aligned} \quad (4.32)$$

For a single damage, p equals 1. Therefore, Eq. (4.32) is converted to

$$\begin{aligned} \frac{\partial MSE_{ij}^{imp}}{\partial \alpha} = & \frac{1}{2} \{\Phi_i\}^T [K_j] \{\Phi_i\} + \frac{1}{2} \sum_{r=1}^n \{\Phi_i\}^T [K_j] \frac{\{\Phi_r\}^T [K_k] \{\Phi_i\}}{\lambda_i - \lambda_r} \{\Phi_r\} \\ & + \frac{1}{2} \sum_{r=1}^n \frac{\{\Phi_r\}^T [K_k] \{\Phi_i\}}{\lambda_i - \lambda_r} \{\Phi_r\}^T [K_j] \{\Phi_i\} \quad (i \neq r) \end{aligned} \quad (4.33)$$

where $K_k=K_j$

The sensitivity matrix can also be formed for m modes and N elements as the following expanded form or matrix notation.

$$S^{MSE} = \frac{\partial MSE}{\partial \alpha_N} = \begin{bmatrix} \frac{\partial MSE_1}{\partial \alpha_1} & \frac{\partial MSE_1}{\partial \alpha_2} & \dots & \frac{\partial MSE_1}{\partial \alpha_N} \\ \frac{\partial MSE_2}{\partial \alpha_1} & \frac{\partial MSE_2}{\partial \alpha_2} & \dots & \frac{\partial MSE_2}{\partial \alpha_N} \\ \vdots & \vdots & \dots & \vdots \\ \frac{\partial MSE_m}{\partial \alpha_1} & \frac{\partial MSE_m}{\partial \alpha_2} & \dots & \frac{\partial MSE_m}{\partial \alpha_N} \end{bmatrix} \quad (4.34)$$

where m is the number of modes under consideration and

MSE_m is the MSE of the system at mode m

N is the number of desired elements

The recent equations of sensitivity matrix, Eqs. (4.32) and (4.34) are used in the next sections for locating and quantifying the damage in the structure.

4.3.3 Locating the damage

The first stage of this method is to detect the location of damage/s in the structure. For this purpose, the amount of the damage location indicator named MSECR is plotted for all elements. Then elements with a higher value of MSECR are selected as the

suspect elements to damage to be further investigated in the second stage. Therefore, the locations of damage/s is a set of elements that acquire the highest amounts of MSECR.

MSECR can be either calculated for a specific single mode as given in Eq. (4.10) or normalized for several modes as set in Eq. (4.11). Hence, to locate the damage, any of Eqs. (4.10) or (4.11) can be separately used for calculating the MSECR indicator. However, in any of these equations, the MSECR or Δ MSE is upgraded to Δ MSE from Eq. (4.30) in the improved method which is very accurate and closer to the actual MSE stored in the elements of the system.

In case of using Eq. (4.10) any of the first five modes can be used i.e. $i =$ any of 1 to 5. Though, the number of modes of damaged structure selected should be necessarily associated with that of an undamaged one. However, using the Eq. (4.11) which mostly gives better results, requires a set of favourite modes, usually the first five modes or more of both damaged and undamaged structures i.e. $i = 5$.

4.3.4 Quantifying the damage

4.3.4.1 Quantifying the elemental damage

The second stage of the improved method is to quantify the damage. Damage quantifying process is conducted among the suspect elements that have primarily been selected in the first stage. In this procedure, the amount of α 's as the extent of damages

of suspect elements are iteratively calculated. Lastly, the amounts of α 's for true damaged elements converge to their real damage percentage while for other suspect elements converge to zero. However, depending on complexity of the structure, number of suspect elements and number of modes under consideration, the exact amount of each set of α 's may be obtained through several iterations. The improved procedure is as follows.

From Eq. (4.34) ignoring coefficient $\frac{1}{2}$, it can be derived.

$$[\beta]\{\alpha\} = \{\text{MSEC}^{\text{imp}}\} \quad (4.35)$$

where MSEC^{imp} is obtained from change between damage and undamaged cases from Eq. (4.25) and β is

$$\begin{aligned} \beta_{k,s} = \frac{\partial \text{MSE}}{\partial \alpha} = & \{\phi_i\}^T [K_s] \{\phi_i\} + \sum_{r=1}^n \{\phi_i\}^T [K_s] \frac{\{\phi_r\}^T [K_k] \{\phi_i\}}{\lambda_i - \lambda_r} \{\phi_r\} \\ & + \sum_{r=1}^n \frac{\{\phi_r\}^T [K_k] \{\phi_i\}}{\lambda_i - \lambda_r} \{\phi_r\}^T [K_s] \{\phi_i\} \quad (i \neq r) \end{aligned} \quad (4.36)$$

where s is a selected element for computation of the MSEC and

k is a suspect damaged element

Substituting for K_j^d from Eq. (4.23) into Eq. (4.25), simplifying and then arranging

$$\text{MSEC}_{ij}^{\text{imp}} = \alpha_j \{\phi_i\}^T [K_j] \{\phi_i\} + \{\phi_i^d\}^T [K_j] \{\phi_i^d\} - \{\phi_i\}^T [K_j] \{\phi_i\} \quad (4.37)$$

Combining Eq. (4.7) and Eq. (4.37) gives

$$\overline{\text{MSEC}}_{ij}^{\text{imp}} = \alpha_j \{\phi_i\}^T [K_j] \{\phi_i\} + \text{MSEC}_{ij} \quad (4.38)$$

Substituting Eqs. (4.36) and (4.38) into Eq. (4.35)

$$\begin{aligned} & \left[\{\phi_i\}^T [K_s] \{\phi_i\} + \sum_{r=1}^n \{\phi_i\}^T [K_s] \frac{\{\phi_r\}^T [K_k] \{\phi_i\}}{\lambda_i - \lambda_r} \{\phi_r\} + \right. \\ & \left. \sum_{r=1}^n \frac{\{\phi_r\}^T [K_k] \{\phi_i\}}{\lambda_i - \lambda_r} \{\phi_r\}^T [K_s] \{\phi_i\} \right] \{\alpha\} = \alpha_s \{\phi_i\}^T [K_s] \{\phi_i\} + \{\text{MSEC}\} \quad (4.39) \\ & (i \neq r) \end{aligned}$$

Simplifying

$$\begin{aligned} & \left[-\{\phi_i^d\}^T [K_s] \{\phi_i^d\} + \{\phi_i\}^T [K_s] \{\phi_i\} + \right. \\ & \left. \sum_{r=1}^n \{\phi_i\}^T [K_s] \frac{\{\phi_r\}^T [K_k] \{\phi_i\}}{\lambda_i - \lambda_r} \{\phi_r\} + \sum_{r=1}^n \frac{\{\phi_r\}^T [K_k] \{\phi_i\}}{\lambda_i - \lambda_r} \{\phi_r\}^T [K_s] \{\phi_i\} \right] \{\alpha\} = \quad (4.40) \\ & \{\text{MSEC}\} \quad (i \neq r) \end{aligned}$$

Combining Eq. (4.7) and Eq. (4.40)

$$\begin{aligned} & \left[-\{\text{MSEC}\} + \sum_{r=1}^n \{\phi_i\}^T [K_s] \frac{\{\phi_r\}^T [K_k] \{\phi_i\}}{\lambda_i - \lambda_r} \{\phi_r\} \right. \\ & \left. + \sum_{r=1}^n \frac{\{\phi_r\}^T [K_k] \{\phi_i\}}{\lambda_i - \lambda_r} \{\phi_r\}^T [K_s] \{\phi_i\} \right] \{\alpha\} \quad (4.41) \\ & = \{\text{MSEC}\} \quad (i \neq r) \end{aligned}$$

Denoting $\beta_{k,s}^* = -\text{MSEC}_{ij}$ and $\beta'_{k,s} = \sum_{r=1}^n \{\phi_i\}^T [K_s] \frac{\{\phi_r\}^T [K_k] \{\phi_i\}}{\lambda_i - \lambda_r} \{\phi_r\} +$

$\{\phi_r\}^T [K_s] \{\phi_i\}$, then, $\beta_{k,s}$ can be written in the following form

$$\beta_{k,s} = \beta_{k,s}^* + \beta'_{k,s} \quad (4.42)$$

Reconstructing Eq. (4.35) in matrix notation,

$$([\beta^*] + [\beta'])\{\alpha\} = \{\text{MSEC}\} \quad (4.43)$$

or

$$\left(\begin{bmatrix} \beta_{11}^* & 0 & \dots & 0 \\ 0 & \beta_{22}^* & \dots & 0 \\ \vdots & \vdots & \ddots & \vdots \\ 0 & 0 & \dots & \beta_{qq}^* \end{bmatrix} + \begin{bmatrix} \beta'_{11} & \beta'_{12} & \dots & \beta'_{1q} \\ \beta'_{21} & \beta'_{22} & \dots & \beta'_{2q} \\ \vdots & \vdots & \ddots & \vdots \\ \beta'_{q1} & \beta'_{q2} & \dots & \beta'_{qq} \end{bmatrix} \right) \begin{bmatrix} \alpha_1 \\ \alpha_2 \\ \vdots \\ \alpha_q \end{bmatrix} = \begin{bmatrix} \text{MSEC}_{i1} \\ \text{MSEC}_{i2} \\ \vdots \\ \text{MSEC}_{iq} \end{bmatrix} \quad (4.44)$$

where q is the number of selected suspected elements

$[\beta^*]$ which is a diagonal matrix is proposed in this study in order to increase the accuracy of $\{\alpha\}$'s. Each array of $[\beta^*]$ is a function of MSEC of the associated element in a specific mode. MSEC is in terms of undamaged stiffness of the structure that can easily be achieved. Finally, from Eq. (4.44), $\{\alpha\}$'s are obtained in expanding form as

$$\begin{bmatrix} \alpha_1 \\ \alpha_2 \\ \vdots \\ \alpha_q \end{bmatrix} = \left(\begin{bmatrix} \beta_{11}^* & 0 & \dots & 0 \\ 0 & \beta_{22}^* & \dots & 0 \\ \vdots & \vdots & \ddots & \vdots \\ 0 & 0 & \dots & \beta_{qq}^* \end{bmatrix} + \begin{bmatrix} \beta'_{11} & \beta'_{12} & \dots & \beta'_{1q} \\ \beta'_{21} & \beta'_{22} & \dots & \beta'_{2q} \\ \vdots & \vdots & \ddots & \vdots \\ \beta'_{q1} & \beta'_{q2} & \dots & \beta'_{qq} \end{bmatrix} \right)^{-1} \begin{bmatrix} \text{MSEC}_{i1} \\ \text{MSEC}_{i2} \\ \vdots \\ \text{MSEC}_{iq} \end{bmatrix} \quad (4.45)$$

Accordingly, to calculate the alpha coefficients, using Eq. (4.45), two sets of mode shapes and natural frequencies of damaged and undamaged structure are required. From Eq. (4.41), the number of mode shapes required from undamaged case is r which can be less than or upmost equal the number of DOFs of the structure under consideration ($r \leq \text{no. of DOFs}$). In numerical models, the number of undamaged modes can be coincided to the analytical mode shapes. However, the process of damage quantifying can be stopped when it converges that may occur at a mode number much lower than the nominated number of DOFs. Whereas, from damaged case, only one mode is adequate, where, the number of required modes is i that equals any of modes from 1 to 5. Since mode one or three normally gives a better result (because of lower natural frequency) as demonstrated by Shi *et al.* (1998), thus $i=1$ or 3.

4.3.4 Quantifying the nodal damage

Similarly, substituting Eq. (4.13) into Eq. (4.9)

$$\text{MSEC}_{ij} = -2\{\phi_i\}^T [K_j] \sum_{r=1}^n \sum_{k=1}^p \sum_{l=1}^2 \frac{\{\phi_r\}^T \frac{\partial [K_k]}{\partial [S_l]} [\Delta S_l] \{\phi_i\}}{\lambda_r - \lambda_i} \{\phi_r\} \quad (4.46)$$

(i ≠ r)

where p is the number of damaged elements of the system

Substituting for $[\Delta S_l] = \alpha_l S$ from Eq. (4.13)

$$\text{MSEC}_{ij} = -2\{\phi_i\}^T [K_j] \sum_{r=1}^n \sum_{k=1}^p \sum_{l=1}^2 \alpha_l S \frac{\{\phi_r\}^T \frac{\partial [K_k]}{\partial [S_l]} \{\phi_i\}}{\lambda_r - \lambda_i} \{\phi_r\} \quad (4.47)$$

(i ≠ r)

However, in the improved method, firstly to derive the MSE change at node n , rewrite

Eq. (4.29), ignoring coefficient $\frac{1}{2}$ and the last two terms.

$$\begin{aligned} \Delta \text{MSE}_{ij}^{\text{imp}} &= \{\phi_i\}^T [\Delta K_j] \{\phi_i\} + \{\phi_i\}^T [K_j] \sum_{r=1}^{\text{md}} \frac{\{\phi_r\}^T [\Delta K] \{\phi_i\}}{\lambda_i - \lambda_r} \{\phi_r\} \\ &+ \sum_{r=1}^{\text{md}} \frac{\{\phi_r\}^T [\Delta K] \{\phi_i\}}{\lambda_i - \lambda_r} \{\phi_r\}^T [K_j] \{\phi_i\} \quad (i \neq r) \end{aligned} \quad (4.48)$$

Substituting for $[\Delta K]$ from Eq. (4.13) into Eq. (4.48) ($[\Delta K] = \sum_{k=1}^p \alpha_k [K_k]$) and

simplifying

$$\begin{aligned}
\Delta \text{MSE}_{ij}^{\text{imp}} &= \sum_{l=1}^2 \{\Phi_i\}^T \frac{\partial [K_j]}{\partial [S_l]} [\Delta S_l] \{\Phi_i\} \\
&+ \{\Phi_i\}^T [K_j] \sum_{r=1}^n \sum_{k=1}^p \sum_{l=1}^2 \frac{\{\Phi_r\}^T \frac{\partial [K_k]}{\partial [S_l]} [\Delta S_l] \{\Phi_i\}}{\lambda_r - \lambda_i} \{\Phi_r\} \\
&+ \sum_{r=1}^n \sum_{k=1}^p \sum_{l=1}^2 \frac{\{\Phi_r\}^T \frac{\partial [K_k]}{\partial [S_l]} [\Delta S_l] \{\Phi_i\}}{\lambda_r - \lambda_i} \{\Phi_r\}^T [K_j] \{\Phi_i\} \\
&\quad (i \neq r)
\end{aligned} \tag{4.49}$$

where p is the number of damaged elements of the system

Substituting for $[\Delta S_l] = \alpha_l S$ from Eq. (4.13) into Eq. (4.49)

$$\begin{aligned}
\Delta \text{MSE}_{ij}^{\text{imp}} &= \sum_{l=1}^2 \{\Phi_i\}^T \frac{\partial [K_j]}{\partial [S_l]} \alpha_l [S_j] \{\Phi_i\} \\
&+ \{\Phi_i\}^T [K_j] \sum_{r=1}^n \sum_{k=1}^p \sum_{l=1}^2 \alpha_l [S_k] \frac{\{\Phi_r\}^T \frac{\partial [K_k]}{\partial [S_l]} \{\Phi_i\}}{\lambda_r - \lambda_i} \{\Phi_r\} \\
&+ \sum_{r=1}^n \sum_{k=1}^p \sum_{l=1}^2 \alpha_l [S_k] \frac{\{\Phi_r\}^T \frac{\partial [K_k]}{\partial [S_l]} \{\Phi_i\}}{\lambda_r - \lambda_i} \{\Phi_r\}^T [K_j] \{\Phi_i\} \\
&\quad (i \neq r)
\end{aligned} \tag{4.50}$$

where S_k is the rotational stiffness of the k th element

At node n , Eq. (4.50) becomes

$$\begin{aligned}
\Delta \text{MSE}_{ij}^{\text{imp}} &= \{\Phi_i\}^T \frac{\partial [K_j]}{\partial [S_j]} \alpha_n [S_j] \{\Phi_i\} \\
&+ \{\Phi_i\}^T [K_j] \sum_{r=1}^n \sum_{k=1}^p \alpha_n [S_k] \frac{\{\Phi_r\}^T \frac{\partial [K_k]}{\partial [S_l]} \{\Phi_i\}}{\lambda_r - \lambda_i} \{\Phi_r\} \\
&+ \sum_{r=1}^n \sum_{k=1}^p \alpha_n [S_k] \frac{\{\Phi_r\}^T \frac{\partial [K_k]}{\partial [S_l]} \{\Phi_i\}}{\lambda_r - \lambda_i} \{\Phi_r\}^T [K_j] \{\Phi_i\} \\
&\quad (i \neq r)
\end{aligned} \tag{4.51}$$

Then, to quantify the damage at node n , rewrite Eq. (4.37) and combine with Eq. (4.13)

$$\text{MSEC}_{ij}^{\text{imp}} = \{\Phi_i^d\}^T \frac{\partial [K_j]}{\partial [S_j]} \alpha_n [S_j] \{\Phi_i^d\} + \{\Phi_i^d\}^T [K_j] \{\Phi_i^d\} - \{\Phi_i\}^T [K_j] \{\Phi_i\} \tag{4.52}$$

Combining Eq. (4.7) and Eq. (4.52) gives

$$\text{MSEC}_{ij}^{\text{imp}} = \{\Phi_i^d\}^T \frac{\partial [K_j]}{\partial [S_j]} \alpha_n [S_j] \{\Phi_i^d\} + \text{MSEC}_{ij} \tag{4.53}$$

Substituting Eq. (4.51) into Eq. (4.53)

$$\begin{aligned}
&\left(\{\Phi_i\}^T \frac{\partial [K_j]}{\partial [S_j]} [S_j] \{\Phi_i\} + \{\Phi_i\}^T [K_j] \sum_{r=1}^n \sum_{k=1}^p [S_k] \frac{\{\Phi_r\}^T \frac{\partial [K_k]}{\partial [S_l]} \{\Phi_i\}}{\lambda_r - \lambda_i} \{\Phi_r\} \right. \\
&\quad \left. + \sum_{r=1}^n \sum_{k=1}^p [S_k] \frac{\{\Phi_r\}^T \frac{\partial [K_k]}{\partial [S_l]} \{\Phi_i\}}{\lambda_r - \lambda_i} \{\Phi_r\}^T [K_j] \{\Phi_i\} \right) \{\alpha\} \\
&= \{\Phi_i^d\}^T \frac{\partial [K_j]}{\partial [S_j]} \alpha_n [S_j] \{\Phi_i^d\} + \text{MSEC}_{ij}
\end{aligned} \tag{4.54}$$

(i ≠ r)

Simplifying

$$\begin{aligned} & \left(-\{\Phi_i^d\}^T \frac{\partial[K_j]}{\partial[S_j]} [S_j] \{\Phi_i^d\} + \{\Phi_i\}^T \frac{\partial[K_j]}{\partial[S_j]} [S_j] \{\Phi_i\} \right. \\ & \quad + \{\Phi_i\}^T [K_j] \sum_{r=1}^n \sum_{k=1}^p [S_k] \frac{\{\Phi_r\}^T \frac{\partial[K_k]}{\partial[S_l]} \{\Phi_i\}}{\lambda_r - \lambda_i} \{\Phi_r\} \\ & \quad \left. + \sum_{r=1}^n \sum_{k=1}^p [S_k] \frac{\{\Phi_r\}^T \frac{\partial[K_k]}{\partial[S_l]} \{\Phi_i\}}{\lambda_r - \lambda_i} \{\Phi_r\}^T [K_j] \{\Phi_i\} \right) \{\alpha\} \\ & = \text{MSEC}_{ij} \end{aligned} \tag{4.55}$$

(i ≠ r)

Combining Eq. (4.7) into Eq. (4.55)

$$\begin{aligned} & \left(-[\text{MSEC}] + \{\Phi_i\}^T [K_j] \sum_{r=1}^n \sum_{k=1}^p [S_k] \frac{\{\Phi_r\}^T \frac{\partial[K_k]}{\partial[S_l]} \{\Phi_i\}}{\lambda_r - \lambda_i} \{\Phi_r\} \right. \\ & \quad \left. + \sum_{r=1}^n \sum_{k=1}^p [S_k] \frac{\{\Phi_r\}^T \frac{\partial[K_k]}{\partial[S_l]} \{\Phi_i\}}{\lambda_r - \lambda_i} \{\Phi_r\}^T [K_j] \{\Phi_i\} \right) \{\alpha\} \\ & = \{\text{MSEC}\} \end{aligned} \tag{4.56}$$

(i ≠ r)

Denoting $\beta_{k,s}^* = -\text{MSEC}_{ij}$ and

$$\beta'_{k,s} = \{\phi_i\}^T [K_j] \sum_{r=1}^n \sum_{k=1}^p [S_k] \frac{\{\phi_r\}^T \frac{\partial [K_k]}{\partial [S_l]} \{\phi_i\}}{\lambda_r - \lambda_i} \{\phi_r\} \\ + \sum_{r=1}^n \sum_{k=1}^p [S_k] \frac{\{\phi_r\}^T \frac{\partial [K_k]}{\partial [S_l]} \{\phi_i\}}{\lambda_r - \lambda_i} \{\phi_r\}^T [K_j] \{\phi_i\}$$

Then, $\beta_{k,s}$ can be written in the following form

$$\beta_{k,s} = \beta_{k,s}^* + \beta'_{k,s} \quad (4.57)$$

Reconstructing Eq. (4.58) in matrix notation,

$$([\beta^*] + [\beta'])\{\alpha\} = \{\text{MSEC}\} \quad (4.58)$$

or

$$\left(\begin{bmatrix} \beta_{11}^* & 0 & \dots & 0 \\ 0 & \beta_{22}^* & \dots & 0 \\ \vdots & \vdots & \ddots & \vdots \\ 0 & 0 & \dots & \beta_{qq}^* \end{bmatrix} + \begin{bmatrix} \beta'_{11} & \beta'_{12} & \dots & \beta'_{1q} \\ \beta'_{21} & \beta'_{22} & \dots & \beta'_{2q} \\ \vdots & \vdots & \ddots & \vdots \\ \beta'_{q1} & \beta'_{q2} & \dots & \beta'_{qq} \end{bmatrix} \right) \begin{bmatrix} \alpha_1 \\ \alpha_2 \\ \vdots \\ \alpha_q \end{bmatrix} = \begin{bmatrix} \text{MSEC}_{i1} \\ \text{MSEC}_{i2} \\ \vdots \\ \text{MSEC}_{iq} \end{bmatrix} \quad (4.59)$$

Similarly, $[\beta^*]$ is a diagonal matrix proposed in this study in order to increase the accuracy of $\{\alpha\}$'s that are nodal damages here. Finally, from Eq. (4.59), $\{\alpha\}$'s are obtained in expanding form as

$$\begin{aligned}
\begin{bmatrix} \alpha_1 \\ \alpha_2 \\ \vdots \\ \alpha_q \end{bmatrix} &= \left(\begin{bmatrix} \beta_{11}^* & 0 & \dots & 0 \\ 0 & \beta_{22}^* & \dots & 0 \\ \vdots & \vdots & \ddots & \vdots \\ 0 & 0 & \dots & \beta_{qq}^* \end{bmatrix} \right. \\
&\quad \left. + \begin{bmatrix} \beta'_{11} & \beta'_{12} & \dots & \beta'_{1q} \\ \beta'_{21} & \beta'_{22} & \dots & \beta'_{2q} \\ \vdots & \vdots & \ddots & \vdots \\ \beta'_{q1} & \beta'_{q2} & \dots & \beta'_{qq} \end{bmatrix} \right)^{-1} \begin{bmatrix} \text{MSEC}_{i1} \\ \text{MSEC}_{i2} \\ \vdots \\ \text{MSEC}_{iq} \end{bmatrix}
\end{aligned} \tag{4.60}$$

4.3.5 Required modes shapes and natural frequencies

The number of mode shapes and natural frequencies required for the two stages of the improved method are as follows, respectively.

- Stage 1 or locating the damage
- The first five (or more) modes of both damaged and undamaged structures
- Stage 2 or quantifying the damage

All analytical mode shapes and natural frequencies or as many as analytical mode shapes and natural frequencies that are available or can be derived.

From undamaged structure, as many modes as possible, the more the better (at least the first five modes used in the first stage with their associated natural frequencies). In numerical models, more analytical mode shapes can be effortlessly derived and used.

In practice, mode measuring may be incomplete because of some parameters such as a smaller number of sensors, improper placement of sensors, difficulty in measuring the rotational DOFs, effect of noise and error in processing the data. Though, normally at least the first five modes can be obtained. So, in this method, there is no difficulty in locating the damage. However, having a smaller number of modes from undamaged structure may decrease the damage quantification accuracy.

To overcome this issue, the mode expansion method proposed by Shi *et al.* (1995) can be used to expand the inadequate number of DOFs measured to the full dimension of FEM. Also, according to Hu (1987), when the stiffness of a structure changes, each perturbed mode shape can be linearly expressed as a combination of the original mode shapes.

4.3.6 Noise effect

To consider some uncertainties and noise effect, Eq. (4.61) is applied to the mode shapes (Shi *et al.*, 2000, Cha and Buyukozturk, 2015).

$$\bar{\varphi}_{ij} = \varphi_{ij}(1 + \gamma_i^\varphi \rho^\varphi |\varphi_{\max,j}|) \quad (4.61)$$

where $\bar{\varphi}_{ij}$ and φ_{ij} are the mode shape components of the j th mode at i th DOF,

γ_i^φ are the random numbers with the mean of zero and a variance of one,

ρ^φ is the noise level (percent), and

$\varphi_{\max,j}$ is the largest component of the j th mode shape

4.4 Concluding remarks

Since energy quantity has been recognized as a reliable index for featuring the structural damage, this chapter proposed an improved MSE-based damage detection method for bridge damage detection. The aim of the study was increasing the damage sensitivity and consequently damage detection accuracy of an existing method. For this purpose, the damaged stiffness matrix of the structure was used to establish a more accurate MSE change equation and sensitivity matrix.

The mathematical formulations were comprehensively improved. In the first step, the MSE equation was accurately established to be used in the first stage for more truthful locating the damage. Then, the sensitivity matrix was derived to be used in the second stage to quantify the more precise damage extent. Both elemental and nodal damage quantifying were well mathematically improved and formulated, respectively. The number of mode shapes and natural frequencies required for applying the method and the way of applying noise effect were also discussed and presented.

The next chapters discuss the comparative studies, numerical and experimental applications of the improved MSE method to some structural models.

CHAPTER 5

COMPARATIVE STUDIES

This Chapter compares the performance of the improved MSE method with its ancestor. Section 5.1 introduces the numerical model selected for performing the comparison. Section 5.2 compares the results for a single damage scenario. Section 5.3 shows the results of both methods for a multiple damage scenario applied to the model. Section 5.4 discusses the results of sections 5.2 and 5.3. Finally, the last section, section 5.5, wraps the overall conclusion.

5.1 The numerical fixed-end beam model

The numerical fixed-end beam model consisting of 12 elements and 13 nodes shown in Figure 5.1 is considered to some comparison between the current study and previous research by Shi *et al.* (2000). The model is a steel beam with a total length of 7.2 m. The material properties and geometric information are as Table 5.1.

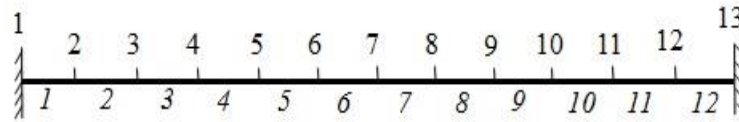


Figure 5.1 The FEM of the fixed-supported beam

Table 5.1 Material properties and geometric information – numerical case study

Material or physical parameter	Symbol	Amount	Unit
Length of each element	L	0.6	M
Total length of the model	L	7.2	m
Modulus of elasticity	E	206×10^9	N/m ²
Cross-sectional area	A	0.0016	m ²
Second moment of area	I	3.4133×10^{-9}	m ⁴
Mass density	ρ	7870	kg/m ³

5.2 Study of the accuracy and convergence of the improved MSE method

As stated in Eq. (4.21), the actual damage extent (α) is a negative coefficient between -1 and 0 or equals 0. However, in this study for more convenience, the sign convention of the damage extent is assumed to be positive. The comparison between the improved method (MSECimp) and the previous method (MSEC) proposed by Shi *et al.* (2000) is performed with the following cases. The Eigen parameters of the model at any case of damaged and undamaged is derived through a MATLAB code.

5.2.1 Single damage

As a single damage scenario, element 5 is damaged with the stiffness loss of 10 percent.

The MSECR of all elements of the model is shown in Figure 5.2.

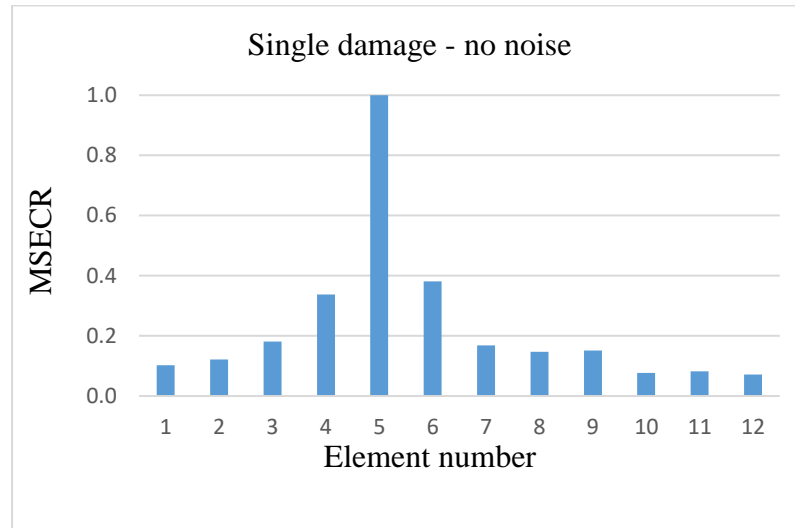


Figure 5.2 The MSECR of the elements, single damage (element 5 with a stiffness loss of 10%)

From Figure 5.2, elements 4, 5 and 6 are selected as suspected elements. Quantifying the extent of the damage performed by increasing the number of analytical mode shapes starting from mode 5. The results of damage extent quantification of element 5 for both methods are shown in Figure 5.3. The results for other suspected elements 4 and 6 are also shown in Figures 5.4 and 5.5, respectively.

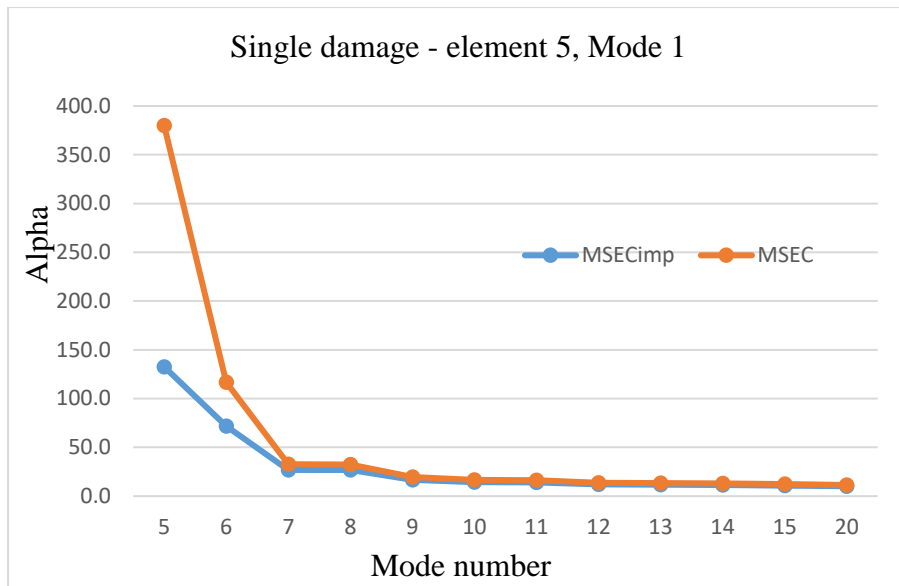


Figure 5.3 Damage extent of element 5 quantified with mode 1 in both MSEC and MSECimp methods

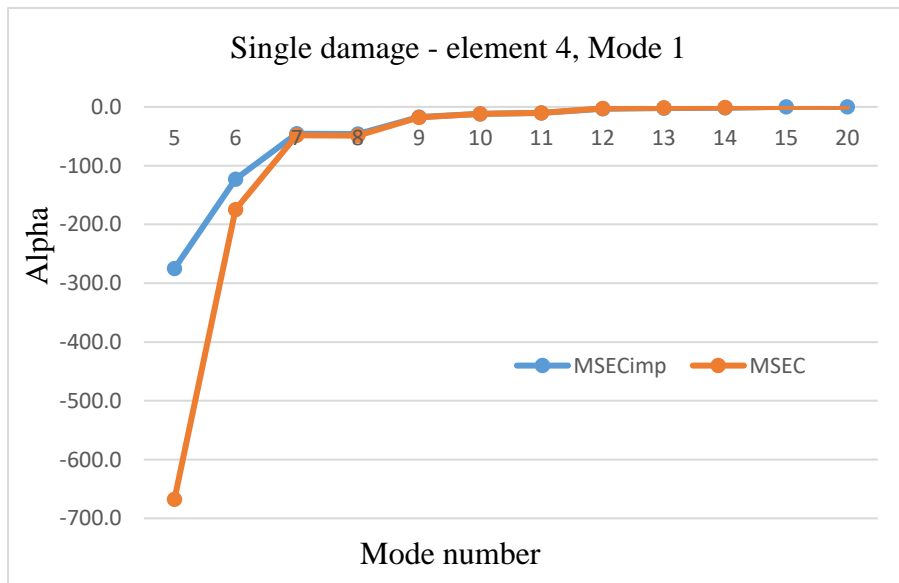


Figure 5.4 Damage extent of element 4 quantified with mode 1 in both MSEC and MSECimp methods

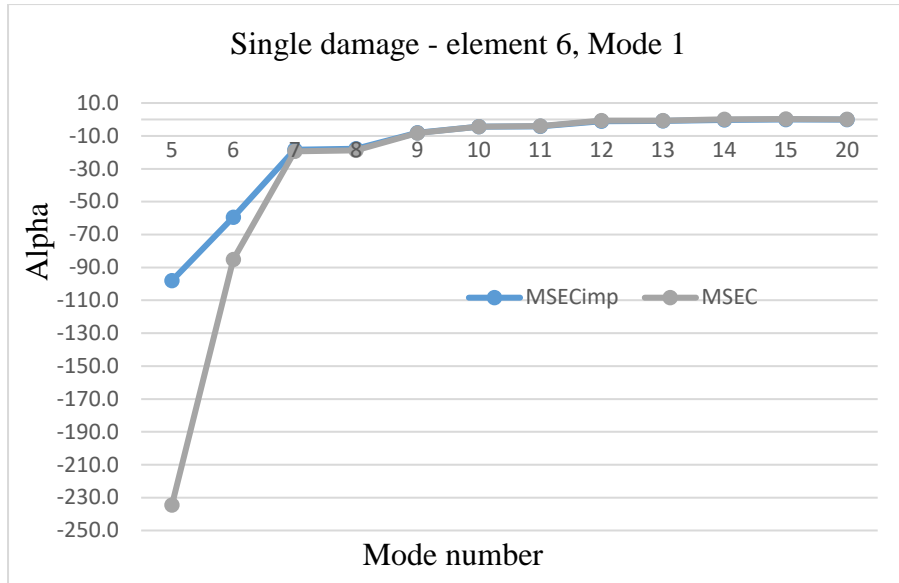


Figure 5.5 Damage extent of element 6 quantified with mode 1 in both MSEC and MSECimp methods

The comparison of damage extents quantified by both MSEC and MSECimp methods for the damaged element (element 5) is shown in Table 5.2.

Table 5.2 Comparison of damage extents quantified using MSEC and MSECimp methods - single damage

Single damage	Damage extent (%)			
	Element no.	Quantified	Actual	Difference (%)
MSECimp	5	10.11	10	+1.11
MSEC	5	11.35	10	+13.47

5.2.2 Multiple damage

Similarly, in multiple damage scenario, elements 4 and 9 are damaged with the stiffness loss of 10 and 15 percent, respectively. The MSECR of all elements of the model is shown in Figure 5.6.

From Figure 5.6, elements 4, 8 and 9 are selected as suspected elements. Quantifying the extent of the damage performed by increasing the number of analytical mode shapes starting from mode 5. The results of damage extent quantification of elements 4, 8 and 9 for both methods are shown in Figures 5.7-5.9, respectively.

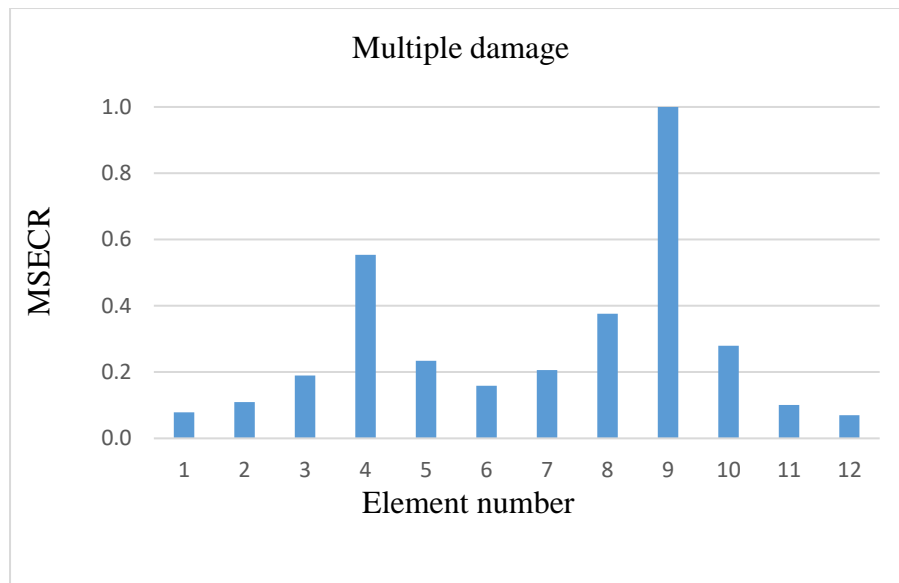


Figure 5.6 MSECR of the elements, multiple damage, (elements 4 and 9 with a stiffness loss of 10 and 15%, respectively)

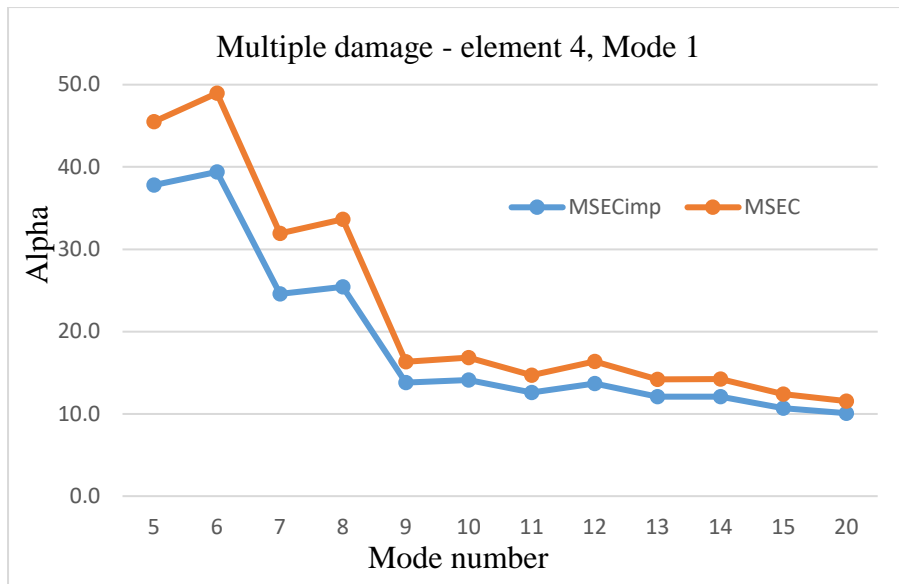


Figure 5.7 Damage extent of element 4 quantified with mode 1 in both MSEC and MSECimp methods

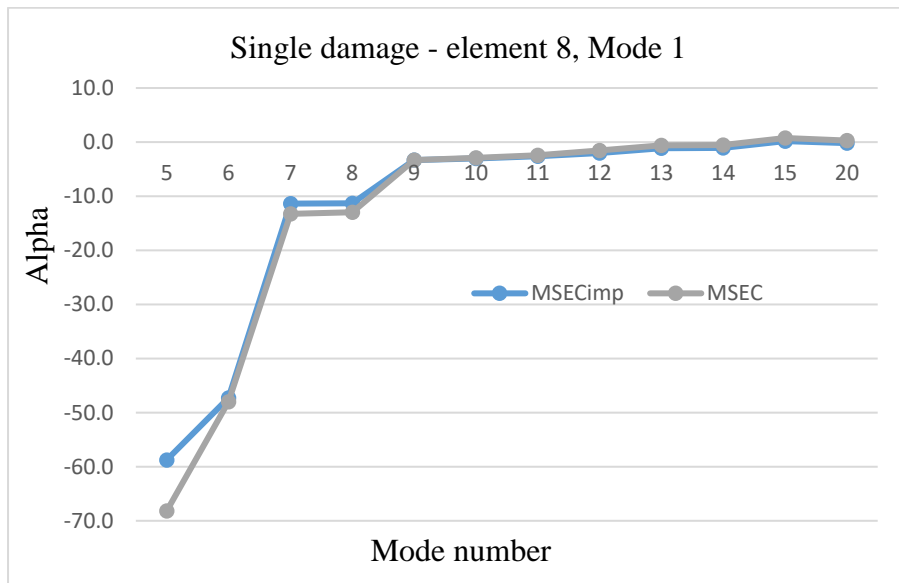


Figure 5.8 Damage extent of element 8 quantified with mode 1 in both MSEC and MSECimp methods

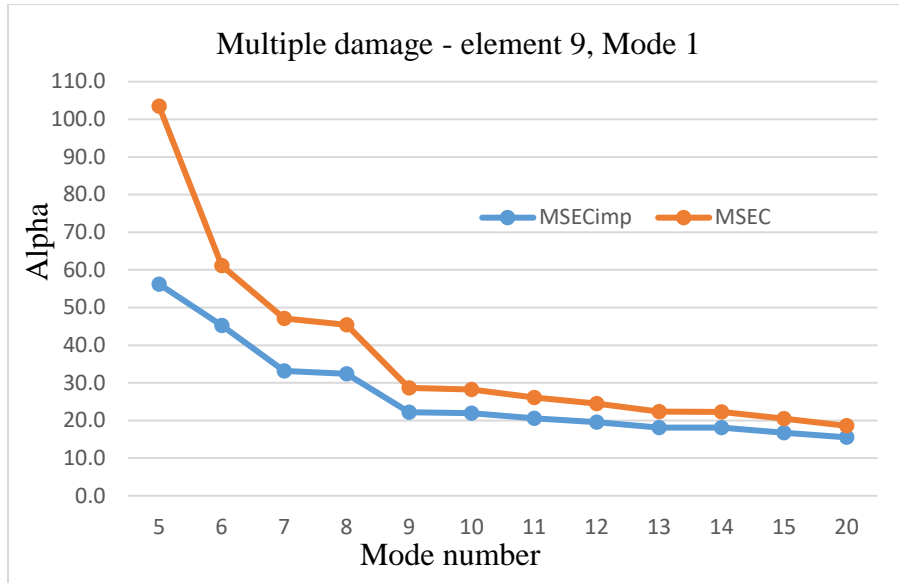


Figure 5.9 Damage extent of element 9 quantified with mode 1 in both MSEC and MSECimp methods

The comparison of the damage extents quantified by both MSEC and MSECimp methods for the damaged elements (elements 4 and 9) is shown in Table 5.3.

Table 5.3 Comparison of damage extents quantified using MSEC and MSECimp methods - multiple damage

Multiple damage	Damage extent (%)			
	Element no.	Quantified	Actual	Difference (%)
MSECimp	4	9.77	10	-2.30
MSEC	4	11.15	10	+11.49
MSECimp	9	15.11	15	+0.75
MSEC	9	17.99	15	+19.92

5.2.3 Results and discussions

From Figures 5.3-5.5 of single damage and Figures 5.7-5.9 of multiple damage, it is seen that MSEC method has a big deviancy at the lower modes. For the single damage, according to the sign convention, Figure 5.3 shows element 5 has damaged. At the beginning that is started with mode 5, MSEC gives 379% damage extent, while MSECimp gives 132% damage extent that shows a considerable deviation between two methods. By increasing the mode number, this trend continues, and both methods converge to the actual damage extent. Although, by increasing the mode number, the difference between quantified damage extents of two methods becomes smaller, the deviation of the MSECimp method from the actual damage extent is always lesser. It means the convergence rate of MSECimp method is faster than that of MSEC method. In other words, for the same mode number, MSECimp method always gives a very much better result i.e. converges with a smaller number of modes. The results of last mode (mode 20) of the both methods are shown in Table 5.2. It is seen that MSEC method has +13.47% difference with the actual damage extent, while the results of current study are deviated only +1.11% from the actual damage extent of 10%. This trend is true for undamaged elements as well. For undamaged elements, the MSECimp converges to zero faster than MSEC.

Similarly, in the multiple damage, Figures 5.7 and 5.9 show elements 4 and 9 have damaged. At mode 5, MSEC gives 45 and 103% damage extent for elements 4 and 9,

respectively. While MSECimp gives 38 and 56% damage extent for those elements, respectively. By increasing the mode number, the convergence is similarly proceeded till mode 20. The significance difference between the two methods is clearly seen in Figures 5.7 and 5.9. The results of the last mode (mode 20) of both methods for the damaged elements 4 and 9 are shown in Table 5.3. The MSEC method shows +11.49 and +19.92% difference with the actual damage extents, while the present study gives only -2.3 and +0.75% from the actual damage extents of 10 and 15%, respectively. It is seen, the MSECimp method always perform better and converges with a smaller number of modes. This trend is also true for the undamaged element 8.

For example, in Figure 5.7, the MSECimp gives 13.8% damage extent at mode 9 that is more accurate than 14.2% damage extent obtained from the MSEC method at mode 14. Similarly, in Figure 5.9, MSECimp and MSEC give 22.2 and 22.3% damage extent at modes 9 and 14, respectively, that shows the accuracy and better performance of the current study at a lower number of mode shapes.

5.3 Conclusion

Studies performed on damage identification using the current study and previous method indicate the improved method is able to identify the damage more accurately by having a smaller number of mode shapes. This highlights the capability of the MSECimp for sensitivity to capture any damage in the structure.

CHAPTER 6

NUMERICAL SIMULATIONS

In this Chapter, Section 6.1 briefly introduces the details of the models studied. Section 6.2 shows the application of the proposed method to a fixed-end steel beam with 2D frame elements. Section 6.3 illustrates the applicability of the proposed method to a three-story steel frame with 2D frame elements. Section 6.4 explains the damage detection of a 2D steel truss structure using the improved MSE method. Section 6.5 describes the performance of the proposed method on a concrete bridge frame. Finally, the last section, section 6.6, wraps the overall conclusion.

6.1 Introduction

This chapter deals with numerical validation of the improved MSE method presented in Chapter 4. The method is applied to different structural models such as a beam, a frame and a truss models with different material properties and element type, size, material properties and structural type. Different damage scenarios including single and multiple damage are also considered for each model. Additionally, all simulations data are contaminated with up to seven percent noise to pretend the actual situation of

noise pollution in the environment. In the last two case studies, the improved method is further verified for two different models representing medium span bridges.

The first case study is a fixed-end beam with frame element as a basic structure that can simply represent a deck of a bridge or a part of any structure. The second case study is a three-story-frame with frame element representing a frame of a building or a frame system supporting the bridge deck. The last two case studies verify the improved method for medium span bridges. In these case studies, in addition to the size and length of the structures, the element type and material properties are also dissimilar. Therefore, the improved method is expansively examined in different aspects using various numerical samples.

The modal analysis of each model at different cases including intact, single and multiple damage is performed using STRAND7 (Strand7_Manual, 2010). The mode shapes and natural frequencies obtained are then used in the improved MSE method using MATLAB to detect the location and quantify the severity of the damage (Smith, 2008, Smith and Pournami, 2013).

6.2 Guideline for practical application of the improved method

The overall guideline for practical application of the current study is as follows.

- a) Stage one is always performed for all structural elements for one specific mode shape or few numbers of modes, for example, mode 1 to 3. Therefore, there is a value of MSECR for each member. The MSECR versus element number from one to n (number of total elements) is drawn.

- b) Calculate the average of MSECRs for all elements. The average of MSECR is the threshold for selecting the suspected elements either for single damage or multiple damage cases. In other words, the elements with MSECR greater than $MSECR_{avg}$ should be selected for quantifying the damage extent for the second stage. However, for the multiple damage, the threshold can be considered slightly around 5% greater than the nominal threshold.

- c) If the number of suspected elements is less than or equals 25% of the total number of elements, continue to stage two of the improved method.

- d) If the number of suspected elements became over 25% of the total number of elements, then
 - i. Select another mode shape or choose few numbers of mode shapes and repeat b and c and repeat this for different modes. If condition c is not satisfied then,

 - ii. Select all suspected element with higher MSECR than $MSECR_{avg}$.

- e) Divide the suspected element (in the same order) to few sets in which the number of elements in each set becomes less than or equals 25% of the total number of elements. Continue to stage two for each set as a separate case and finally combine all the extents obtained from different sets for each case or scenario.
- f) Finally, the true damage elements will be identified with non-zero extent in stage two of the method.

6.3 Case study 1: A fixed-end steel beam

The first numerical simulation is a simple structure which is a fixed-end steel beam consisting of 12 elements and 13 nodes with 33 DoFs as shown in Figure 6.1. The material properties and geometric information are as follows.

Table 6.1 Material properties and geometric information – numerical case study 1

Material or physical parameter	Symbol	Amount	Unit
Length of each element	l	0.6	m
Total length of the model	L	7.2	m
Modulus of elasticity	E	206×10^9	N/m^2
Cross-sectional area	A	0.0016	m^2
Second moment of area	I	3.4133×10^{-9}	m^4
Mass density	ρ	7870	kg/m^3

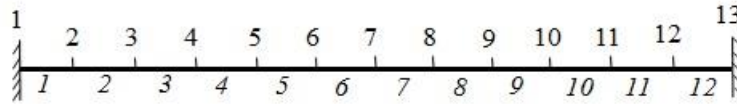


Figure 6.1 The FEM model of the steel fixed-supported beam

Three damage scenarios are assumed to be occurred in the beam. Scenario 1 is a single-damage that occurs in element 7 with a stiffness loss of 5% and scenario 2 is a multiple-damage with damage in elements 4 and 10 with stiffness loss of 5 and 10%, respectively. Scenario 3 is a multiple damage with damage in elements 3, 6 and 11 with stiffness loss of 5, 3 and 8%, respectively. Three, five and seven percent of noise are also considered in each damage scenario, respectively.

Initially, the model is analysed in STRAND7 to get its Eigenvalues and Eigen vectors representing the frequencies and mode shapes of the structure, respectively. The analysis is done for three different cases including, undamaged, single damaged and multiple damaged. The damages are applied to the model by decreasing the local stiffness of the desired elements. It should be noted that the sign convention of the damage extent in this dissertation is considered positive as assumed in Chapter 5.

6.3.1 Results of case study 1

In the first stage, to detect the location of the single damage, the MSCER indicator is calculated and shown in Figure 6.2 using Eq. (4.11). For this purpose, the first five mode shapes of both single damaged and undamaged cases are used i.e. m equals 5.

The second stage is to calculate the alpha coefficients as the damage extents. According to Eq. (4.29), the number of analytical modes required for undamaged case is r which equals or is less than the number of DoFs of the structure ($r \leq \text{no of DoFs}$). While, for damaged case, the number of required modes is i that equals any of modes from 1 to 5. Since, mode one normally gives better solution (because of lower frequency), generally i equals 1. So, in this case study, $r=33$ and $i=1$. Finally, the α 's of the improved method are calculated from Eq. (4.44). The calculation is performed through an iteration process. In each iteration, the global stiffness of the structure is updated as a new undamaged case considering the stiffness of the selected elements using obtained α 's of the previous iteration. Following that the system is reanalysed, and the process is repeated until convergence in α 's. The computation results of five iterations for scenarios 1-3 are shown in Tables 6.2-6.4, respectively. It is seen, the damage extent quantification process normally converges after two or three iterations.

The single damage coefficients (α 's) of iteration 3 using the improved method quantified with the first mode are shown in Figure 6.3. Similarly, the results of the first and second stage for the multiple damages (scenarios 2 and 3) are shown in Figures 6.4-6.7, respectively.

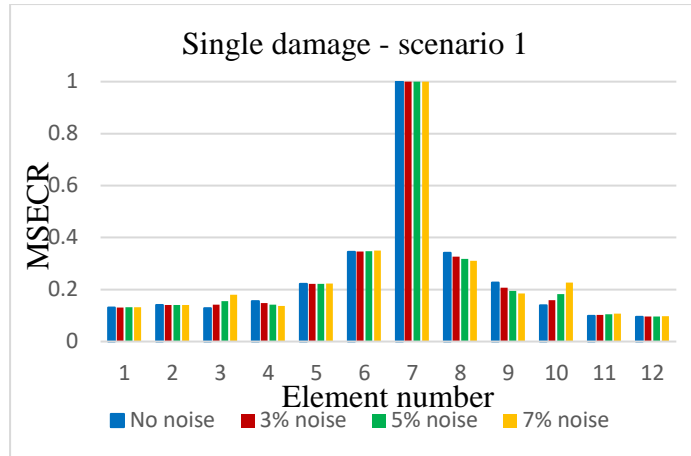


Figure 6.2 The MSECR of the elements, single damage, scenario 1 (element 7 with a stiffness loss of 5%)

According to Figure 6.2, elements 6, 7 and 8 are selected for stage 2 to quantify their damage extents because of getting the higher MSECR. The details are shown in Table 6.2 and Figure 6.3. As mentioned in Eq. (4.21), in reality, the damage extent (α) is a negative coefficient between -1 and 0 or equals 0. However, in this study, the real damage extent conventionally considered positive, because showing the amount of damage upward positive is more convenient. Therefore, α with a negative amount makes little sense and automatically considered 0.

Table 6.2 Damage extent of selected element at each iteration, single damage, scenario 1
(element 7 with a stiffness loss of 5%)

Element number	Iteration number				
	1	2	3	4	5
	no noise				
6	-0.0464	-0.0485	-0.0485	-0.0485	-0.0485
7	5.0321	5.0091	5.0092	5.0092	5.0092
8	-0.0512	-0.0506	-0.0506	-0.0506	-0.0506
	3% noise				
6	0.1710	0.1682	0.1682	0.1682	0.1682
7	5.0307	5.0070	5.0072	5.0072	5.0072
8	0.0952	0.0951	0.0951	0.0951	0.0951
	5% noise				
6	0.3118	0.3085	0.3085	0.3085	0.3085
7	4.9785	4.9546	4.9547	4.9547	4.9547
8	0.1504	0.1501	0.1501	0.1501	0.1501
	7% noise				
6	0.4452	0.4415	0.4416	0.4416	0.4416
7	4.8854	4.8618	4.8619	4.8619	4.8619
8	0.1749	0.1746	0.1746	0.1746	0.1746

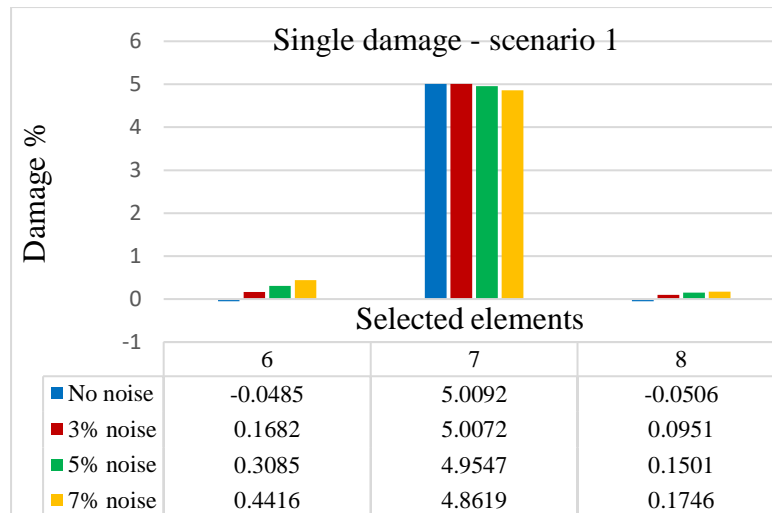


Figure 6.3 The extent of the damage, single damage, scenario 1 (element 7 with a stiffness loss of 5%)

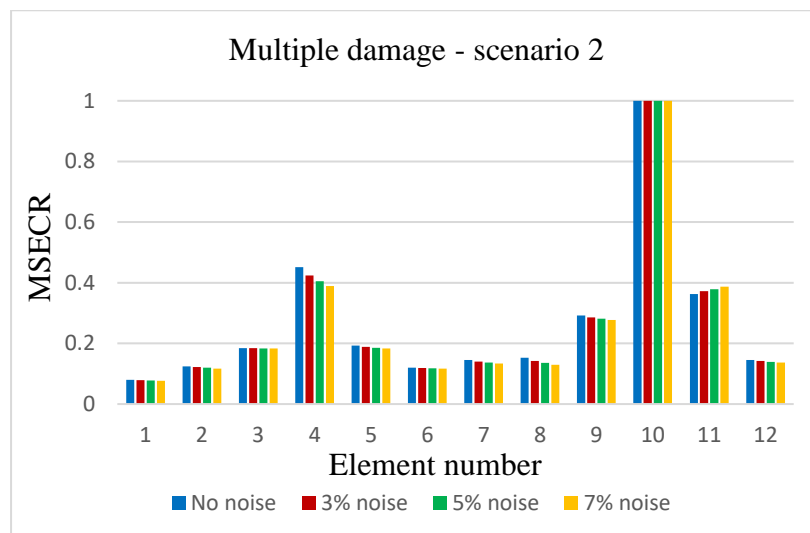


Figure 6.4 The MSECR of the elements, multiple damage, scenario 2 (elements 4 and 10 with stiffness loss of 5 and 10%, respectively)

For the second scenario as shown in Figure 6.4, elements 4, 9, 10 and 11 are selected for next stage to quantify their damage extents because of receiving the higher MSECR.

The details are shown in Table 6.3 and Figure 6.5.

Table 6.3 Damage extent of selected element at each iteration, multiple damage, scenario 2 (elements 4 and 10 with stiffness loss of 5 and 10%, respectively)

Element number	Iteration number				
	1	2	3	4	5
			no noise		
4	5.0819	5.0148	5.0157	5.0157	5.0157
9	0.0132	0.0153	0.0152	0.0152	0.0152
10	10.3934	10.2503	10.2523	10.2522	10.2522
11	-0.0321	-0.0293	-0.0293	-0.0293	-0.0293
			3% noise		
4	4.9830	4.9150	4.9160	4.9160	4.9160
9	-0.6910	-0.6801	-0.6802	-0.6802	-0.6802
10	10.3188	10.1723	10.1745	10.1744	10.1744
11	-0.1061	-0.1024	-0.1025	-0.1025	-0.1025
			5% noise		
4	4.8724	4.8045	4.8055	4.8055	4.8055
9	-1.1252	-1.1084	-1.1087	-1.1087	-1.1087
10	10.2484	10.1006	10.1028	10.1027	10.1027
11	-0.1603	-0.1561	-0.1562	-0.1562	-0.1562
			7% noise		
4	4.7283	4.6613	4.6623	4.6623	4.6623
9	-1.5279	-1.5056	-1.5059	-1.5059	-1.5059
10	10.1693	10.0209	10.0231	10.0231	10.0231
11	-0.2155	-0.2107	-0.2108	-0.2107	-0.2107

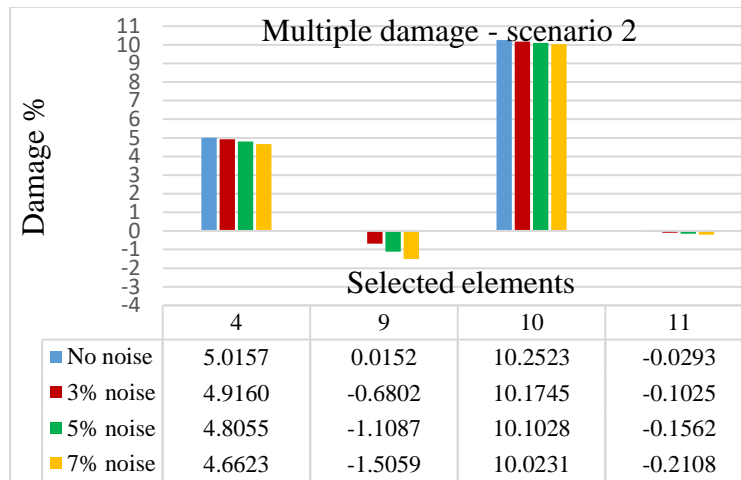


Figure 6.5 The extent of the damage, multiple damage, scenario 2 (elements 4 and 10 with stiffness loss of 5 and 10%, respectively)

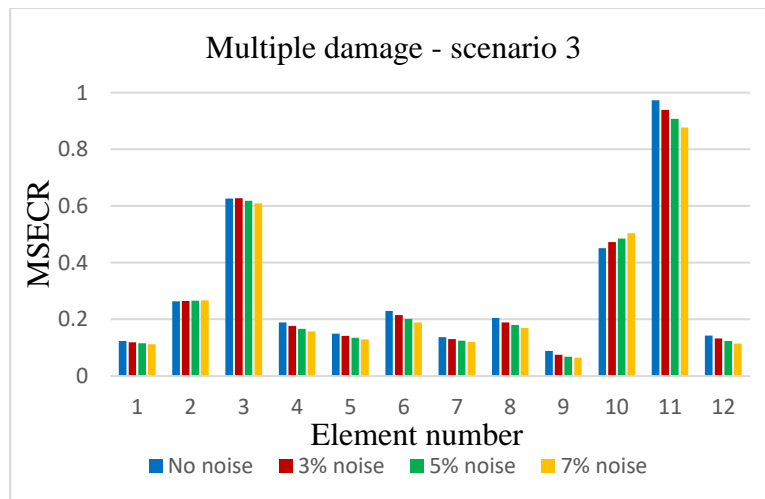


Figure 6.6 The MSECR of the elements, multiple damage, scenario 3 (elements 3, 6 and 11 with stiffness loss of 5, 3 and 8%, respectively)

In the last case, according to Figure 6.6, elements 2, 3, 6, 10 and 11 are suspected to damage because of receiving the higher MSECR. The process of quantifying the damage extents is shown in Table 6.4 and Figure 6.7.

Table 6.4 Damage extent of selected element at each iteration, multiple damage, scenario 3 (elements 3, 6 and 11 with stiffness loss of 5,3 and 8%, respectively)

Element number	Iteration number				
	1	2	3	4	5
			no noise		
2	-0.0129	-0.0137	-0.0137	-0.0137	-0.0137
3	5.1528	5.0831	5.0840	5.0840	5.0840
6	3.0105	2.9683	2.9689	2.9689	2.9689
10	-0.0702	-0.0709	-0.0709	-0.0709	-0.0709
11	8.0422	7.9367	7.9381	7.9381	7.9381
			3% noise		
2	-0.0287	-0.0292	-0.0292	-0.0292	-0.0292
3	5.2319	5.1581	5.1591	5.1591	5.1591
6	3.3850	3.3362	3.3369	3.3369	3.3369
10	-0.0827	-0.0837	-0.0837	-0.0837	-0.0837
11	8.2465	8.1337	8.1353	8.1353	8.1353
			5% noise		
2	-0.0371	-0.0374	-0.0374	-0.0374	-0.0374
3	5.2645	5.1882	5.1893	5.1893	5.1893
6	3.6329	3.5797	3.5805	3.5805	3.5805
10	-0.0885	-0.0897	-0.0897	-0.0897	-0.0897
11	8.3729	8.2554	8.2571	8.2571	8.2571
			7% noise		
2	-0.0442	-0.0443	-0.0443	-0.0443	-0.0443
3	5.2848	5.2065	5.2076	5.2076	5.2076
6	3.8766	3.8189	3.8198	3.8198	3.8198
10	-0.0995	-0.1006	-0.1006	-0.1006	-0.1006
11	8.4911	8.3692	8.3710	8.3710	8.3710

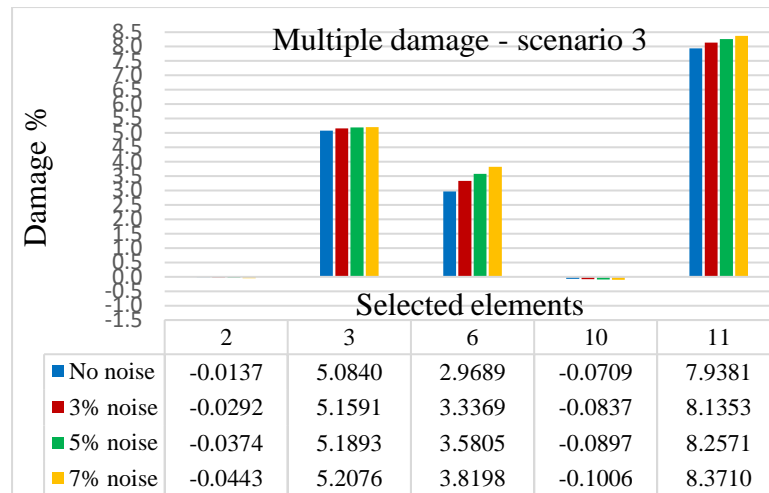


Figure 6.7 The extent of the damage, multiple damage, scenario 3 (elements 3, 6 and 11 with stiffness loss of 5,3 and 8%, respectively)

6.3.2 Discussion on case study 1

Scenario 1: The first scenario investigates the performance of the improved method when single damage occurs in the structure. As shown in Figure 6.2, for the case of no noise, the MSECR peaks at element 7 that represents it is the highly suspected element to damage. Even though, elements 5, 6, 8 and 9 are also likely exposure to damage because of having the higher MSECR index. However, to decrease the computation cycles, few suspected elements such as 6, 7, and 8 are selected for next stage to quantify their damage extents as the α coefficients. Quantifying the α coefficient for selected elements is depicted in Figure 6.3. From this figure, it is seen that for the case of no noise, the amount of α 's converge to zero except α_7 which converges to 5 that accurately equals the assumed damage.

Similarly, in presence of noise, it is seen that although the amount of MSECR index in Figure 6.2 is slightly affected by noise, the elements with a higher amount of MSECR are same with case of no noise. However, in the second stage, the extent of damages quantified in those elements varies. In other words, by increasing the noise, the accuracy of the method to detect the actual extent of the damage decreases. From Figure 6.3 it is seen, the method shows the extent of the damage at element 7 with 0.14, -0.91 and -2.76% error for the noise level of 3, 5 and 7 percent, respectively. It means, by increasing the percentage of the random noise level, the accuracy of the method to quantify the damage slightly decreases.

Scenario 2: The second scenario deals with multiple damage in the structure. As shown in Figure 6.4, for the case of no noise, the MSECR tops at elements 4, 9, 10 and 11. These elements are selected as the suspected elements for the next stage to quantify their damage extents as the α coefficients. Quantifying the α coefficient for selected elements is depicted in Figure 6.5. From this figure, it is seen that for the case of no noise, the amount of α 's converge to zero except α_4 and α_{10} which converge to 5.02 and 10.25, respectively, that almost equals the assumed damage.

Similarly, in presence of noise, the same elements are selected for the next stage. However, in the second stage, the extent of damages quantified in those elements slightly changes. From Figure 6.5 it is seen, the method shows the extent of damage at element 4 with -1.68, -3.89 and -6.75% error for the noise level of 3, 5 and 7 percent,

respectively. For element 10 the errors are 1.75, 1.03 and 0.02% for the noise levels applied, respectively.

Scenario 3: For the last scenario as another multiple damage scenario by assuming damage in three elements, the results are shown in Figures 6.6 and 6.7. The MSECR indicator identifies elements 2, 3, 6, 10 and 11 as suspected elements. After quantifying the damage at these elements in presence of three levels of noise as shown in Figure 6.7, it is seen, elements 3, 6 and 11 are the true damage elements with damage extents of 5.08, 2.97 and 7.93% for the case of no noise, respectively. The amount of error for each element at each level of noise is as follows.

Table 6.5 The percentage of error of damage extent for selected elements with different noise level, scenario 3 (elements 3, 6 and 11 with stiffness loss of 5,3 and 8%, respectively)

Element number	Noise level			
	No noise	3%	5%	7%
3	1.68	3.18	3.76	4.15
6	-1.33	11.23	19.35	27.32
11	-0.77	1.69	3.21	4.63

The above Table shows that the improved method is noise sensitive and performs better with lower noise level up to 5 percent.

6.4 Case study 2: A three-story steel frame

The second case study is a three-story steel frame with frame elements of three DoFs at each end consisting of nine elements and eight nodes with 18 DoFs as shown in Figure 6.8. The material properties and geometric information are as follows.

Table 6.6 Material properties and geometric information – numerical case study 2

Material or physical parameter	Symbol	Amount	Unit
Length	L	3.0	m
Modulus of elasticity	E	206×10^9	N/m ²
Cross-sectional area	A	0.0015	m ²
Second moment of area	I	1.125×10^{-7}	m ⁴
Mass density	ρ	7870	kg/m ³

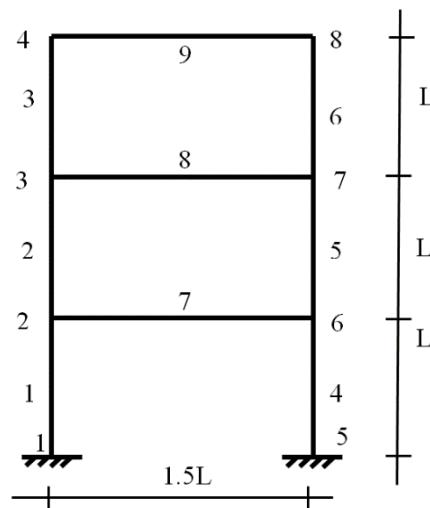


Figure 6.8 FEM of the three-story steel frame

Similarly, two damage cases, single and multiple damage scenarios, are assumed to be occurred in the frame. Scenario 1 is a single-damage that occurs in a beam (element

7), with a stiffness loss of 8% and scenario 2 is a multiple-damage with damages in a column and a beam, elements 4 and 8, with stiffness loss of 5 and 8 percent, respectively. Three and five percent noise are also considered in each damage scenario, respectively.

Primarily, the modal analysis of the model is performed in STRAND7 to acquire the Eigenvalues and Eigenvectors. The damages are applied to the model by decreasing the local stiffness of the elements under consideration. Three different analysis including undamaged, single damaged and multiple damaged are performed. Then the noise is applied to the mode shape and natural frequencies of each case.

6.4.1 Results of case study 2

In the first stage, to detect the location of the damages, using the pair of the first five mode shapes of both damaged and undamaged of each case using Eq. (4.11) with m equals 5. The MSCER indicator for all elements of the single and multiple damage cases is calculated and shown in Figures 6.9 and 6.11, respectively. In the second stage, to get the alpha coefficients, Eq. (4.44) is used, however, in this case study $r=18$ and $i=1$. The single and multiple damage coefficients (α 's) using the improved method quantified with the first mode are shown in Figures 6.10 and 6.12, respectively.

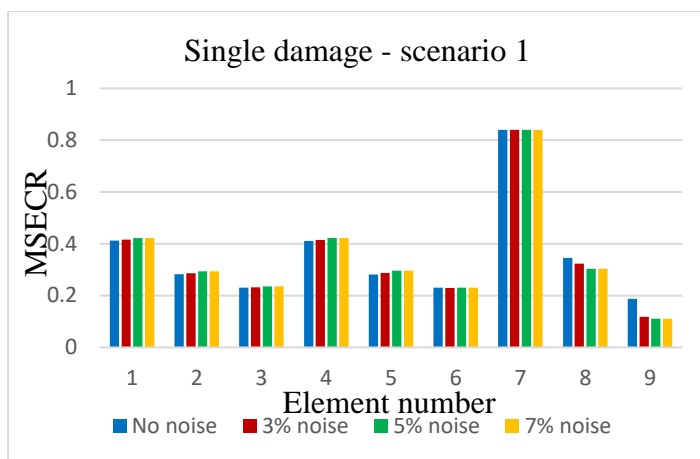


Figure 6.9 The MSECR of the elements, single damage, scenario 1 (element 7 with stiffness loss of 8%)

According to Figure 6.9, for single damage, suspected elements are 1, 4 and 7. The computation results of five iterations for scenarios 1 are shown in Table 6.7 and drawn in Figure 6.10.

Table 6.7 Damage extent of selected element at each iteration, single damage, scenario 1
(element 7 with stiffness loss of 8%)

Element number	Iteration number				
	1	2	3	4	5
	no noise				
1	-0.0464	-0.0327	-0.0328	-0.0328	-0.0328
4	-0.0464	-0.0329	-0.0330	-0.0330	-0.0330
7	7.7281	7.6595	7.6603	7.6603	7.6603
	3% noise				
1	0.1522	-0.0336	-0.0328	-0.0328	-0.0328
4	0.1572	-0.0338	-0.0330	-0.0330	-0.0330
7	7.3424	7.6616	7.6603	7.6603	7.6603
	5% noise				
1	0.2826	-0.0344	-0.0328	-0.0328	-0.0328
4	0.2912	-0.0346	-0.0330	-0.0330	-0.0330
7	7.0733	7.6623	7.6603	7.6603	7.6603
	7% noise				
1	-0.0011	-0.0352	-0.0328	-0.0328	-0.0328
4	0.4235	-0.0353	-0.0330	-0.0330	-0.0330
7	6.7935	7.6632	7.6602	7.6603	7.6603

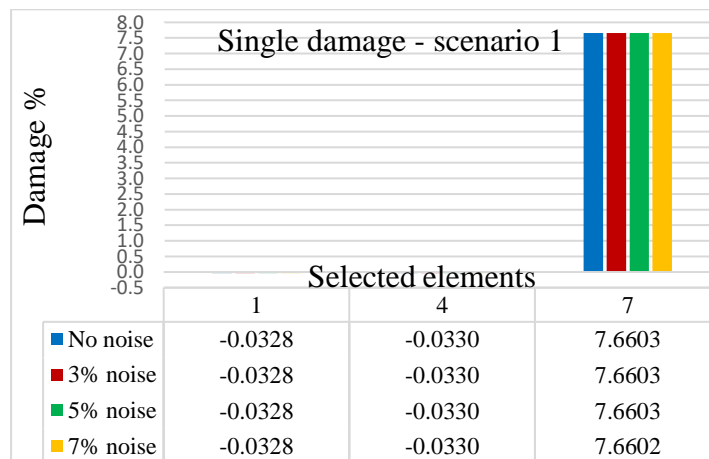


Figure 6.10 The extent of the damage, single damage, scenario 1 (element 7 with stiffness loss of 8%)

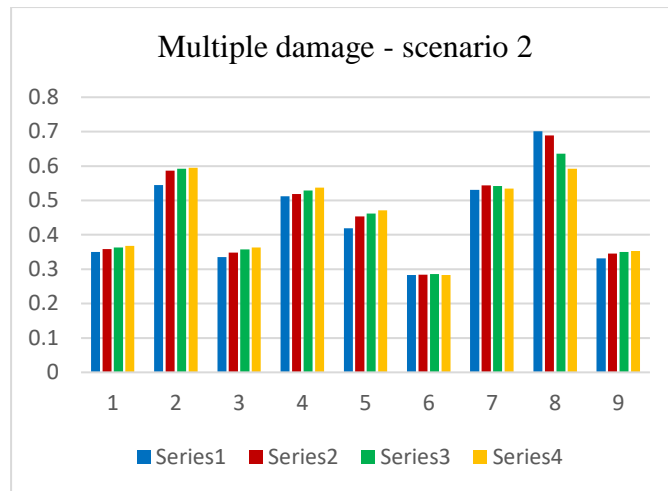


Figure 6.11 MSECR of the elements, multiple damage, scenario 2 (elements 4 and 8 with stiffness loss of 5 and 8%, respectively)

According to Figure 6.11, for the multiple damage, suspected elements are 2, 4, 7 and 8. The details of iteration and extents are shown in Table 6.8 and drawn in Figure 6.12.

Table 6.8 Damage extent of selected element at each iteration, multiple damage, scenario 2 (elements 4 and 8 with stiffness loss of 5 and 8%, respectively)

Element number	Iteration number				
	1	2	3	4	5
			no noise		
2	-0.3041	-0.3095	-0.3093	-0.3093	-0.3093
4	4.8214	4.7727	4.7735	4.7734	4.7734
7	-0.2355	-0.2151	-0.2153	-0.2153	-0.2153
8	7.6789	7.5599	7.5617	7.5617	7.5617
			3% noise		
2	-0.6984	-0.3077	-0.3093	-0.3093	-0.3093
4	4.4756	4.7739	4.7734	4.7734	4.7734
7	-0.7387	-0.2152	-0.2153	-0.2153	-0.2153
8	6.9753	7.5666	7.5616	7.5617	7.5617
			5% noise		
2	-0.9410	-0.3066	-0.3093	-0.3093	-0.3093
4	4.2388	4.7747	4.7734	4.7734	4.7734
7	-1.0531	-0.2154	-0.2153	-0.2153	-0.2153
8	6.5269	7.5709	7.5615	7.5617	7.5617
			7% noise		
2	-1.1650	-0.3056	-0.3094	-0.3093	-0.3093
4	3.9976	4.7755	4.7734	4.7734	4.7734
7	-1.3480	-0.2156	-0.2153	-0.2153	-0.2153
8	6.0982	7.5752	7.5615	7.5617	7.5617

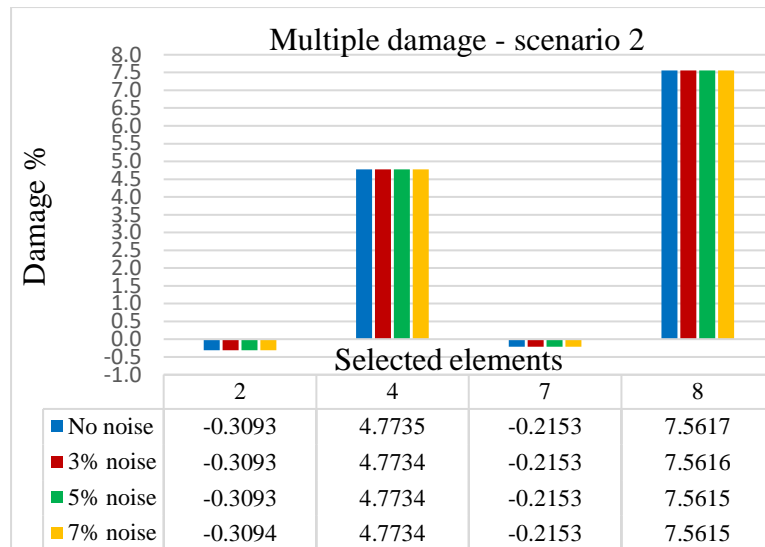


Figure 6.12 The extent of the damage, multiple damage, scenario 2 (elements 4 and 8 with stiffness loss of 5 and 8%, respectively)

6.4.2 Discussion on case study 2

Similarly, in single-damage scenario, according to Figure 6.9, element numbers 1, 4 and 7 are selected as the suspect damaged elements. The obtained coefficient of α_7 is 7.66 percent as shown in Figure 6.10. The error in damage extent quantified is -4.25 percent for any noise levels applied. In multiple-damage scenario also based on Figure 6.11, among the selected suspect elements 2, 4, 7 and 8, the amount of α_4 and α_8 are calculated 4.77 and 7.56, respectively, as shown in Figure 6.12. Almost for all noise level studied, the amount of error is -4.6 and -5.5 percent for elements 4 and 8, respectively.

It should be mentioned that for selecting the suspect damaged elements, there is no limitation neither in the number nor order of elements. It is because of that only the

true damaged elements will finally converge to a non-zero coefficient of damage. However, selecting many suspected elements at the same time could increase the computational cycles, particularly for complex structures, but it does not affect identifying the true damaged elements.

6.5 Case study 3: A 2D steel truss structure

For further investigation, the improved method is applied to two other models, a steel truss bridge and a concrete bridge frame as the models of the short- and medium-span of bridges framework. These simulations, firstly, examine the efficiency of the improved method on this category of bridges in terms of dimension and type of structure and element. In addition, the effect of material properties on performance of the improved method is observed.

The next numerical case study is a 2D steel truss bridge with truss element of two DoFs at each end consisting of 12 nodes and 21 elements with 20 DoFs as shown in Figure 6.13. The material properties and geometric information are as follows.

Table 6.9 Material properties and geometric information – numerical case study 3

Material or physical parameter	Symbol	Amount	Unit
Length	L	5.0	m
Modulus of elasticity	E	206×10^9	N/m ²
Cross-sectional area	A	0.04	m ²
Mass density	ρ	7870	kg/m ³

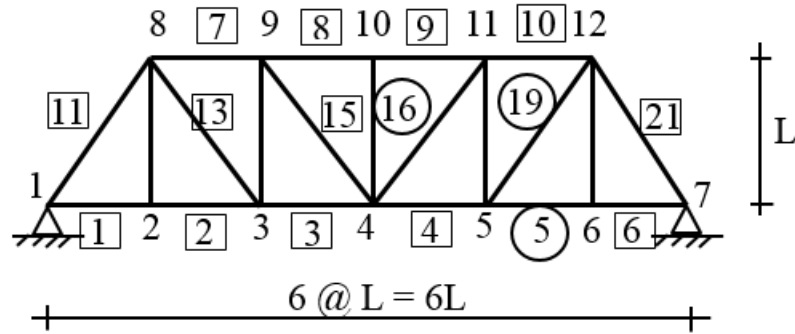


Figure 6.13 The FEM model of the steel truss model

Two damage scenarios including single- and multiple-damage are considered being occurred in each structure. Scenario one is a single-damage that occurs in element 5 with a stiffness loss of 3% and scenario two is a multiple-damage with damages in elements 16 and 19 with stiffness loss of 5 and 12%, respectively, as encircled in Figure 6.13. Modal analysis is performed for structure at a different state of the intact and damaged (both single- and multiple-damage scenarios) structure using STRAND7. The effect of up to 5 percent noise is also comprised. The simulated mode shapes and natural frequencies derived are then used in MATLAB to identify the damage.

6.5.1 Results of case study 3

To apply the improved method and determine the suspected elements, MSECR indicator is calculated using Eq. (4.11). Attempt for finding the true damaged elements is then performed among the suspected elements using the Eq. (4.44). The effect of noise is also included using Eq. (4.61) for two different assumed percentages of 3 and 5.

Locating the single- and multiple-damage are shown in Figures 6.12 and 6.14, respectively. The alpha coefficients of single- and multiple-damage quantified with the first mode are also shown in Figures 6.13 and 6.15, respectively. The last iteration of stage 2 for quantifying the single- and multiple-damage extents are shown in Tables 6.10 and 6.11, respectively.

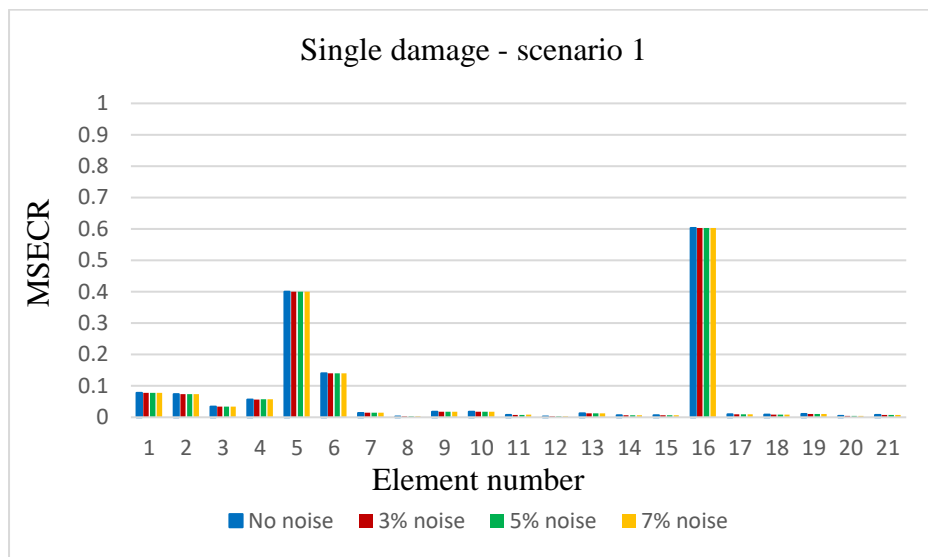


Figure 6.14 The MSECR of the elements, single damage, scenario 1 (element 5 with stiffness loss of 3%)

Like previous case studies, as seen in the Figure 6.14, for the single damage, suspected elements are 5, 6 and 16. The details of iteration and extents of damages are shown in Table 6.10 and drawn in Figure 6.15.

Table 6.10 Damage extent of selected element at each iteration, single damage, scenario 1
(element 5 with stiffness loss of 3%)

Element number	Iteration number				
	L	2	3	4	5
no noise					
5	3.0262	3.0098	3.0099	3.0099	3.0099
6	-0.0072	-0.0050	-0.0050	-0.0050	-0.0050
16	-0.0001	-0.0001	-0.0001	-0.0001	-0.0001
3% noise					
5	2.5737	3.0106	3.0099	3.0099	3.0099
6	0.6046	-0.0058	-0.0050	-0.0050	-0.0050
16	-0.0325	-0.0001	-0.0001	-0.0001	-0.0001
5% noise					
5	2.1457	3.0120	3.0099	3.0099	3.0099
6	0.9508	-0.0064	-0.0050	-0.0050	-0.0050
16	-0.0683	-0.0001	-0.0001	-0.0001	-0.0001
7% noise					
5	1.7319	3.0136	3.0098	3.0099	3.0099
6	1.1988	-0.0069	-0.0050	-0.0050	-0.0050
16	-0.1175	-0.0002	-0.0001	-0.0001	-0.0001

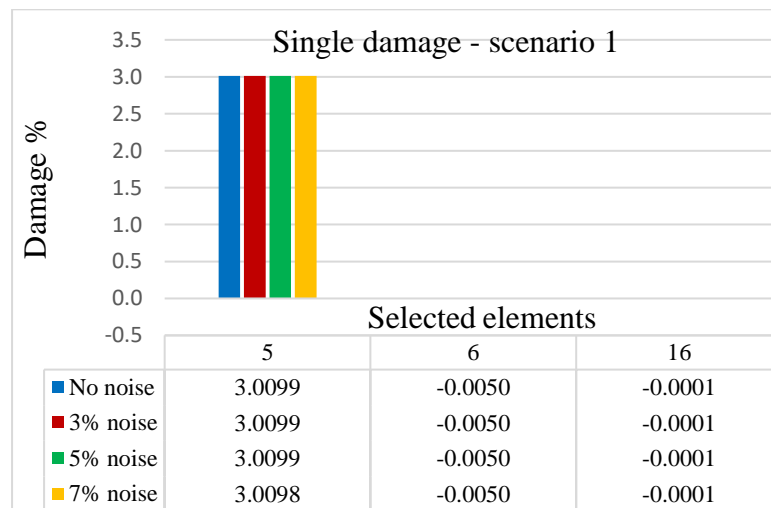


Figure 6.15 The extent of the damage, single damage, scenario 1 (element 5 with stiffness loss of 3%)

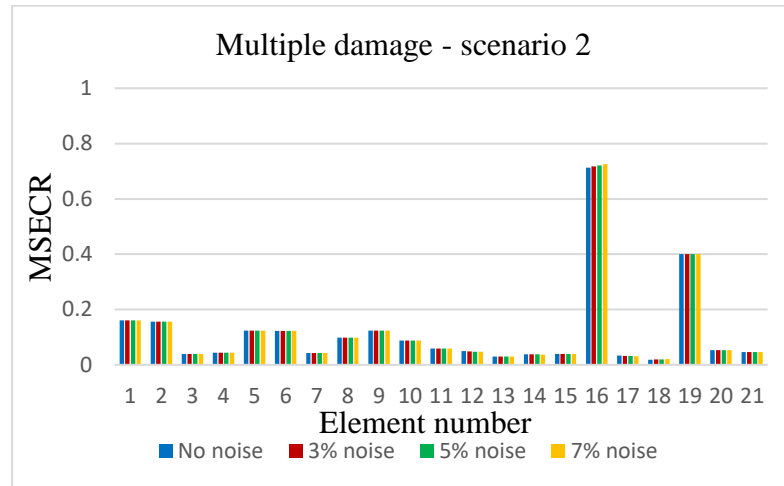


Figure 6.16 The MSECR of the elements, multiple damage, scenario 2 (elements 16 and 19 with stiffness loss of 5 and 12%, respectively)

Similar to the previous case study, as seen in Figure 6.16, for the multiple damage, suspected elements are 1, 16 and 19. The details of iteration and extent of damages are shown in Table 6.11 and drawn in Figure 6.17.

Table 6.11 Damage extent of selected element at each iteration, multiple damage, scenario 2 (elements 16 and 19 with stiffness loss of 5 and 12%, respectively)

Element number	Iteration number				
	1	2	3	4	5
	no noise				
1	-0.1061	-0.1940	-0.1927	-0.1927	-0.1927
16	5.0355	4.9593	4.9605	4.9605	4.9605
19	12.6110	12.4825	12.4835	12.4835	12.4835
	3% noise				
1	-2.8596	-0.1720	-0.1928	-0.1927	-0.1927
16	1.9586	4.9977	4.9601	4.9605	4.9605
19	12.3161	12.4741	12.4837	12.4835	12.4835
	5% noise				
1	-6.6947	-0.1450	-0.1930	-0.1927	-0.1927
16	-0.2967	5.0222	4.9598	4.9605	4.9605
19	11.5311	12.4626	12.4839	12.4835	12.4835
	7% noise				
1	-11.2071	-0.1188	-0.1930	-0.1927	-0.1927
16	-2.5106	5.0012	4.9600	4.9605	4.9605
19	10.4281	12.4450	12.4842	12.4835	12.4835

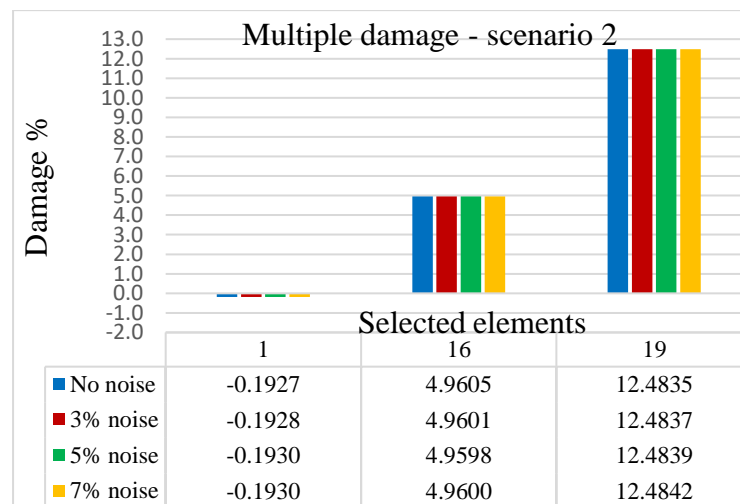


Figure 6.17 The extent of the damage, multiple damage, scenario 2 (elements 16 and 19 with stiffness loss of 5 and 12%, respectively)

6.5.2 Discussion on case study 3

In the single-damage scenario, shown in Figure 6.14, it is seen that the MSECR crests at elements 5 and 16 which represent they are highly suspected elements to damage. Element 6 also has probably damaged because of getting the high amount of the MSECR. Figure 6.15 shows the amounts of alphas versus element number that indicates the amount of all alphas converge to zero except α_5 which converges to a non-zero amount around 3%. In other words, it means for this damage scenario, only element 5 is a true damaged element. It is evident that since other suspected elements 6 and 16 have got the alphas with the amount of almost zero, so no damage has occurred in those elements. Element 16 has received a high MSECR, but it is not damaged at all. It may because of the location of the element at the middle of the structure that has received a lot of energy, but it has not actually damaged.

Similarly, in the multiple-damage scenario, shown in Figure 6.16, the MSECR peaks at elements 16 and 19 which represents their highly possibility of damage. Elements 1, 2, 5, 6 and 9 are also probably damaged elements because of getting the higher MSECR. Figure 6.17 shows that the amount of α_{16} and α_{19} converge to 4.96 and 12.48%, respectively, while element 1 converges to zero. Likewise, the single-damage scenario, it can be concluded that elements 16 and 19 are the true damaged elements, however other suspected elements have experienced no damage.

6.6 Case study 4: A concrete bridge frame

The last case study is a concrete bridge frame with frame elements of three DoFs at each end consisting of eight nodes and seven elements with 12 DoFs as shown in Figure 6.16. The material properties and geometric data are as follows.

Table 6.12 Material properties and geometric information – numerical case study 4

Material or physical parameter	Symbol	Amount	Unit
Length	L	6.0	m
Modulus of elasticity	E	30×10^9	N/m ²
Cross-sectional area	A	0.75	m ²
Second moment of area	I	0.140625	m ⁴
Mass density	ρ	2500	kg/m ³

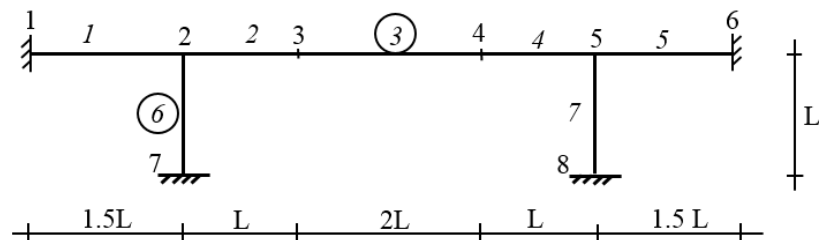


Figure 6.18 The FEM model of the concrete bridge frame

Two damage scenarios are assumed to be happened in the frame structure. Scenario 1 is a single-damage that occurs in a beam with element number of 3 with a stiffness loss of 6% and scenario 2 is a multiple-damage with damage in elements 3 and 6 with stiffness loss of 6 and 4%, respectively.

Modal analysis is done for structure at three different states of the intact, single damaged and multiple damaged using STRAND7. The data is polluted by up to 7 percent noise as well. The simulated mode shapes and natural frequencies derived are lastly used to identify the damage via MATLAB.

6.6.1 Results of case study 4

Similarly, Eqs. (4.11), (4.44) and (4.61) are used to calculate the MSECR indicator, the amounts of alphas and effects of 3, 5 and 7% noise, respectively. Locating the single- and multiple-damage are shown in Figures 6.19 and 6.21, respectively. The amounts of alphas coefficients of the suspected elements of single- and multiple-damage quantified with the first mode are also shown in Figures 6.20 and 6.22, respectively. The calculated results of the five iterations for scenarios 1-2 are shown in Tables 6.13-6.14, respectively.

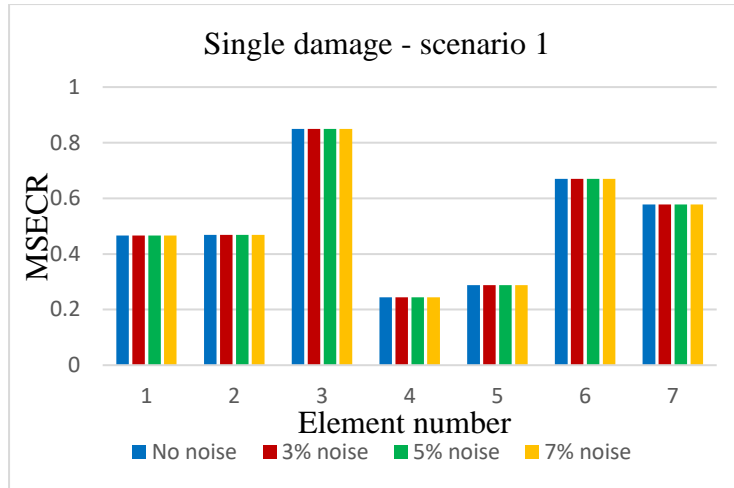


Figure 6.19 The MSECR of the elements, single damage, scenario 1 (element 3 with stiffness loss of 6%)

As seen in the Figure 6.19, for the single damage, suspected elements are 3, 6 and 7. The details of iterations and extent of damages are shown in Table 6.13 and Figure 6.20. Similarly, for the multiple damage scenario, also, the same elements are selected. However, the details of iterations and extent of damages are shown in Table 6.14 and drawn in Figure 6.22, respectively.

Table 6.13 Damage extent of selected element at each iteration, single damage, scenario 1
(element 3 with stiffness loss of 6%)

Element number	Iteration number				
	1	2	3	4	5
			no noise		
3	5.6643	5.6264	5.6267	5.6267	5.6267
6	-0.1306	-0.1289	-0.1289	-0.1289	-0.1289
7	-0.1307	-0.1199	-0.1200	-0.1200	-0.1200
			3% noise		
3	5.4700	5.6218	5.6267	5.6267	5.6267
6	-0.6552	-0.1283	-0.1289	-0.1289	-0.1289
7	-0.4646	-0.1202	-0.1200	-0.1200	-0.1200
			5% noise		
3	5.3696	5.6192	5.6267	5.6267	5.6267
6	-0.9470	-0.1279	-0.1289	-0.1289	-0.1289
7	-0.6543	-0.1204	-0.1200	-0.1200	-0.1200
			7% noise		
3	5.2911	5.6170	5.6267	5.6267	5.6267
6	-1.1733	-0.1276	-0.1289	-0.1289	-0.1289
7	-0.8311	-0.1205	-0.1200	-0.1200	-0.1200

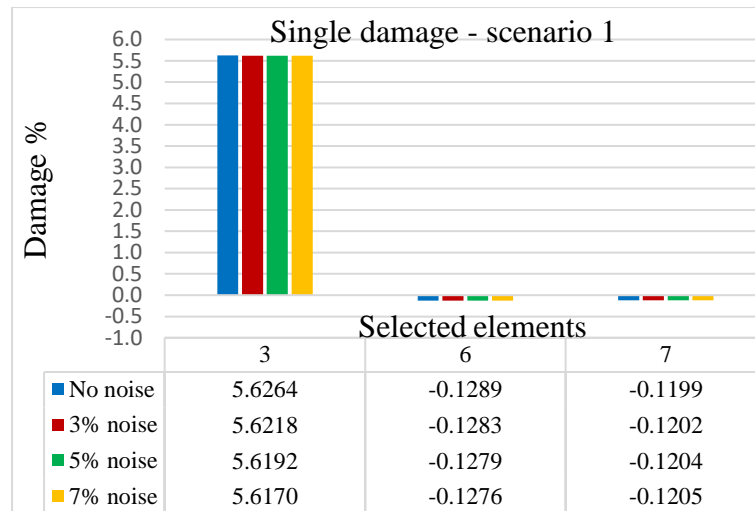


Figure 6.20 The extent of the damage, single damage, scenario 1 (element 3 with stiffness loss of 6%)

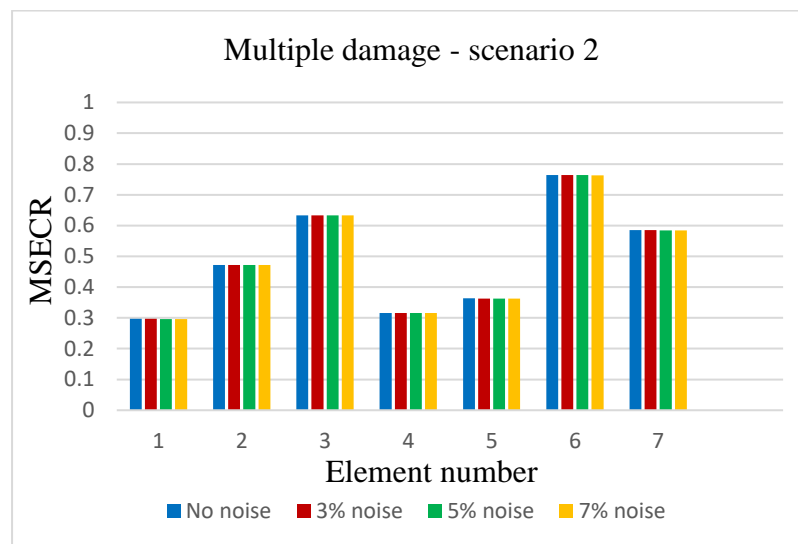


Figure 6.21 The MSECR of the elements, multiple damage, scenario 2 (elements 3 and 6 with stiffness loss of 6 and 4%, respectively)

Table 6.14 Damage extent of selected element at each iteration, multiple damage, scenario 2 (elements 3 and 6 with stiffness loss of 6 and 4%, respectively)

Element number	Iteration number				
	1	2	3	4	5
	no noise				
3	5.692986	5.623254	5.624419	5.6244	5.624401
6	3.85973	3.792221	3.793276	3.793259	3.79326
7	-0.12064	-0.0911	-0.09149	-0.09148	-0.09148
	3% noise				
3	5.039364	5.632981	5.624246	5.624403	5.624401
6	2.821409	3.803218	3.793118	3.793262	3.79326
7	-0.92053	-0.09427	-0.09143	-0.09148	-0.09148
	5% noise				
3	4.663839	5.640296	5.624124	5.624405	5.624401
6	2.077853	3.810915	3.793005	3.793264	3.79326
7	-1.26413	-0.0961	-0.09139	-0.09148	-0.09148
	7% noise				
3	4.364969	5.647602	5.624007	5.624407	5.624401
6	1.359343	3.818214	3.792896	3.793265	3.79326
7	-1.44111	-0.09757	-0.09135	-0.09148	-0.09148

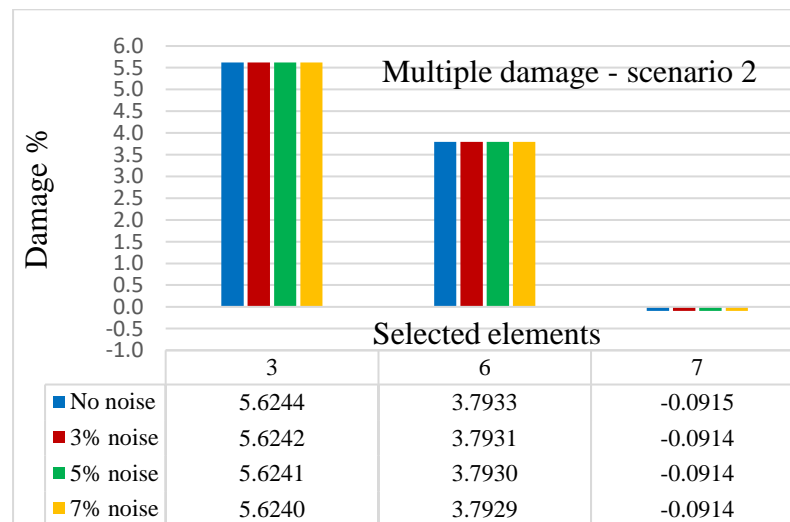


Figure 6.22 The extent of the damage, multiple damage, scenario 2 (elements 3 and 6 with stiffness loss of 6 and 4%, respectively)

6.6.2 Discussion on case study 4

In the single-damage scenario, shown in Figure 6.19, it is seen that the MSECR peaks at element 3 which represents it is a highly suspected element to damage. Elements 6 and 7 also have probably damaged because of getting the high amount of the MSECR. Figure 6.20 shows the alpha versus element number that indicates the amount of all alphas converge to zero except α_3 which converges to a non-zero amount around 5.63%. In other words, it means for this damage scenario, only element 3 is a true damaged element.

In multiple-damage scenario also among the suspected elements of 3, 6 and 7 as shown in Figure 6.21, the amount of α_3 and α_6 and are calculated as 5.62 and 3.79%, respectively, whereas, α_7 converges to zero that are drawn in Figure 6.22. This also represents that elements 3 and 6 are the correct damaged elements with reduction stiffness of 5.62 and 3.79%, respectively.

6.7 Quantifying the minimum damage magnitude

In this section, it is tried to evaluate the improved method for diagnosis of a very small damages in the structures. For this purpose, two scenarios are considered for the model studied in case study one. Scenario 1 is a single damage at element 7 with the amount of 1% and scenario 2 is a multiple damage with the amount of 0.5, 1 and 0.75% at

elements 3, 6 and 11, respectively. The computation results of the five iterations for scenarios 1-2 are shown in Tables 6.15-6.16, respectively.

The results shown in the following Tables and Figures perfectly indicate that the method is strongly able to detect the small damages assumed and even smaller ones. The application can be applied to any other model, and the method is nicely able to detect any minor damages in the system.

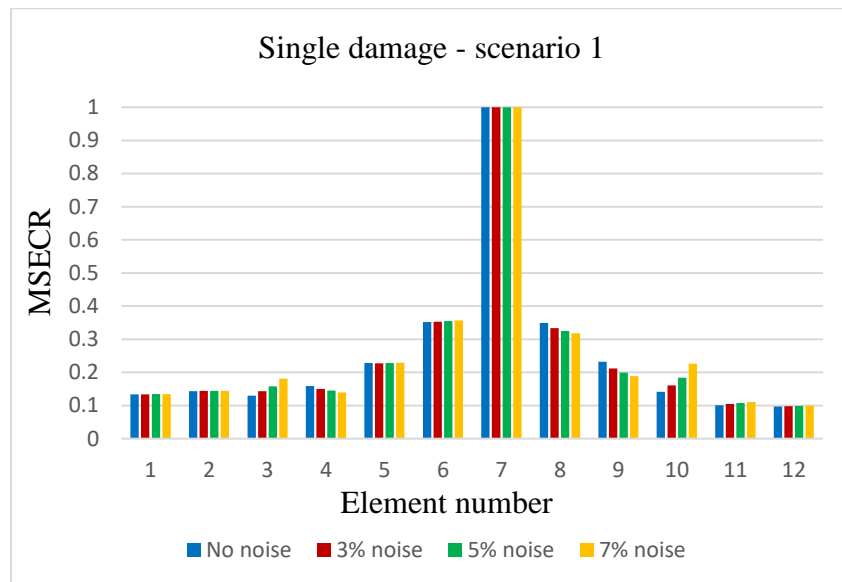


Figure 6.23 The MSECR of the elements, single damage, scenario 1 (element 7 with stiffness loss of 1%)

As seen in Figure 6.23, this scenario is like scenario 1 in case study 1, however, it is in a very smaller scale. So, elements 6, 7 and 8 are selected for the next stage to quantify their damage extents because of receiving a higher MSECR. The details are shown in Table 6.15 and drawn in Figure 6.24, respectively.

Table 6.15 Damage extent of selected element at each iteration, single damage, scenario 1
(element 7 with stiffness loss of 1%)

Element number	Iteration number				
	1	2	3	4	5
			no noise		
6	-0.00175	-0.00185	-0.00185	-0.00185	-0.00185
7	1.00135	1.00043	1.00043	1.00043	1.00043
8	-0.00193	-0.00193	-0.00193	-0.00193	-0.00193
			3% noise		
6	0.04098	0.04086	0.04086	0.04086	0.04086
7	1.00119	1.00022	1.00022	1.00022	1.00022
8	0.02671	0.02669	0.02669	0.02669	0.02669
			5% noise		
6	0.06844	0.06830	0.06830	0.06830	0.06830
7	0.99035	0.98937	0.98937	0.98937	0.98937
8	0.03719	0.03716	0.03716	0.03716	0.03716
			7% noise		
6	0.09425	0.09410	0.09410	0.09410	0.09410
7	0.97097	0.97001	0.97001	0.97001	0.97001
8	0.04141	0.04138	0.04138	0.04138	0.04138

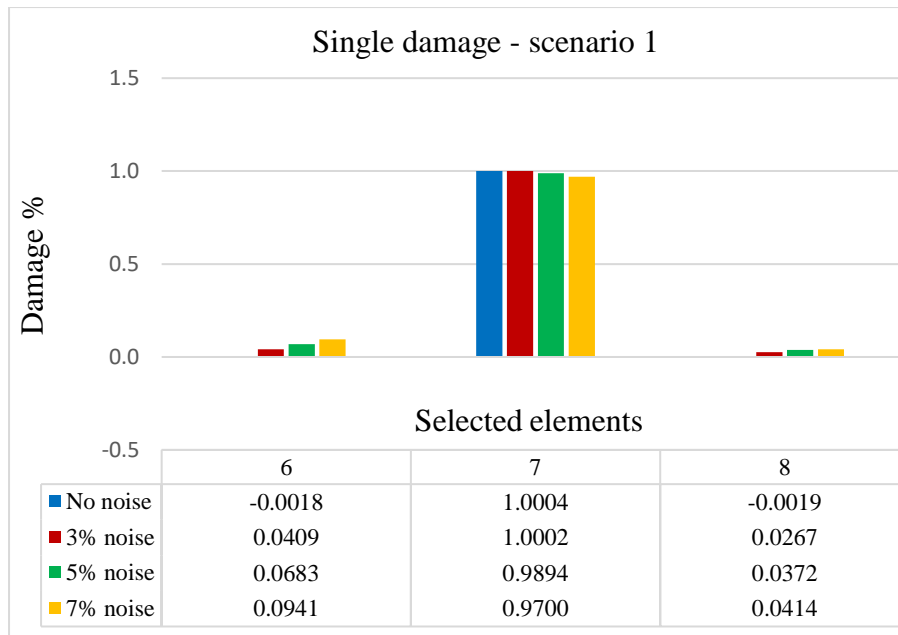


Figure 6.24 The extent of the damage, single damage, scenario 1 (element 7 with stiffness loss of 1%)

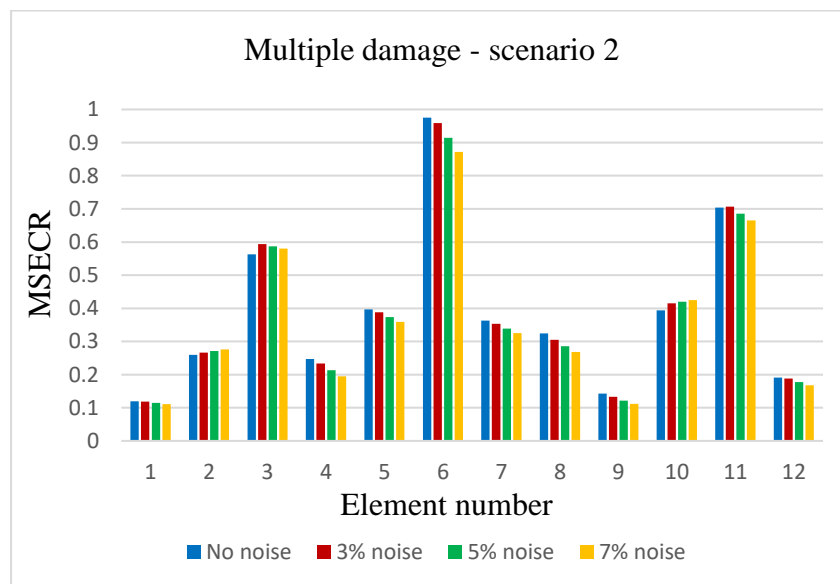


Figure 6.25 The MSECR of the elements, multiple damage, scenario 2 (elements 3, 6 and 11 with stiffness loss of 0.5, 1 and 0.75%, respectively)

As seen in Figure 6.25, elements 3, 6 and 11 are selected for the next stage to quantify their damage extents because of receiving a higher MSECR. The details are shown in Table 6.16 and drawn in Figure 6.26, respectively.

Table 6.16 Damage extent of selected element at each iteration, multiple damage, scenario 2 (elements 3,6 and 11 with stiffness loss of 0.5, 1 and 0.75%, respectively)

Element number	Iteration number				
	1	2	3	4	5
			no noise		
3	0.50385	0.50283	0.50283	0.50283	0.50283
6	1.00199	1.00005	1.00005	1.00005	1.00005
11	0.75014	0.74864	0.74864	0.74864	0.74864
			3% noise		
3	0.48211	0.48114	0.48114	0.48114	0.48114
6	1.03134	1.02926	1.02926	1.02926	1.02926
11	0.84701	0.84525	0.84526	0.84526	0.84526
			5% noise		
3	0.47023	0.46928	0.46928	0.46928	0.46928
6	1.04813	1.04596	1.04596	1.04596	1.04596
11	0.91208	0.91015	0.91015	0.91015	0.91015
			7% noise		
3	0.46116	0.46021	0.46021	0.46021	0.46021
6	1.06292	1.06066	1.06066	1.06066	1.06066
11	0.97662	0.97450	0.97451	0.97451	0.97451

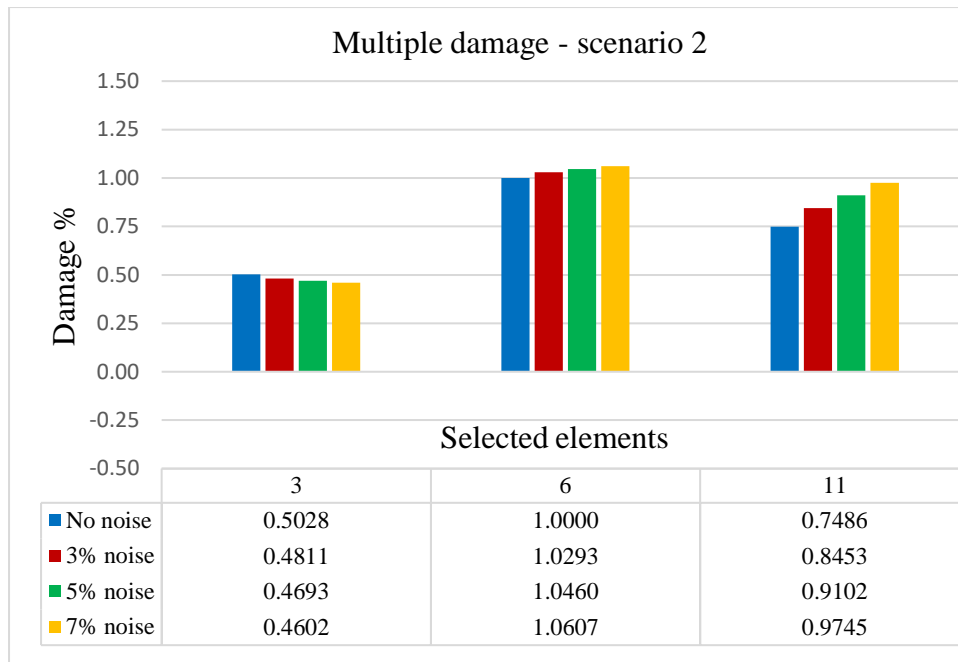


Figure 6.26 The extent of the damage, multiple damage, scenario 2 (elements 3,6 and 11 with stiffness loss of 0.5, 1 and 0.75%, respectively)

6.7.1 Discussion on quantifying the small damages

As shown in Figure 6.23, in single-damage scenario, elements 6, 7 and 8 are selected as the suspect damaged elements. The calculated coefficient of α_7 is 1.0004 percent as shown in Figure 6.24. The error in damage extent quantification is 0.04, 0.02, -1.06 and -3 percent for the conditions of no noise, 3, 5 and 7 percent noise level applied, respectively. In multiple-damage scenario also based on Figure 6.25, among the selected suspected elements 3, 6 and 11, the amount of α_3 , α_6 and α_{11} are calculated 0.50 1.00 and 0.75, respectively, as shown in Figure 6.26. The amount of error is shown in the following Table.

Table 6.17 The percentage of error of damage extent for selected elements with different noise level, scenario 2 (elements 3,6 and 11 with stiffness loss of 0.5, 1 and 0.75%, respectively)

Element number	Noise level			
	No noise	3%	5%	7%
3	0.56	-4.0	-6.2	-7.96
6	0	2.93	4.6	6.07
11	-0.186	12.7	21	29.93

6.8 Conclusion

Verification of the improved method in Chapter 4 was performed by applying it to several plane structures from simple to multi-part structures with different types of element, material properties, dimensions and numbers of DoFs. Single and multiple damage scenarios were considered for each structure as well. The mode shapes and natural frequencies were also contaminated by 3, 5 and 7 percent noise to simulate the environmental noise pollution. The improved method perfectly recognizes the damage in two stages. Stage one uses the first five modes to discriminate the probable elements that are exposure to damage. Stage two quantifies the extent of the damage among the suspected elements recognized from stage one.

The results indicate that the performance of the improved method is in a good agreement with the numerically assumed damages doing few computational cycles. It is because of that the improved method, firstly, has been established based on a very accurate MSE equation that decreases the error accumulation in computations.

Secondly, it employs a more accurate sensitivity matrix that helps decrease computations and accelerates convergence.

Besides, the method shows applicability to detect the damage in different types of structures such as beam, frame and truss models. Moreover, it can diagnose the damage in structures with a different type of elements such as beam, frame and truss elements and even different type of material properties. In this method, the size and dimension of the structure is not an issue, whatsoever. Furthermore, the method is capable of detecting any single and multiple damage in the structure. Finally, in presence of up to 7 percent noise, it quite performs well with almost the same number of iterations that normally requires for the case of no noise. Although the method is able to correspondingly detect the damage in presence of higher noise percentage, however, quantifying the damage in the second stage will require more efforts that demands more time and computational cycles which may not be cost effective for complex structure.

CHAPTER 7

EXPERIMENTAL VERIFICATIONS

This chapter illustrates experimental verifications of the improved MSE method proposed in Chapter 4. The proposed method is applied to some laboratory models with different features such as beam and frame like structures. Section 7.1 concisely presents the details of the models studied. Section 7.2 demonstrates the application of the proposed method to a simply-support steel beam. Section 7.3 explains the applicability of the proposed method to a cantilever beam model. Section 7.4 gives details of the damage detection of a three-story steel frame model using the improved MSE method. Lastly, section 8.5, concludes the overall results and observations.

7.1 Introduction

The laboratory tests were conducted at Banyo Pilot Plant Precinct of QUT and the HKPU to examine the performance of the improved method. Each model was tested at two cases, healthy and damaged. To collect the data, a sensory system was installed at the defined nodes. Each model was excited by an impact hammer as the input force. Then, the time history data was measured. Finally, the natural frequencies and mode

shapes were extracted from the measured time history data (acceleration) and FRFs (Fu and He, 2001).

Simulation of the damage was performed by either increasing the mass at selected elements (specimen 1) or decreasing the cross section of the elements (specimens 2 and 3). The numerical Eigen parameters of each model at two cases of damaged and undamaged are obtained through a MATLAB code or SAP2000. However, experimental mode shapes and natural frequencies are derived through DIAMOND (Doebling *et al.*, 1997a). Similar to the numerical studies, the performance of the improved method for each model is evaluated using a pair of datasets obtained from the damaged and undamaged cases of each model through a MATLAB code. To accurately acquire the experimental data, each test was repeated several times and averaged to overwhelm the effect of errors. However, the data are associated with only translational DoFs, since measuring the rotational DoFs is a difficult and expensive task. Although having those DoFs could give a better result and help understand the real behaviour of the structure.

In addition to performing each test in two cases, damage and undamaged, the models are also numerically modelled, and all analytical characteristics are derived as the healthy structures. The results are then compared with the experimental ones. The selected models studied are as follows.

The first specimen is a simply-support steel beam with the frame element as a basic structure that can simply characterize a part of any bridge or structure. The second model is a cantilever beam representing a part of any structure. The last sample is a three-story steel frame model representing a part of a building or a bridge. In these case studies, damages are created in different ways by adding mass or decreasing the stiffness of the desired elements. Moreover, different single and multiple damage scenarios at different parts of the models are studied. The results of each model are compared with its own FEM analysis, as well. Therefore, the improved method is comprehensively examined in different aspects.

7.1.1 Data processing

To process the data in the experimental case studies, the following equations are primarily used for normalization and standardization of the data.

7.1.1.1 Data normalization

To make the numerical and experimental data comparable, firstly, there is a need to all the time signals be normalized (Nair *et al.*, 2003) as follows.

$$y_{s,l}(t) = \frac{y_l(t)}{\sqrt{\sum_{j=1}^n y_{jl}(t)^2}} \quad (7.1)$$

where

S= Sensor location

l =Direction of measurement

j = the number of data points of the signal

7.1.1.2 Data standardization

In the next step, the data should be standardized (Lei *et al.*, 2003, Nair *et al.*, 2003, Nair *et al.*, 2006b, Krishnan Nair and Kiremidjian, 2007).

$$y_{sn,l}(t) = \frac{y_{s,l}(t) - \mu}{\sigma} \quad (7.2)$$

μ : The mean and

σ : Standard deviation of $y_{s,1}(t)$ (of normalized data)

7.2 Case study 1 (Specimen 1): A simply-support steel beam

The first experimental case study is a simply-support steel beam consisting of eight elements and nine nodes with 23 DoFs as shown in Figure 7.1 conducted at the QUT.

The FEM model of the specimen is shown in Figure 7.2, as well. The material properties, geometric data and damage details are as follows.

Table 7.1 Material properties and geometric information – experimental case study 1

Material or physical parameter	Symbol	Amount	Unit
Length of each element	l	0.4125	m
Total length of the model	L	3.30	m
Modulus of elasticity	E	206×10^9	N/m ²
Cross-sectional area (Hollow rectangular)	A	3.1064×10^{-4}	m ²
Second moment of area	I	3.18853×10^{-8}	m ⁴
Mass density	ρ	7870	kg/m ³

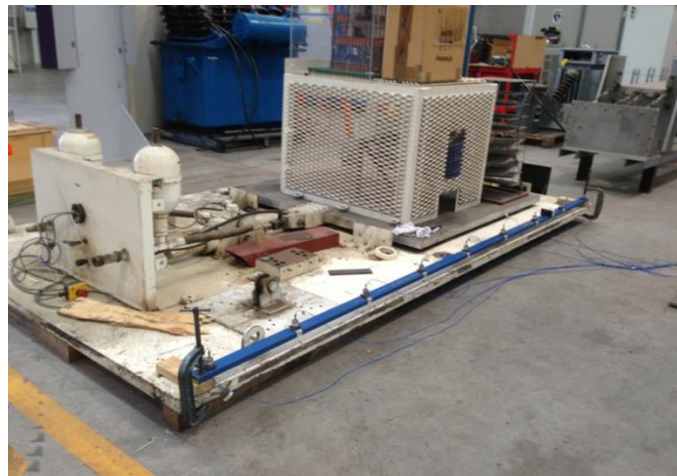


Figure 7.1 Physical model of the simply-support beam sample

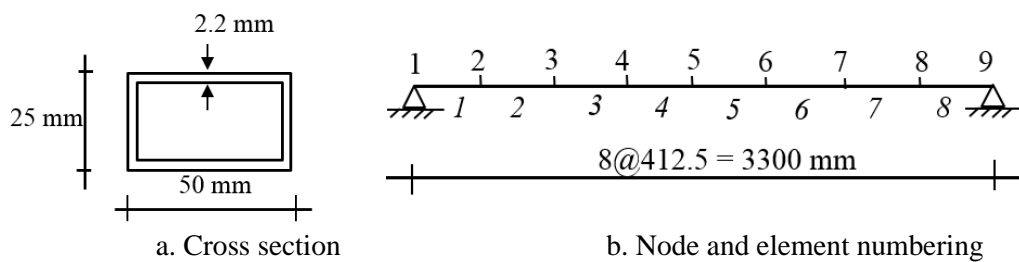


Figure 7.2 The FEM model of the simply-support beam

The current method uses the Eigenvalues and Eigenvectors of the structure in both damaged and undamaged cases and the stiffness of the structure in undamaged case. From the solution to the governing equation $M\ddot{x} + Kx = f(t)$ as an Eigen problem, it is mathematically clear that the effect of decreasing the stiffness of the system on

Eigenvalues and Eigenvectors equals adding a mass of the system. Therefore, in this study besides studying the effect of the stiffness reduction, an attempt was made to experimentally investigate the equivalency of adding mass and decreasing the stiffness and compare the experimental results with the numerical studies. Definitely, any damage that can be scaled or measured as a fraction reduction of the stiffness or increase of mass of the elements of a system can be recognized by the proposed method. However, there are many other types of damage that cannot be included in this category. Hence those types of damage are out of the scope of this study.

7.2.1 Damage cases made

One damage scenario is created in the model. The single damage created at element 7 by adding one kg mass on the element. The damage and the data measurement for each case is separately performed by exciting the structure using an impact hammer at a point near the left support. The excitation location is selected in such a way to acquire more experimental mode shapes.

7.2.2 Results of case study 1

In stage 1, to detect the damage location, the MSCER indicator is calculated and shown in Figure 7.3 using experimental data and Eq. (4.11). For this purpose, the first five mode shapes of both damaged and undamaged cases are used i.e. $m = 5$. The

suspected elements are picked up for further investigation in stage 2. As a single damage, elements 2, 3, 5 and 7 are selected because of having higher MSECR.

In stage 2, it is attempted to find the alpha coefficients to quantify the damage among the suspected elements. The single damage coefficients (α 's) using the improved method, applying Eq. (4.29) are shown in Figure 7.4.

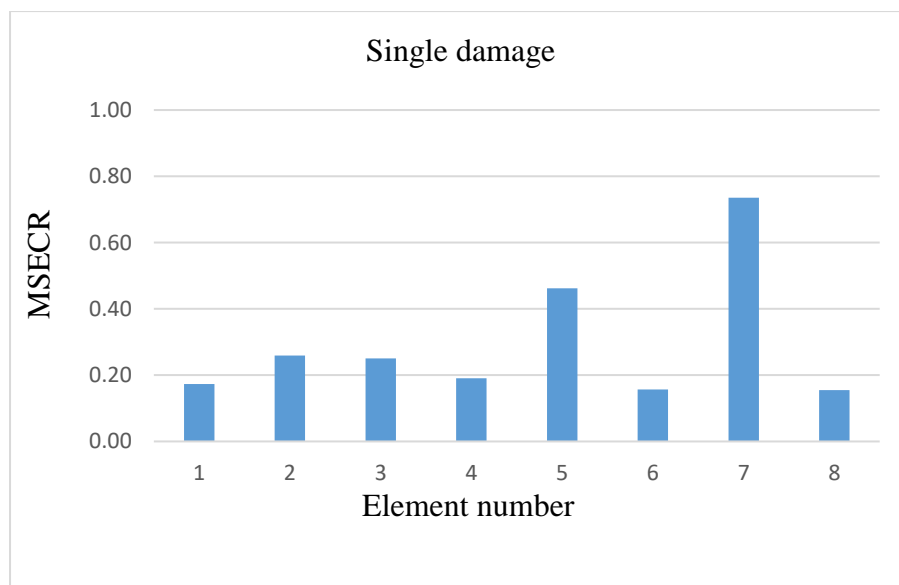


Figure 7.3 Experimental elemental MSECR, single damage scenario (element 7 with added mass of 1 kg)

As, it is seen from Figure 7.3, elements 2, 3, 5 and 7 are the suspected elements. So, they are selected, and their damage extent are quantified as Figure 7.4.

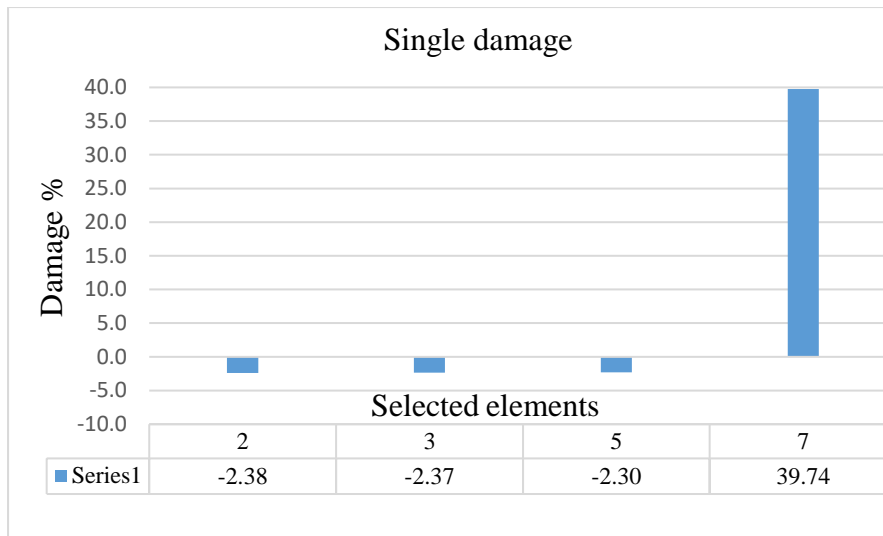


Figure 7.4 Experimental damage extents, single damage scenario (element 7 with added mass of 1 kg)

To find the equivalent damage caused by adding mass on the structure, the modal analysis of the system is performed considering it as a lumped mass added to the mass of the element under consideration. The natural frequencies and mode shape of the healthy and the damaged structure by adding mass are compared with those of damaged structure by loss in the stiffness. By interpolation, it is found that for a single damage, effect of adding 1 kg on element 7 equals around 31% loss in the stiffness of that element. The natural frequency of the structure for the first ten modes at different cases including healthy, damaged by adding mass and damaged by stiffness loss of 25-35% in element 7 are given in Table 7-2.

Table 7.2 Natural frequency of the structure in different cases, single damage (element 7 with added mass of 1 kg)

Mode no	Natural frequency (Hz)					
	A	B	C	D	E	F
1	7.48	7.31	7.38	7.35	7.35	7.32
2	29.91	28.58	28.95	28.70	28.64	28.41
3	67.38	65.00	65.26	64.75	64.65	64.21
4	120.10	117.73	117.97	117.47	117.37	116.94
5	188.65	185.24	186.46	185.85	185.72	185.17
6	274.08	268.26	269.61	268.40	268.15	267.06
7	377.76	372.08	371.13	369.61	369.30	368.01
8	531.10	525.41	522.23	520.30	519.91	518.32
9	661.23	651.20	649.77	647.09	646.53	644.20
10	780.17	786.55	759.25	753.80	752.65	747.78

A: Healthy structure
 B: Damaged by adding 1 kg mass on element 7
 C: Damaged By stiffness loss of 25% at element 7
 D: Damaged By stiffness loss of 30% at element 7
 E: Damaged By stiffness loss of 31% at element 7
 F: Damaged By stiffness loss of 35% at element 7

To compare the applicability of the improved method, the numerical data obtained from loss of stiffness of 31% at both damage scenarios are presented in the following figures.

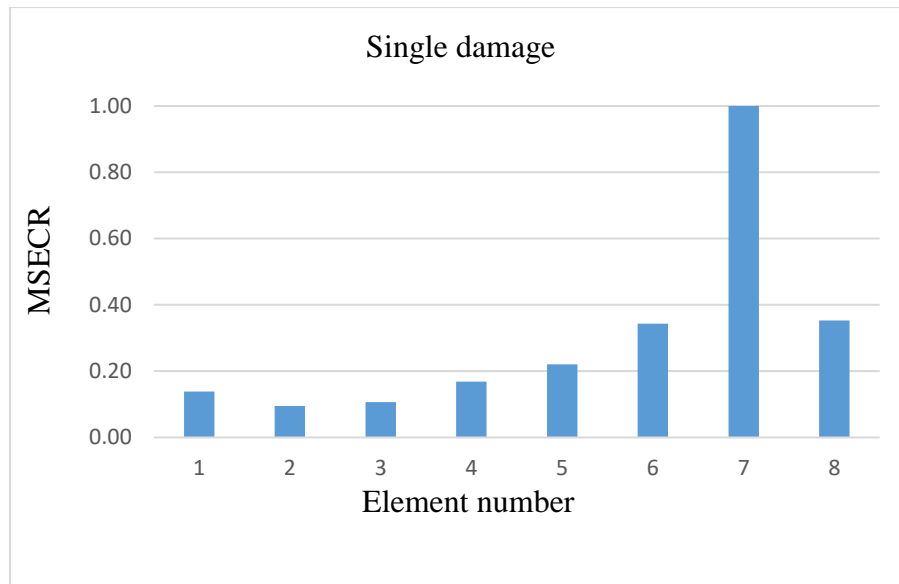


Figure 7.5 Numerical elemental MSECR, single damage scenario (elements 7 with added mass of 1 kg)

Figure 7.5 shows the suspected elements are 6, 7 and 8. The alphas are calculated and shown in Figure 7.6. It is seen that the only damaged element is element 7 with the amount of 32.80%.

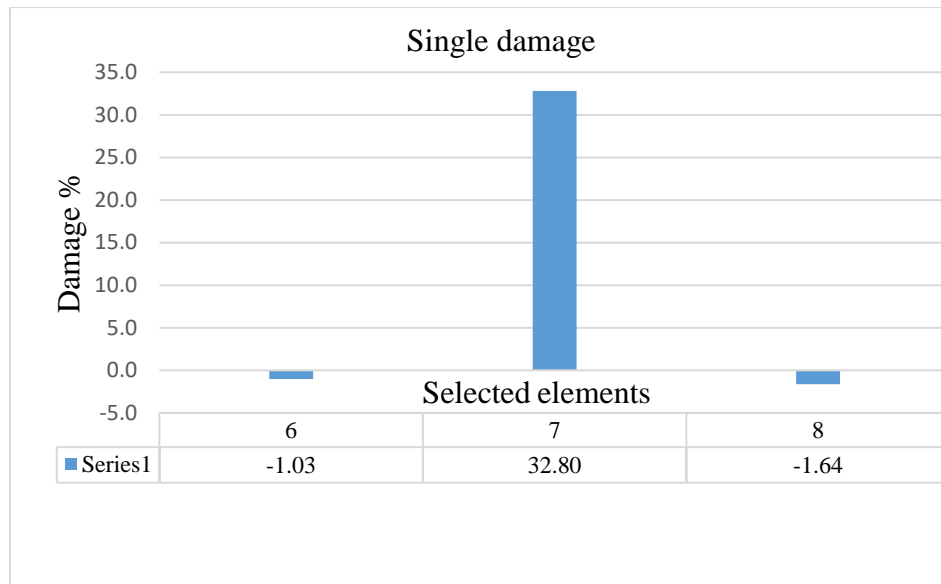


Figure 7.6 Numerical extent of the damage, single damage scenario (element 7 with added mass of 1 kg)

7.2.3 FEM analysis

FEM analysis is accomplished in order to, firstly, evaluate the correlation between mode shapes and natural frequencies from experiment and simulation that is presented in section 7.2.4. Secondly, to observe the theoretical equivalent damage in the model by adding the masses instead of damaging the cross sectional of the elements. From the Table 7.2, it is realized that for the single damage; the damage created by adding 1 kg mass equals around 31% decrease in local stiffness of the element under consideration.

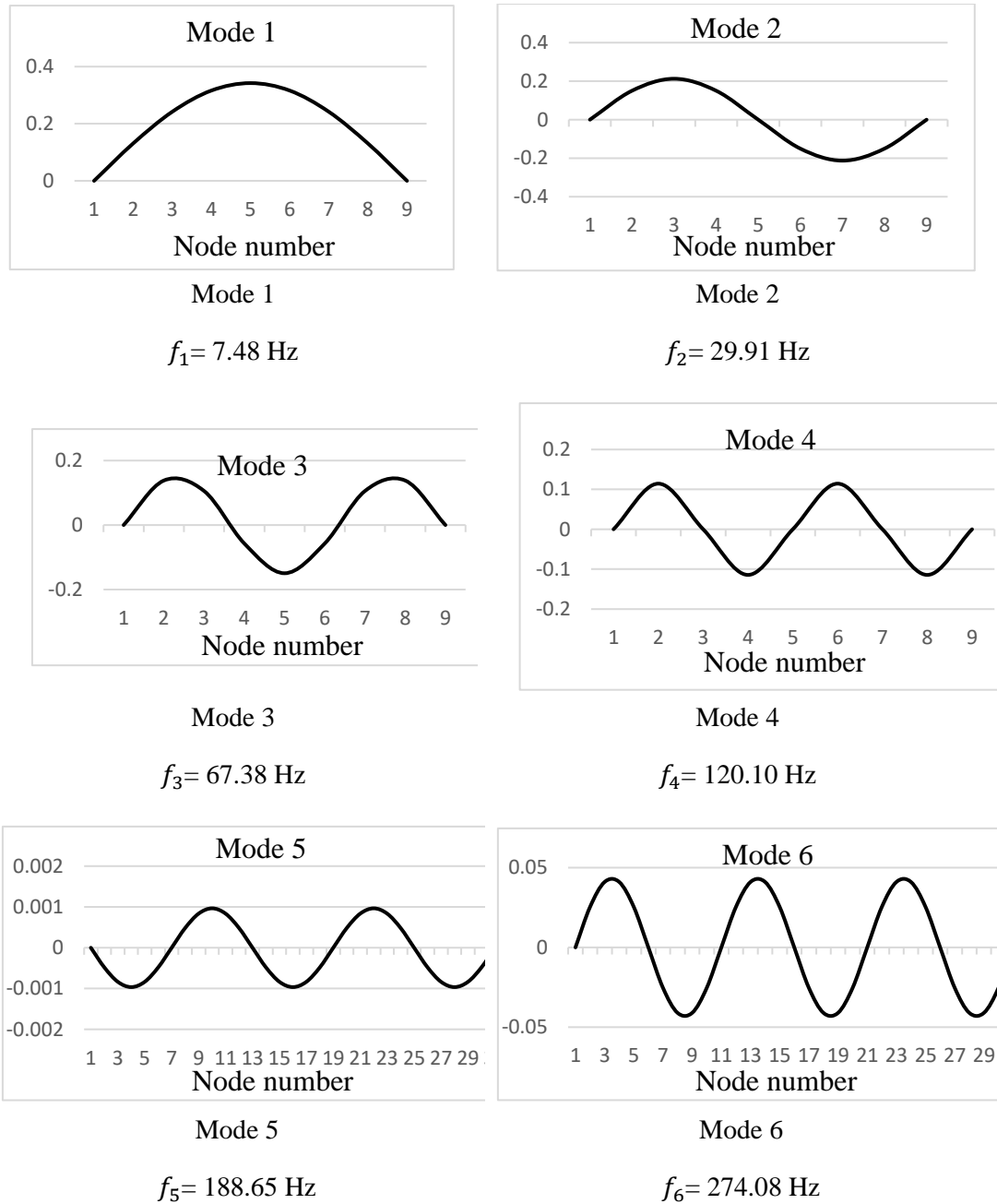


Figure 7.7 The first six numerical mode shapes of undamaged - sample 1

7.2.4 MAC value comparison

The MAC or modal correlation coefficient is used to determine the level of correlation between the mode shapes obtained from the experimental tests and the finite element

method (FEM) through the following equation (Farrar *et al.*, 2000, Sinou, 2009, Allemang, 2003)

$$MAC(\phi_{1i}, \phi_{2i}) = \frac{(\phi_{1i}^T \phi_{2i}^T)^2}{(\phi_{1i}^T \phi_{1i})(\phi_{2i}^T \phi_{2i})} \quad (7.3)$$

where i is the mode shape

The MAC values for the first eight mode shapes identified from FEM are compared with those mode shapes acquired from experiments to evaluate their correlation. This index is shown in Table 7.3 using Eq. (7.3) for the single damage.

Table 7.3 MAC values for comparison mode shapes identified from FEM compared with mode shapes acquired from experiments, single damage, case study 1

Mode/Test	1/Exp	2/Exp	3/Exp	4/Exp	5/Exp	6/Exp	7/Exp	8/Exp
1/FEM	1.000	0.005	0.009	0.001	0.021	0.000	0.024	0.000
2/FEM	0.000	0.991	0.018	0.017	0.000	0.041	0.000	0.022
3/FEM	0.020	0.002	0.977	0.012	0.029	0.000	0.042	0.001
4/FEM	0.000	0.035	0.001	0.984	0.004	0.034	0.000	0.027
5/FEM	0.021	0.000	0.035	0.000	0.992	0.009	0.025	0.001
6/FEM	0.000	0.032	0.000	0.033	0.002	0.979	0.017	0.027
7/FEM	0.021	0.000	0.030	0.001	0.039	0.005	0.968	0.002
8/FEM	0.000	0.018	0.000	0.016	0.000	0.031	0.008	0.996

7.2.5 Discussion on case study 1

According to Figure 7.3, as a single-damage scenario, element 7 has received the highest amount of the MSECR. Therefore, in addition to element 7, elements 2, 3, 5 and 7 are selected as the suspected damaged elements. The α coefficients calculated

in the second stage are shown in Figure 7.4 which indicate that the only true damaged element is element 7 with the extent of 39.74% loss in its local stiffness. Whilst the extent of the damage in other elements is negative and consequently zero.

It is seen, the MAC values shown in Table 7.3 demonstrate that the amount of mode shapes obtained from analytical solution and experimental studies has a good agreement.

However, there is some errors and false results. Because, the difference between the assumed and the actual boundary conditions of the model, effect of a high level of the noise, dis-connectivity of the mass added to the structure, and difference between the assumed and actual material properties of the model may contribute to error.

7.3 Case study 2 (Specimen 2): A cantilever beam model

The second experimental model is a cantilever steel beam consisting of eight elements and nine nodes as shown in Figure 7.8. The FEM model of the specimen is shown in Figure 7.9, also. The material properties, geometric data and damage details are as follows.

Table 7.4 Material properties and geometric information – experimental case study 2

Material or physical parameter	Symbol	Amount	Unit
Length of each element	l	0.10	m
Total length of the model	L	0.80	m
Modulus of elasticity	E	207×10^9	N/m^2
Cross-sectional area	A	2.500×10^{-4}	m^2
Second moment of area	I	5.208×10^{-10}	m^4
Mass density	ρ	7870	kg/m^3



a) Before installing the sensors



b) After installing the sensors

Figure 7.8 The cantilever beam model

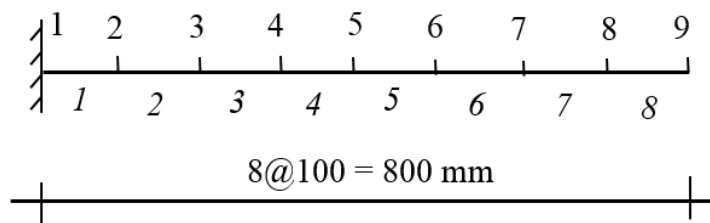


Figure 7.9 The FEM model of the cantilever beam model (dimensions are in mm)

7.3.1 Damage case created

The beam is divided into eight equal elements as shown in Figure 7.10. The only damage is introduced at the first element by reduction of cross section width from 50 mm to 30 mm as shown in Figure 7.10. Since the ratio of width of the cross section after damage to before damage is $3/5=0.60$, therefore, the ratio of reduction in the area and second moment of inertia are also 0.60. As stiffness is directly related to the area and the second moment inertia of the cross section, so the remaining stiffness is 0.60 which represents 0.40 loss. Practically, inducing a larger damage in the model is better to decrease the error in measurement of the geometry and overcome the noise pollution of the lower damage percentage in the environment. Therefore, in this case study, damage of 40% is applied to the model.

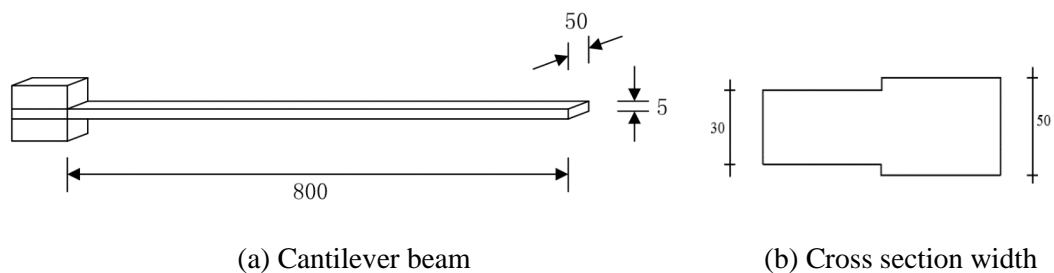


Figure 7.10 The cantilever beam model (dimensions are in mm)

7.3.2 Results of case study 2

In stage 1, to detect the damage locations, the MSCER parameter is calculated and shown in Figure 7.11 using Eq. (4.11). For this purpose, damage extent of 40% is

applied to the model and shown in Figure 7.12. The suspected elements are selected for further investigation in stage 2. In stage 2, it is tried to find the alpha coefficients to quantify the damage among the suspected elements of 1, 2 and 3 as the elements with the higher amounts of MSECR. The single damage coefficients (α 's) using the improved method for different percentages, using Eq. (4.29) are shown in Figure 7.16.

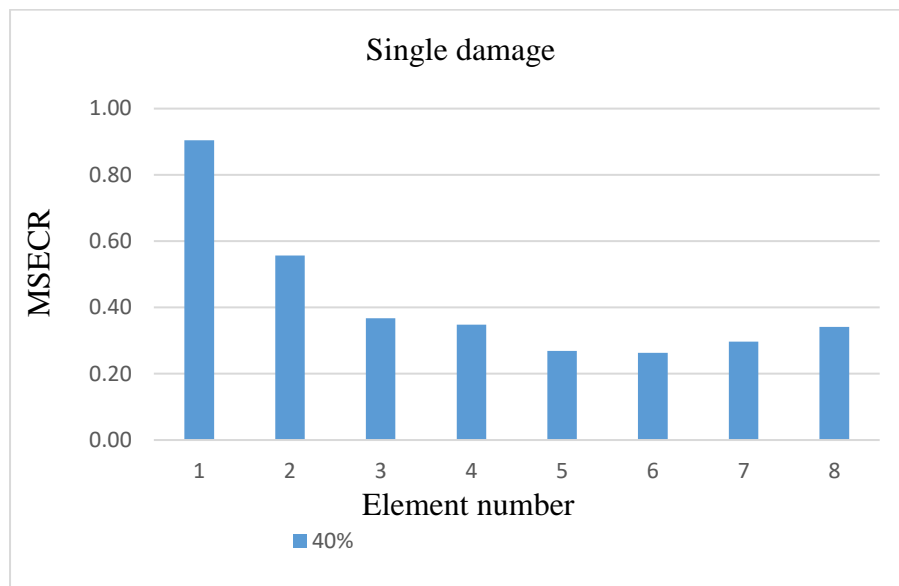


Figure 7.11 Numerical MSECR of the elements, single damage scenario (element 1 with stiffness loss of 40%)

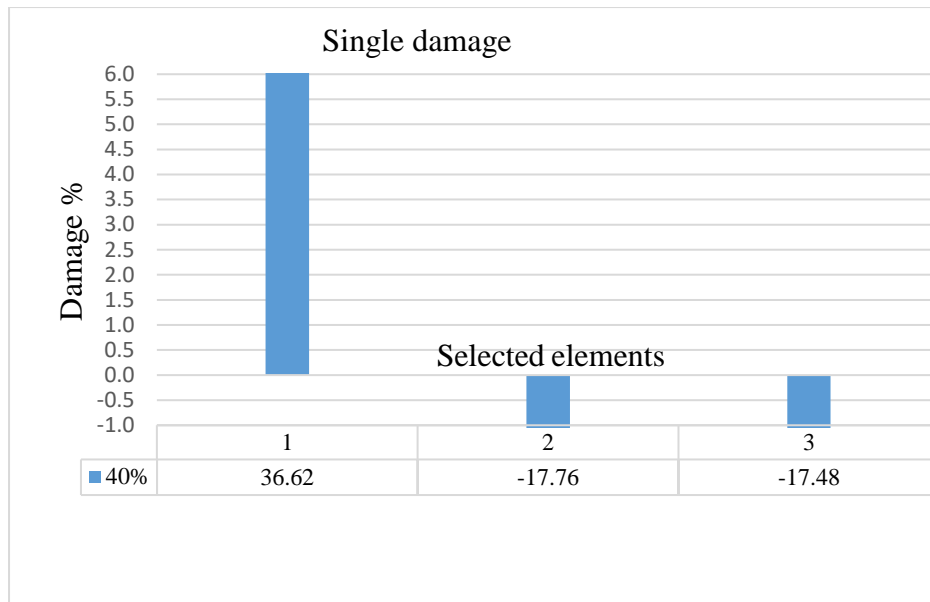


Figure 7.12 Numerical extent of the damage, single damage scenario (element 1 with stiffness loss of 40%)

To compare with the experimental observation, the results of the experimental single damage with stiffness loss of 40% in element 1 are shown in Figure 7.13. It is seen, elements 1 and 2 are the suspected elements. Figure 7.14 shows the alphas for suspected elements.

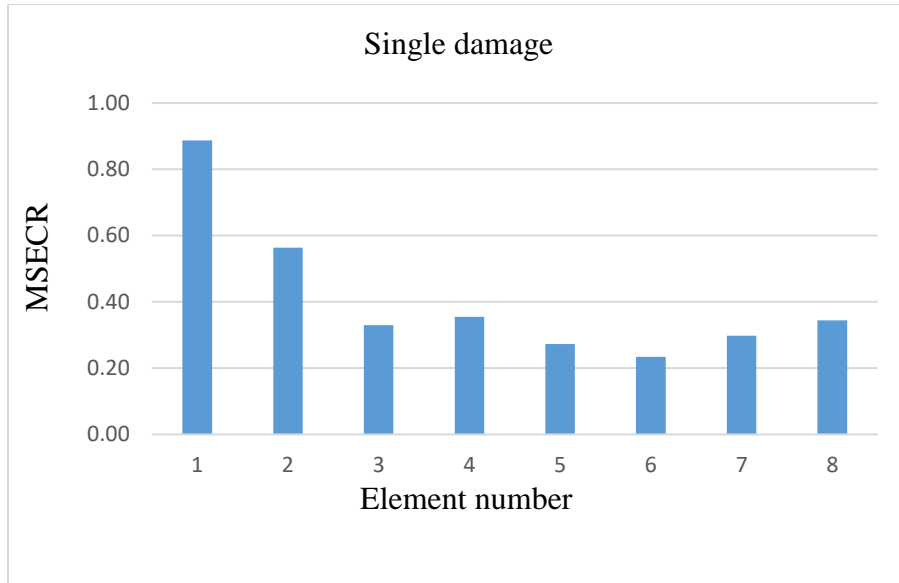


Figure 7.13 Experimental MSECR of the elements, single damage scenario (element 1 with stiffness loss of 40%)

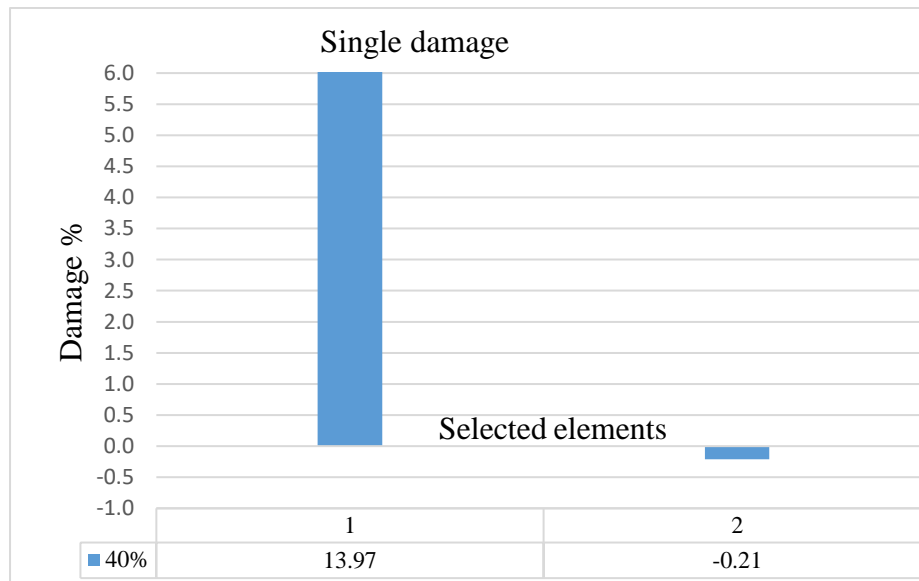


Figure 7.14 Experimental extents of the damage, single damage scenario (element 1 with stiffness loss of 40%)

7.3.3 FEM analysis

Similar to the case study 1, the FEM analysis is performed to assess the correlation between mode shapes and natural frequencies from experimental test and numerical simulation that is shown in section 7.3.4. It is seen that the FEM analysis of the damaged model gives a good agreement with experimental results. For more information, the first six numerical mode shapes of undamaged model are shown in Figure 7.15.

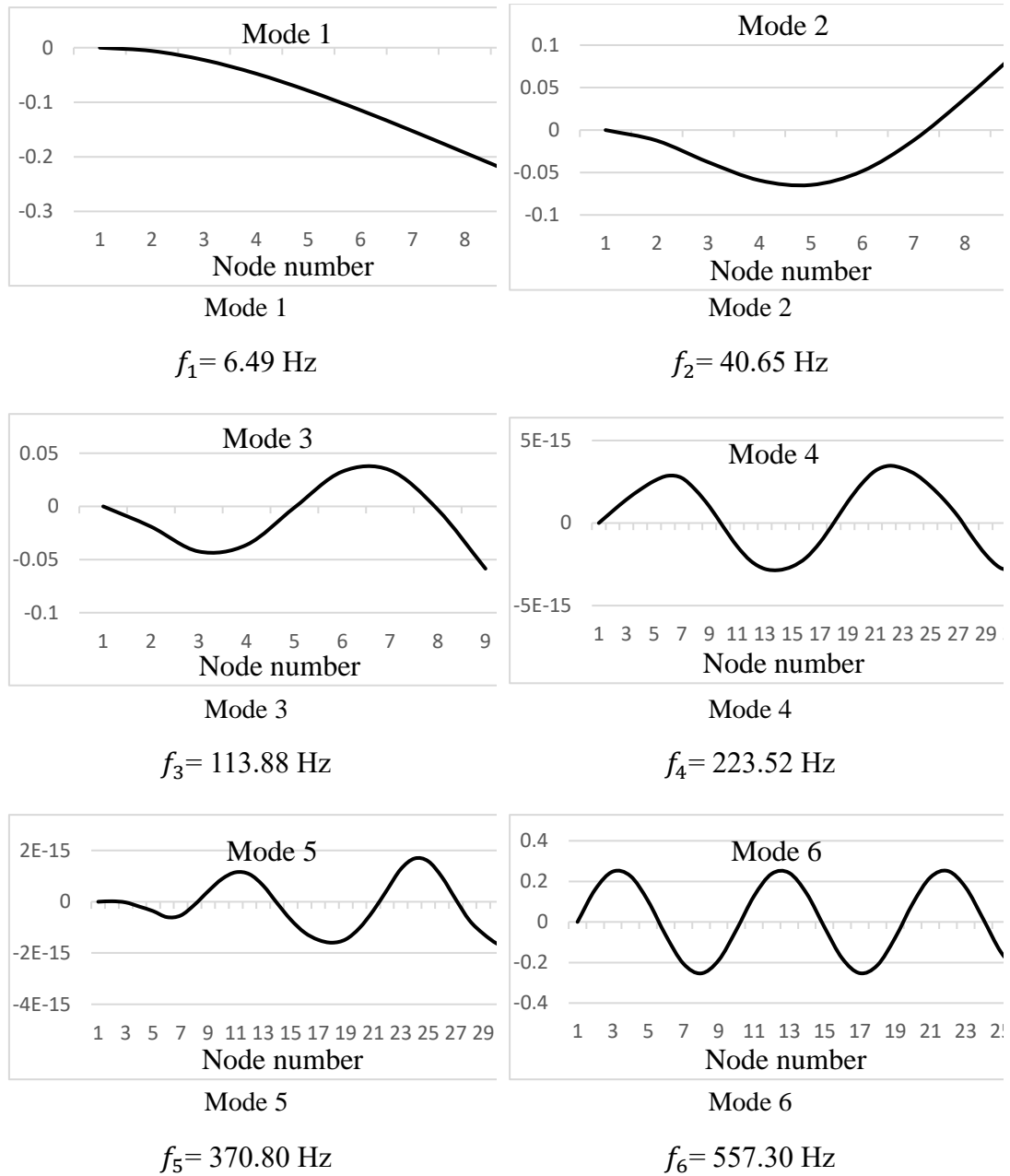


Figure 7.15 The first six numerical mode shapes of undamaged sample 1

7.3.4 MAC value comparison

The comparison of the MAC values of the first eight mode shapes identified from FEM are shown in Table 7.5.

Table 7.5 MAC values for comparison mode shapes identified from FEM compared with mode shapes acquired from experiments, single damage, case study 2

Mode/Test	1/Exp	2/Exp	3/Exp	4/Exp	5/Exp	6/Exp	7/Exp	8/Exp
1/FEM	0.999	0.370	0.078	0.107	0.056	0.061	0.061	0.057
2/FEM	0.351	1.000	0.288	0.097	0.140	0.094	0.097	0.125
3/FEM	0.076	0.284	0.996	0.216	0.086	0.131	0.098	0.136
4/FEM	0.115	0.103	0.174	0.986	0.183	0.075	0.148	0.084
5/FEM	0.049	0.154	0.096	0.104	0.990	0.184	0.046	0.226
6/FEM	0.067	0.079	0.135	0.084	0.101	0.992	0.261	0.013
7/FEM	0.045	0.114	0.069	0.138	0.057	0.134	0.974	0.429
8/FEM	0.070	0.101	0.192	0.054	0.236	0.028	0.225	0.925

7.3.5 Discussion on case study 2

In this case study only one single damage scenario is conducted. As shown in Figure 7.13, element 1 has received the highest amount of the MSECR. Other elements have received a lesser amount of the MSECR. So, element 1 is one of the suspected elements with a strong possibility of damage. The damage extents calculated in stage 2, shown in Figure 7.14, state that element 1 is really damaged although other elements also show some damage extents.

Besides, in is also seen, the method recognizes the damage using numerical mode shapes in Figures 7.11 and 7.12. It is seen that there is an agreement between analytical solution and experimental damage implemented in the model. Another reason for this is the MAC values which also shows a good agreement between analytic and experimental mode shapes as has indicated in Table 7.2.

However, there are some errors and false results. For this case, the similar reasons stated at section 7.2.5 are possible. In addition, creating the exact damage in the model is difficult and even may increase the modelling error. For the last model studied, limited sensors to simultaneously measure the required DoFs, and therefore data processing, also impacts the results.

7.4 Case study 3 (Specimen 3): A three-story steel frame model

The last experimental case study is a three-story steel frame consisting of 15 elements and 14 nodes with 36 DoFs as shown in Figure 7.16 conducted at HKPU. The FEM model of the specimen is also shown in Figure 7.17. The material properties, geometric data and damage details are as follows.

Table 7.6 Material properties and geometric information – experimental case study 3

Material or physical parameter	Symbol	Amount	Unit
Beam cross-sectional area	A_b	1.476×10^{-3}	m^2
Column cross-sectional area	A_c	1.449×10^{-4}	m^2
Beam second moment of area	I_b	1.074×10^{-7}	m^4
Column second moment of area	I_c	1.029×10^{-10}	m^4
Modulus of elasticity	E	207×10^9	N/m^2
Mass density	ρ	7870	kg/m^3



a) Top view



b) Side view

Figure 7.16 Physical model of the three-story steel frame

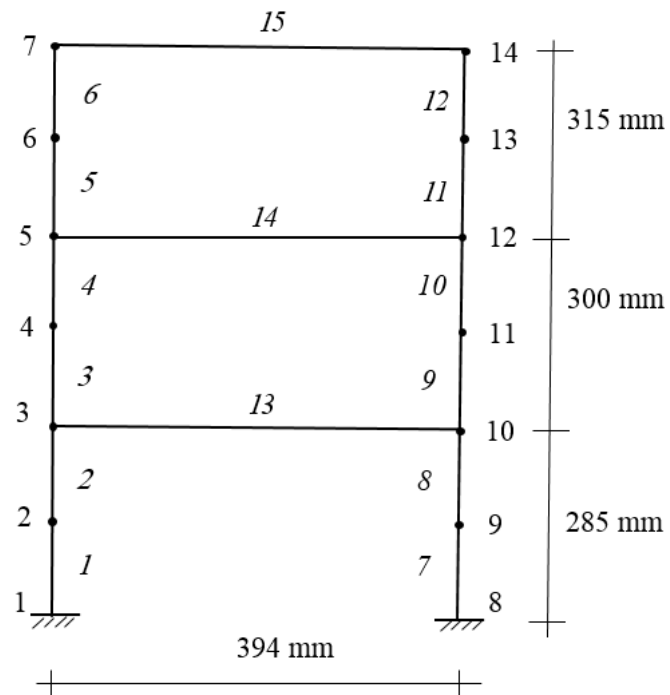


Figure 7.17 FEM model of the three-story steel frame model

Several tests are performed at different cases of entire and damaged model. The discrete time data is collected via accelerometers using an impact hammer. The details of the sensor's sensitivity are tabulated in Table 7.7.

Table 7.7 Sensitivity of accelerometer sensors

Channel no.	1	2	3	4	5
Sensitivity (pc/ms ⁻²)	3.15	3.16	12.09	9.99	3.22
Channel no.	6	7	8	Hammer	
Sensitivity (pc/ms ⁻²)	3.17	11.49	11.28	4.19	

The model is excited using an impact hammer. Each dataset includes accelerations at nine channels (including force) during 90 sec with the frequency of 1000 Hz. A typical vibration from sensor 4 (data set 155), case 1 is shown in Figure 7.18 considering only the first 10 seconds.

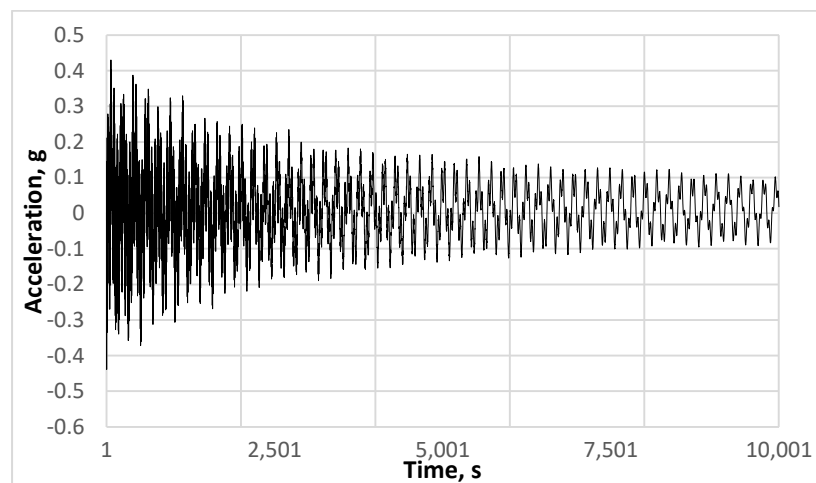


Figure 7.18 Typical time series data acquired from Channel 4, case 1

There were only eight sensors available, which are very limited to measure 24 DOFs. Therefore, several tests were done with different locations of the eight sensors and then the data were combined. One of the typical sensor locations is shown in Figure 7.19.

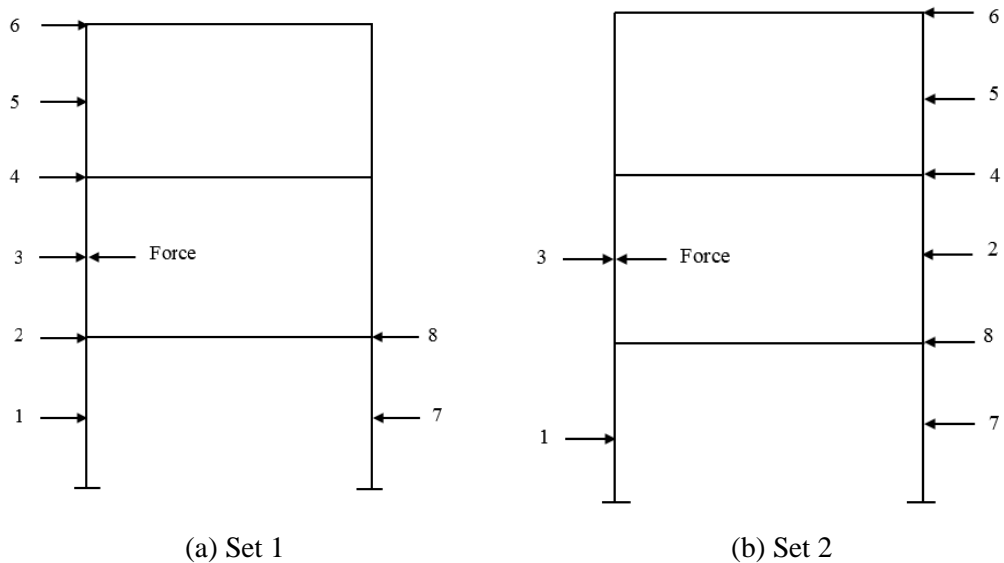


Figure 7.19 Typical sensor placement

7.4.1 Damage cases created

Three damage scenarios were created in the model as follows.

- a) Case 1: Single damage at left column in the third floor (note, the column is also considered as two elements.)
- b) Case 2: Multiple damage at both columns in the third floor (note, this column is also considered as two elements.)

- c) Case 3: Multiple damage at left column in the third floor and a beam in the second floor

To get more accuracy, each column is divided into two elements, therefore, the amount of damage implemented at each case is as follows.

- a) Case 1: 20% damage in any of element 5 and 6. The damage was created by decreasing the width of the beam by 20%, 10 percent from each side.
- b) Case 1: 20% damage in any of element 5, 6, 11 and 12. The damage was created like case 1.
- c) Case 3: 20% damage in any of element 5 and 6 and 99% in element 14. The damage at elements 5 and 6 was created like case 1 and 2 and the damage in the beam was conducted by adding a beamlike mass as shown in Figure 7.20.

7.4.2 Results of case study 3

In stage 1, for experimental studies, to detect the single and multiple damage locations, the MSCER indicator is calculated and shown in Figures 7.20, 7.26 and 7.31, respectively, using Eq. (4.11). For this purpose, the first five mode shapes of both damaged and undamaged cases are used i.e. $m=5$. The suspected elements are selected for further investigation in stage 2. In stage 2, it is tried to find the alpha coefficients

to quantify the damage among the suspected elements. The single and multiple damage coefficients (α 's) using the improved method, applying Eq. (4.29) are shown in Figures 7.21-22, 7.27-28 and 7.32, respectively. For each case, the numerical study comes after the experimental as follows.

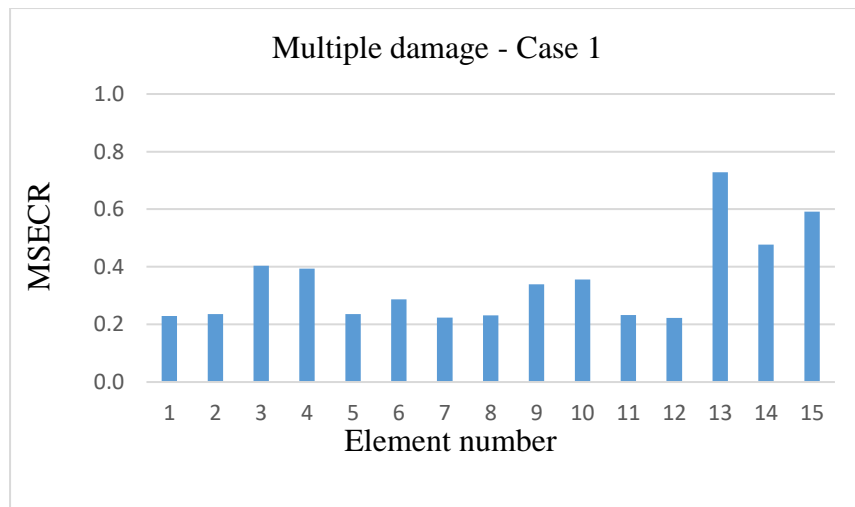


Figure 7.20 The Experimental elemental MSECR, Multiple damage, Case 1 (elements 5 and 6 with stiffness loss of 20% in each)

From Figure 7.20, elements 3, 4, 6, 10, 13, 14 and 15 have received a higher amount of the MSECR. These are selected as the suspected elements. However, it is better to select a smaller set of elements at each iteration step in order to get more accuracy. Normally, selecting a maximum 25% of the total number of elements as a set gives a reasonable result. So, here, the suspected element is divided by two sets. Set 1, elements 3, 4, 6, 9 and 10 and set 2 elements 13, 14 and 16. The stage two (quantifying the damage) separately applies to each set as shown in Figures 7.21 and 7.22. It is seen, some elements receive a negative amount of the damage that means there is no damage.

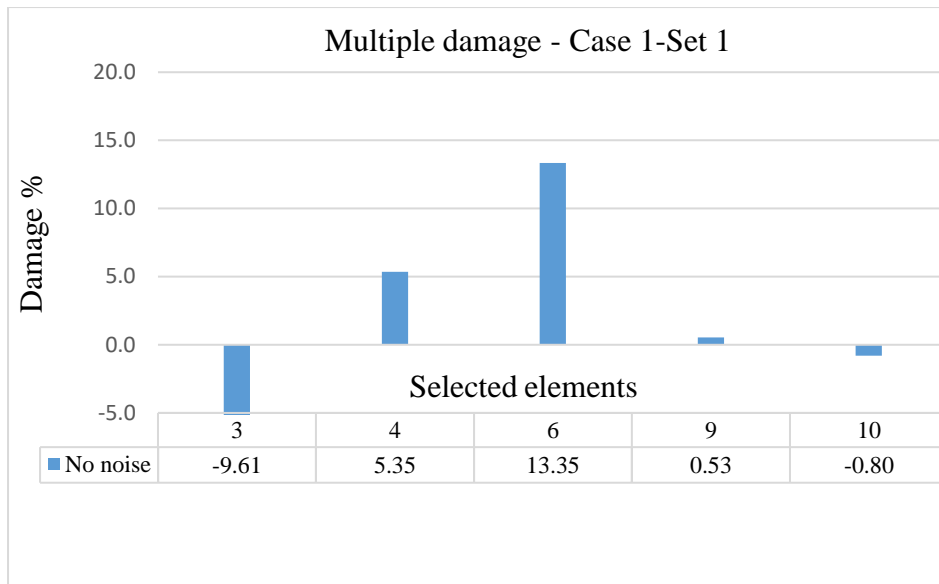


Figure 7.21 Experimental damage extent, Multiple damage, Case 1, Set 1 (elements 5 and 6 with stiffness loss of 20% in each)

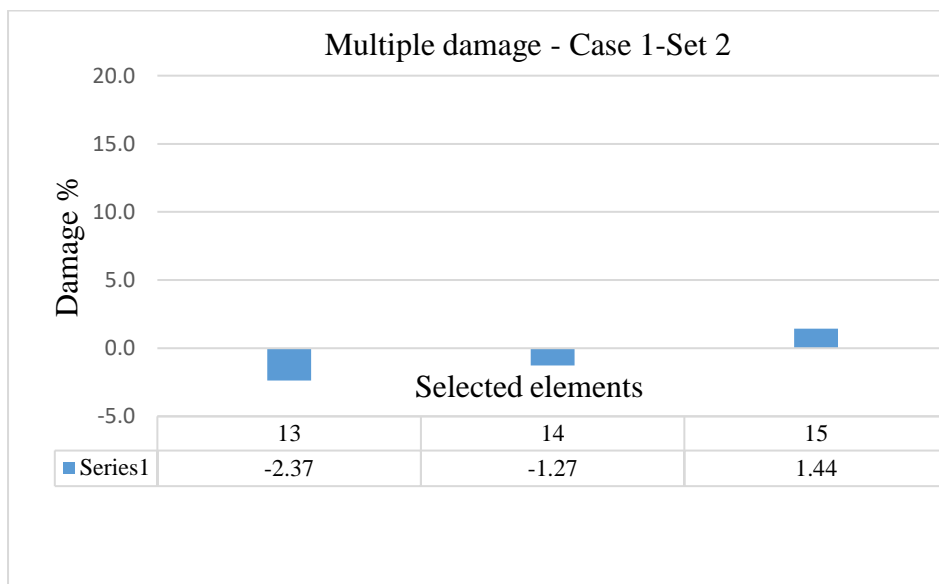


Figure 7.22 Experimental damage extent, Multiple damage, Case 1, Set 2 (elements 5 and 6 with stiffness loss of 20% in each)

Numerical simulation is also conducted for each case and instantly presented after that experimental case. However, the procedure of damage detection for numerical and experimental of each case is same.

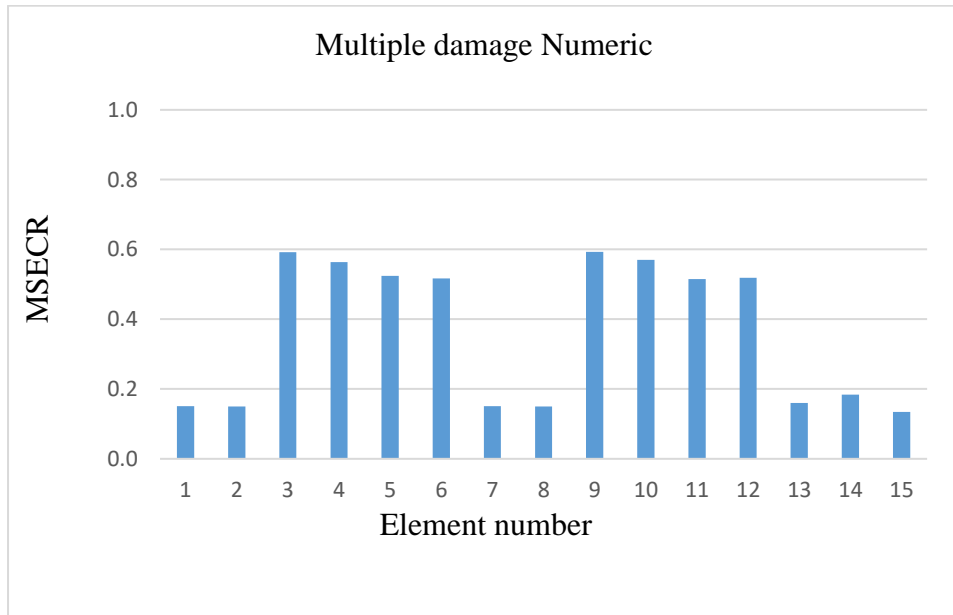


Figure 7.23 Numerical elemental MSECR, Multiple damage, Case 1 (elements 5 and 6 with stiffness loss of 20% in each)

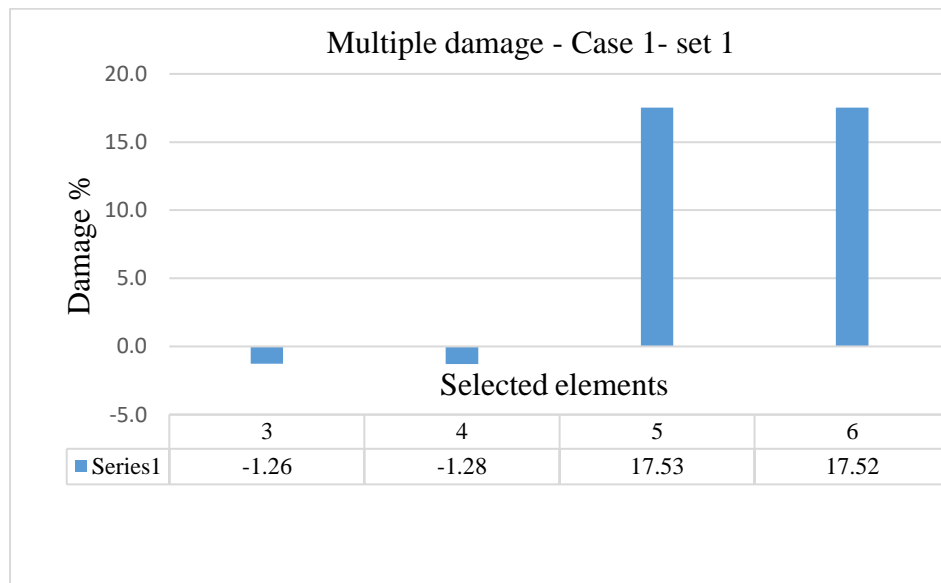


Figure 7.24 Numerical damage extent, Multiple damage, Case 1, Set 1 (elements 5 and 6 with stiffness loss of 20% in each)

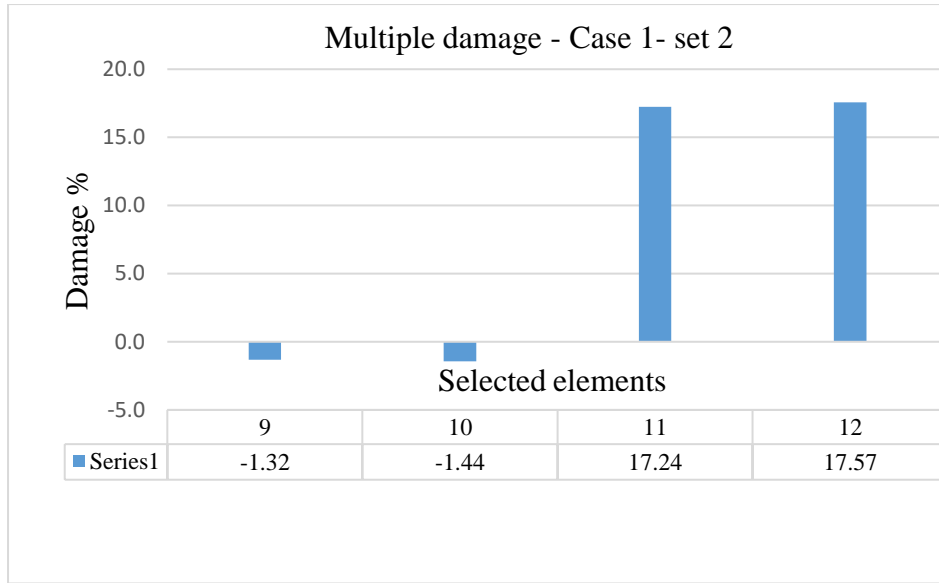


Figure 7.25 Numerical damage extent, Multiple damage, Case 1, Set 2 (elements 5 and 6 with stiffness loss of 20% in each)

For the second case, since there are many suspected candidates for damage, again the elements are divided into two set to get the better results.

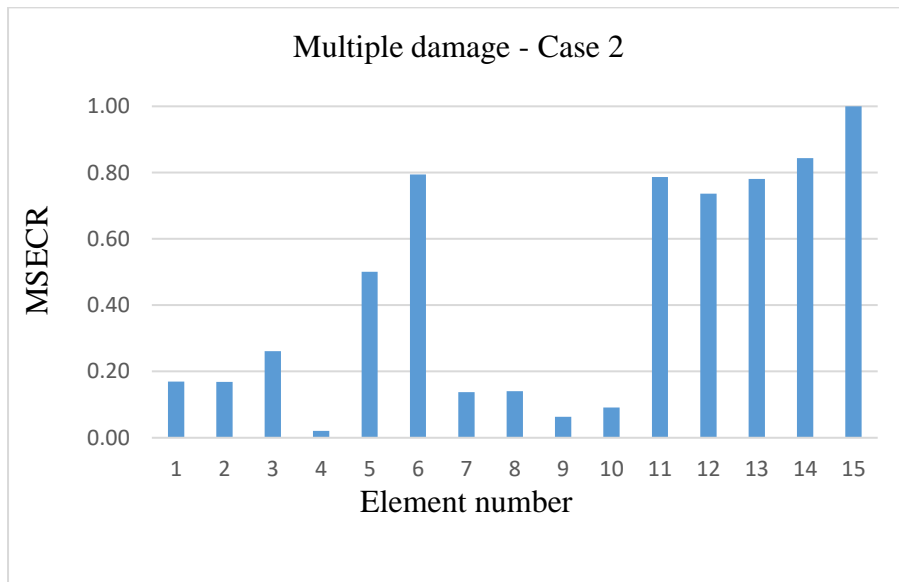


Figure 7.26 Experimental elemental MSECR, Multiple damage, Case 2 (elements 5, 6, 11 and 12 with stiffness loss of 20% in each)

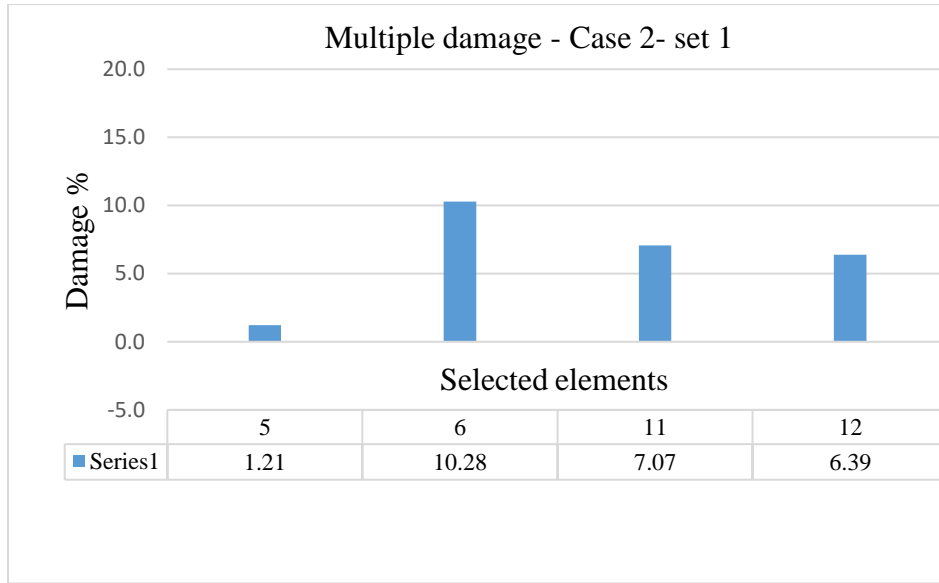


Figure 7.27 Experimental damage extent, Multiple damage, Case 2, Set 1 (elements 5, 6, 11 and 12 with stiffness loss of 20% in each)

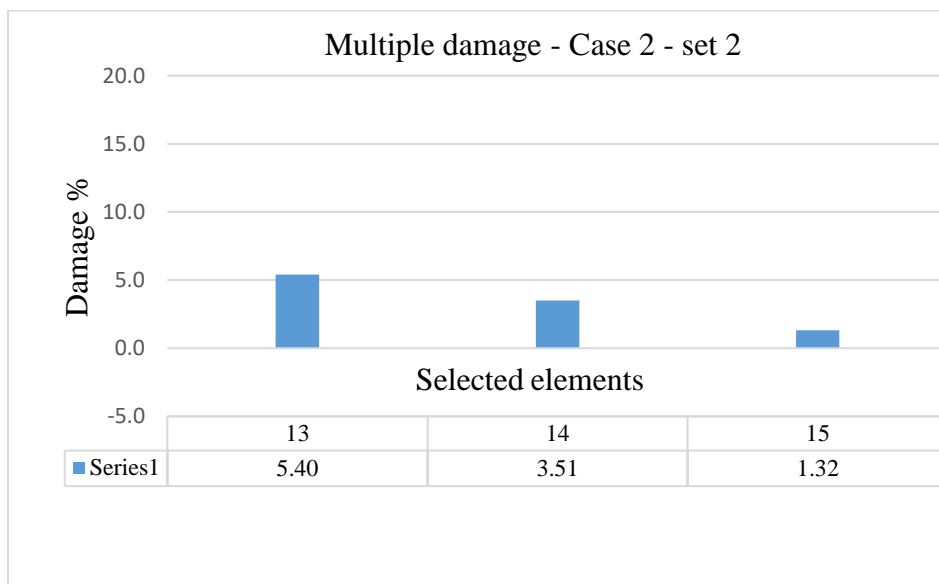


Figure 7.28 Experimental damage extent, Multiple damage, Case 2, Set 1 (elements 5, 6, 11 and 12 with stiffness loss of 20% in each)

The following numerical case is very perfect and recognizes the damage in one set of suspected elements.

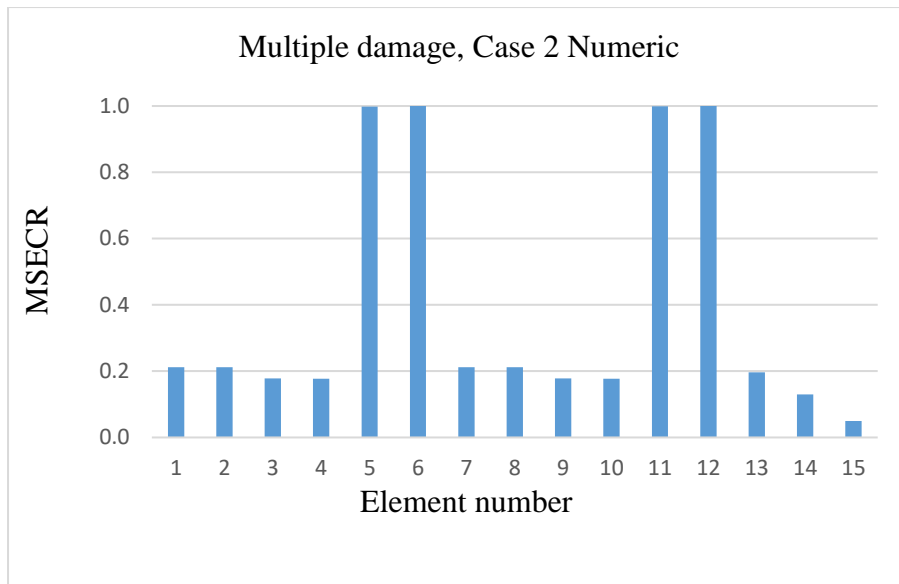


Figure 7.29 Numerical elemental MSECR, Multiple damage, Case 2 (elements 5, 6, 11 and 12 with stiffness loss of 20% in each)

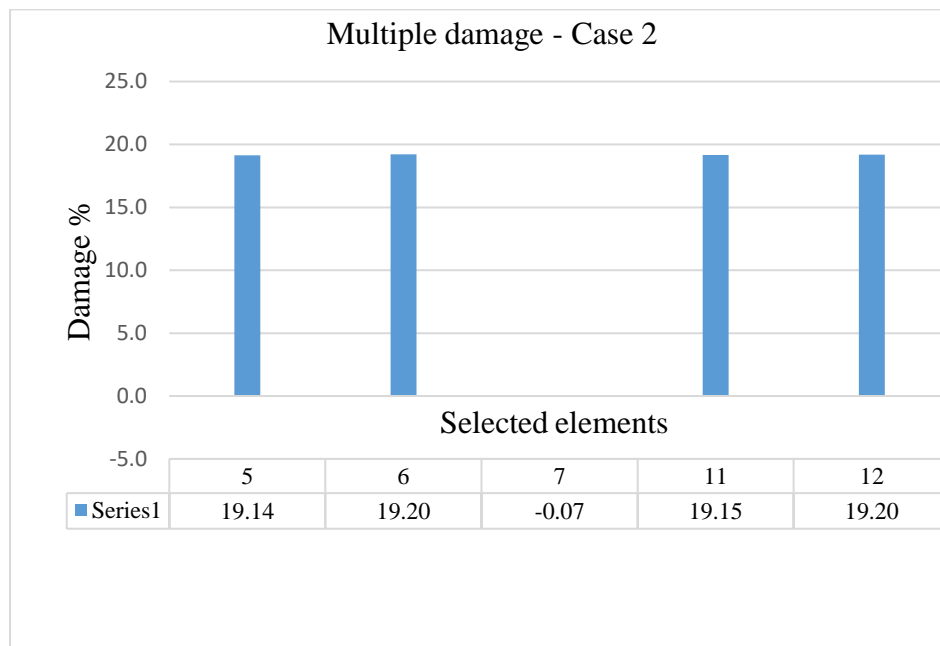


Figure 7.30 Numerical damage extent, Multiple damage, Case 2 (elements 5, 6, 11 and 12 with stiffness loss of 20% in each)

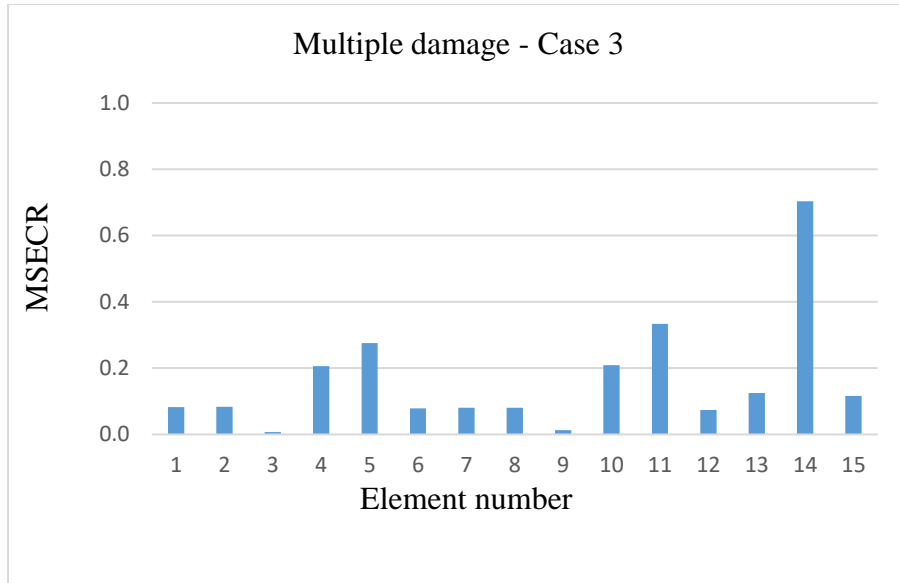


Figure 7.31 Experimental elemental MSECR, Multiple damage, Case 3 (elements 5, 6 and 14 with stiffness loss of 20, 20 and 99%, respectively)

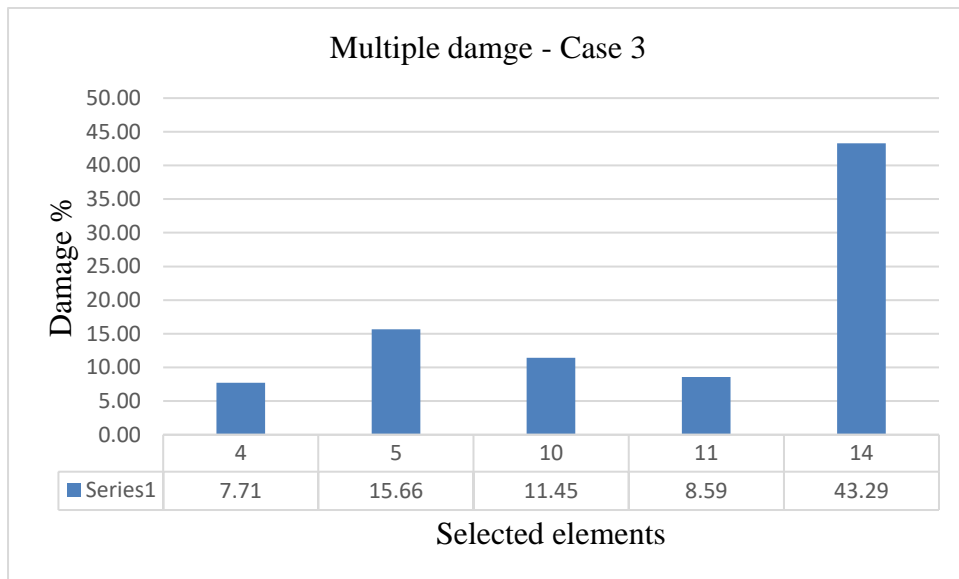


Figure 7.32 Experimental damage extent, Multiple damage, Case 3 (elements 5, 6 and 14 with stiffness loss of 20, 20 and 99%, respectively)

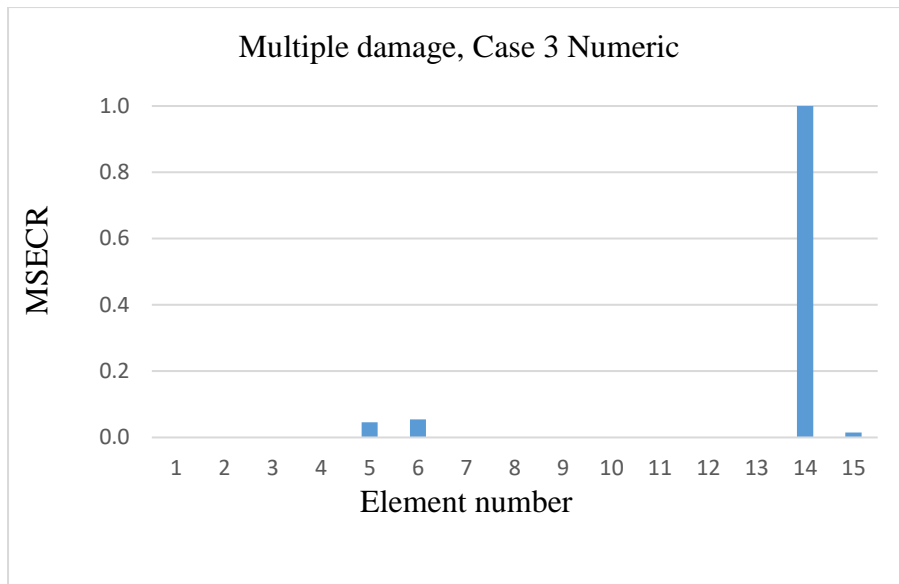


Figure 7.33 Numerical elemental MSECR, Multiple damage, Case 3 (elements 5, 6 and 14 with stiffness loss of 20, 20 and 99%, respectively)

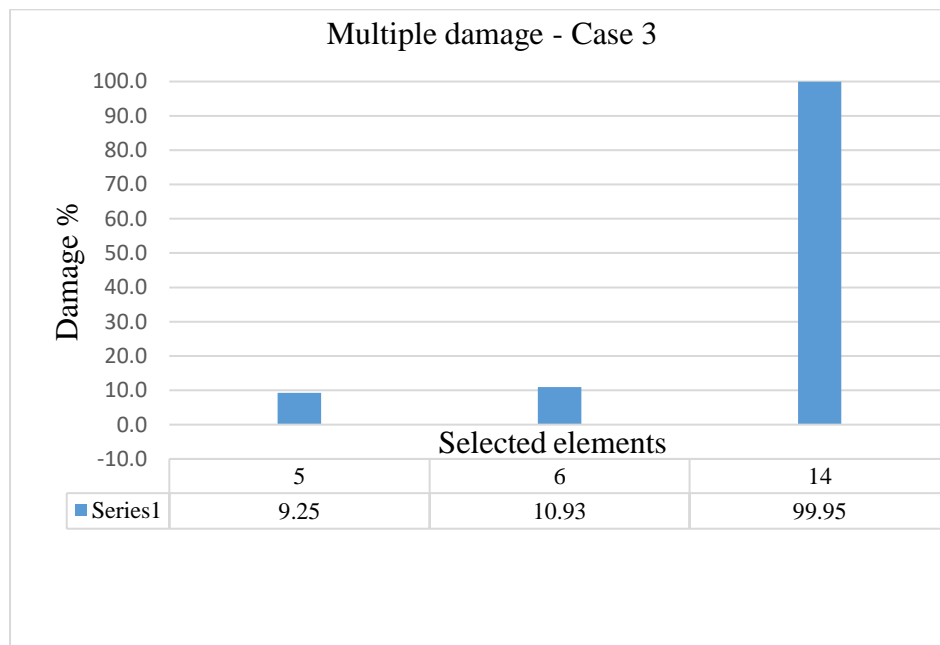


Figure 7.34 Numerical damage extent, Multiple damage, Case 3 (elements 5, 6 and 14 with stiffness loss of 20, 20 and 99%, respectively)

7.4.3 FEM analysis

Similarly, the FEM analysis is performed using SAP2000 and MATLAB to assess the correlation between mode shapes and natural frequencies from experiment and simulation that is shown in section 7.4.4. Also, FEM analysis of the damaged model shows a good agreement with experimental results. For more information, the first six numerical mode shapes of undamaged model are shown in Figure 7.35.

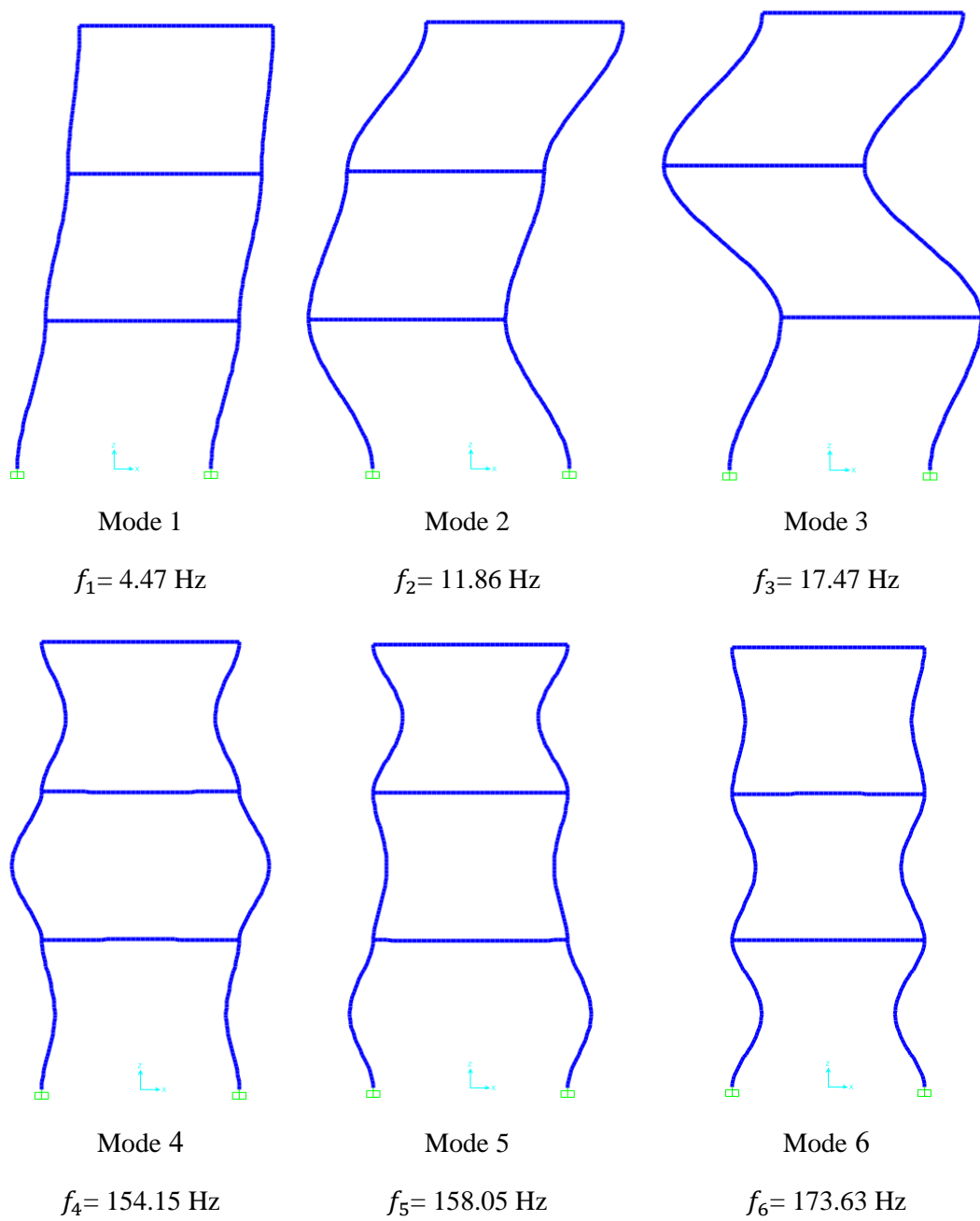


Figure 7.35 The first six numerical mode shapes of undamaged sample 3

7.4.4 MAC value comparison

The comparison of the MAC values of the first eight mode shapes identified from FEM for three cases of single and multiple damages are shown in Tables 7.8-7.10, respectively.

Table 7.8 MAC values for comparison mode shapes identified from FEM compared with mode shapes acquired from experiments, single damage, case 1, case study 3

Mode/Test	1/Exp	2/Exp	3/Exp	4/Exp	5/Exp	6/Exp	7/Exp	8/Exp
1/FEM	0.998	0.001	0.000	0.001	0.014	0.000	0.010	0.000
2/FEM	0.005	0.995	0.000	0.000	0.002	0.000	0.040	0.000
3/FEM	0.000	0.014	0.999	0.000	0.015	0.000	0.004	0.000
4/FEM	0.000	0.000	0.000	0.989	0.000	0.000	0.000	0.000
5/FEM	0.010	0.002	0.020	0.010	0.999	0.000	0.000	0.000
6/FEM	0.000	0.000	0.000	0.000	0.000	1.000	0.000	0.000
7/FEM	0.011	0.042	0.003	0.000	0.000	0.000	1.000	0.000
8/FEM	0.000	0.000	0.000	0.000	0.000	0.000	0.000	1.000

Table 7.9 MAC values for comparison mode shapes identified from FEM compared with mode shapes acquired from experiments, multiple damage, case 2, case study 3

Mode/Test	1/Exp	2/Exp	3/Exp	4/Exp	5/Exp	6/Exp	7/Exp	8/Exp
1/FEM	0.992	0.000	0.001	0.001	0.000	0.002	0.024	0.000
2/FEM	0.013	0.983	0.001	0.000	0.000	0.005	0.004	0.001
3/FEM	0.002	0.033	0.996	0.000	0.000	0.001	0.017	0.000
4/FEM	0.000	0.000	0.000	0.953	0.020	0.000	0.022	0.000
5/FEM	0.010	0.001	0.021	0.045	0.996	0.003	0.055	0.001
6/FEM	0.000	0.000	0.000	0.000	0.000	0.954	0.061	0.001
7/FEM	0.014	0.042	0.002	0.001	0.002	0.142	0.967	0.006
8/FEM	0.000	0.000	0.000	0.000	0.000	0.000	0.000	0.981

Table 7.10 MAC values for comparison mode shapes identified from FEM compared with mode shapes acquired from experiments, multiple damage, case 3, case study 3

Mode/Test	1/Exp	2/Exp	3/Exp	4/Exp	5/Exp	6/Exp	7/Exp	8/Exp
1/FEM	0.966	0.001	0.000	0.000	0.000	0.001	0.000	0.030
2/FEM	0.000	0.974	0.024	0.116	0.369	0.000	0.103	0.077
3/FEM	0.000	0.022	0.997	0.068	0.031	0.000	0.468	0.005
4/FEM	0.000	0.113	0.030	0.998	0.383	0.000	0.000	0.008
5/FEM	0.000	0.346	0.021	0.384	0.985	0.015	0.000	0.027
6/FEM	0.004	0.001	0.000	0.000	0.000	0.998	0.000	0.029
7/FEM	0.000	0.105	0.469	0.000	0.000	0.000	0.980	0.000
8/FEM	0.040	0.000	0.000	0.000	0.000	0.000	0.000	0.977

7.4.5 Discussion on case study 3

In case 1, Figure 7.20 shows a high possibility for damage at elements 3, 4, 6, 10, 13, 14 and 15. After performing stage two, results of quantifying damage from candidate elements are obtained. Elements 4 and 6 are recognized as damaged elements as shown in Figure 7.21. Actually, element 4 is a false damage element and has not been damaged. While element 6 which is a truly damaged element and element 5 form one member (a column) of the frame model on the third floor.

In case 2, as a multiple damage scenario shown in Figure 7.26, the suspected elements to damage are 5, 6, 11, 12, 13, 14 and 15. Proceeding to the second stage shown in Figures 7.27-7.28, clarifies that the actual damaged elements are elements 6, 11 and 12. Each pair of elements 5 and 6 and elements 11 and 12 form a column on third floor of the model.

The last case is also a multiple damage scenario (damage in one column and one beam) shown in Figure 7.31. The candidate elements to damage are 5, 6, 10, 11 and 14. Performing the second stage shown in Figure 7.32 leads to identifying the true damaged elements 5, 11 and 14 although their damage extents are not very accurate. Also, there is a false in elements 4 and 10. As it is observed, in all cases, the elements and damages detected mostly agree with the experimental damages created in the models or analytical solutions. It is also seen, in all cases, the numerical verification mostly agrees with experimental studies.

The correlation between modes of simulated and experimental are shown in Tables 7.10-7.12 which indicates the good agreement and coincidence.

However, for the error and false results occurred, the similar reasons stated at sections 7.2.5 and 7.3.5 are likely. Besides, limited sensors to simultaneously measure the required DoFs, and therefore data processing, also impact the results.

7.5 Conclusion

In this chapter, verification of the improved method proposed in Chapter 4 was performed by applying to some laboratory models. Different damage scenario including single and multiple damage scenarios were considered and studied.

The results show that the improved method performs in a good agreement between the implemented damages in the models by reducing the cross section or adding mass and those of from closed form solution. Furthermore, the MAC values of all models studied in this Chapter are also a good witness of well data measurement and efficiency of the improved method, too.

However, for the experimental cases studied in this Chapter, there are some error and false results. Generally, the issue can be originated from some sources including, effect of a high level of the noise, difference between the physical model of the structure and its FEM model, incomplete and limited measurements, data processing and unknown parameters and uncertainties. Moreover, for case 1, the actual boundary conditions of the model, dis-connectivity of the mass added to the structure, and difference between the assumed and actual material properties of the model contributes to error. For case 2, the similar reasons are possible. In addition, creating the exact amount of the damage in the model is difficult and even may increase the modelling error. For the last model studied, limited sensors to simultaneously measure the required DoFs, and therefore data processing, also impacts the results.

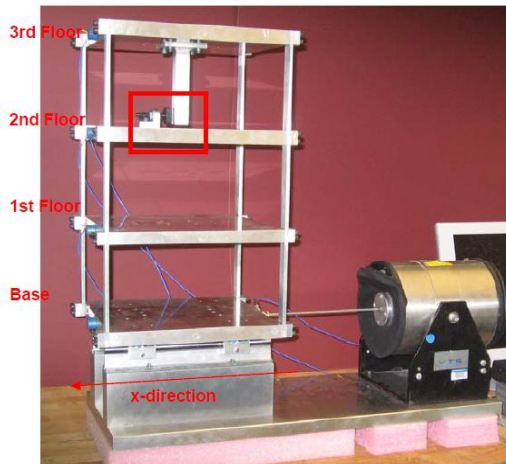
CHAPTER 8

APPLICATION OF THE IMPROVED MODAL STRAIN ENERGY METHOD TO LOS ALAMOS NATIONAL LABORATORY MODEL AND A REAL BRIDGE

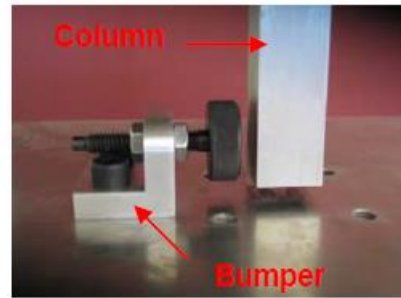
This chapter outlines the application of the improved MSE-based damage detection method in reality. The Los Alamos National Laboratory (LANL) 4-DOF three-story structure is studied as a real-world structure and I-40 Bridge is examined as a real bridge using the available data. Section 8.1 is allocated to application of the improved method to the LANL bookshelf. The model is a complete model of 3D steel structure with several damage cases. Subsequently, section 8.2 demonstrates the application of the improved MSE method to the real bridge of the I-40 in the US using the available data from Los Alamos National Laboratory. The details of application, comparison of the results with the FEM analysis and MAC values are also described. Lastly, concluding remarks are presented in section 8.3.

8.1 Case study 1: LANL 4-DOF Three-story Model

The LANL 4-DOF three-story structure is shown in Figure 8.14. The structure consists of aluminium columns and plates gathered using bolted joints with a rigid Base. There are four columns at each floor located at the corners connected to the aluminium plates. The dimension of column and aluminium plates are (17.7x2.5x0.6 cm) and (30.5x30.5x2.5 cm), respectively. Moreover, a centre column (15.0x2.5x2.5 cm) is suspended from the top floor, which is used to induce nonlinear behaviour, shown in Figure 8.14 (b). The structure can only move in the x-direction using the rails, as shown in Figure 8.14 (a). The dimension of the structure from different angles are also shown in Figure 8.15. The structure can be modelled as Figure 8.16 as a four-DOF structure.



(a) Three-story frame structure



(b) The adjustable bumper and suspended column

Figure 8.1 The LANL 4-DOF three-story structure

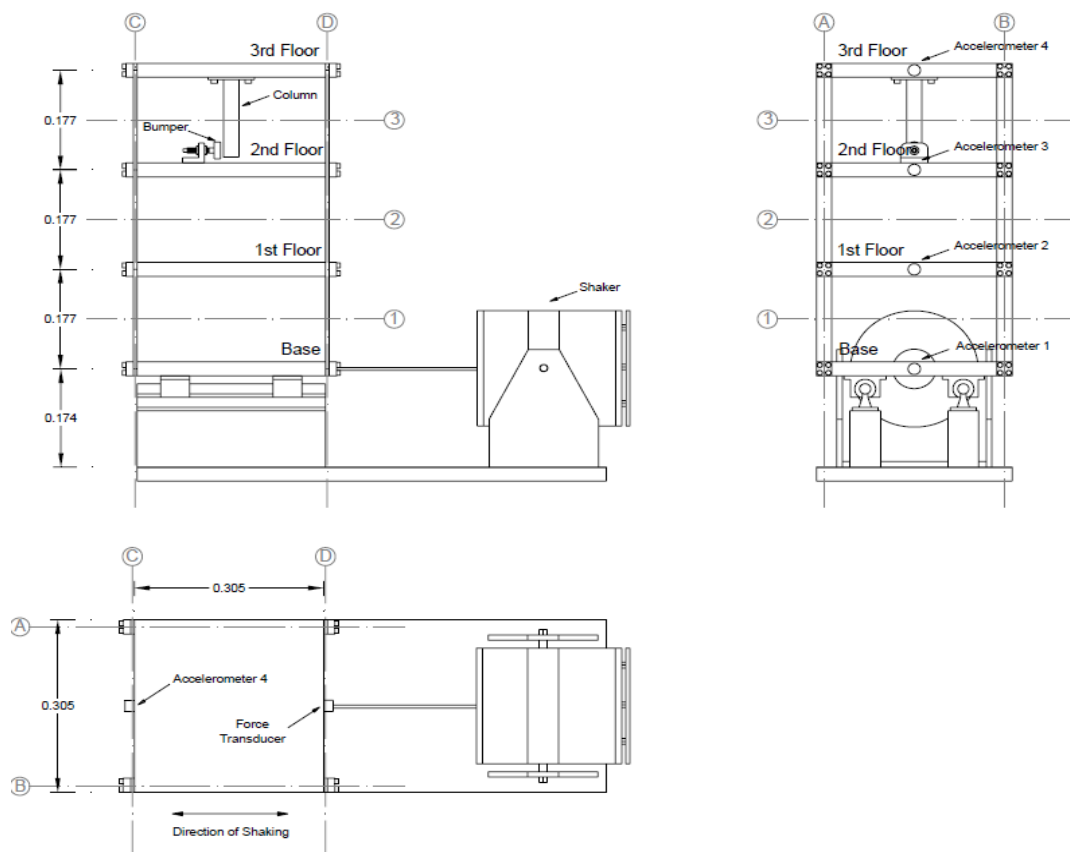


Figure 8.2 Basic dimensions of the LANL three-story structure

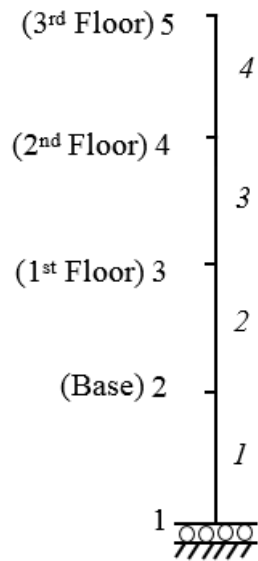


Figure 8.3 The FEM model of the LANL three-story structure

8.1.1 Results of different damage states

Eight damage states including states 1, 2, 17, 18, 21, 22, 23 and 24 as shown in Table 8-1 are considered for evaluating the performance of the improved method. For each damage state, state 13 which is the baseline condition is considered as undamaged states. As stated in section 4.3.5 of Chapter 4, the required mode shape for the improved method is at least the first five mode shapes. However, the case study structure has only four DOFs which is less than even the required mode shapes for the first stage of the improved method, which is damage locating. Although, more than five mode shapes are required to accurately quantify the damage extents. Therefore, it is predicted that the improved method does not properly detect or especially quantify the damages. The experimental Eigen parameters of the model at each state of damaged and undamaged are derived through DIAMOND. The results of two stages

of each states are shown in the following Figures, respectively, using Eqs. (4.10), (4.11) and (4.44) and a MATLAB code. Since the number of elements is limited to four, in all studied states, all elements are selected in both stages of the improved method.

Table 8.1 List of damage states

No	State	Condition of damage
1	1	Mass on the 1st floor
2	2	Mass at the base
3	13	Baseline condition
4	17	Column: 1BD – 50% stiffness reduction
5	18	Column: 1AD + 1BD – 50% stiffness reduction
6	21	Column: 3BD – 50% stiffness reduction
7	22	Column: 3AD + 3BD – 50% stiffness reduction
8	23	Column: 2AD + 2BD – 50% stiffness reduction
9	24	Column: 2BD – 50% stiffness reduction

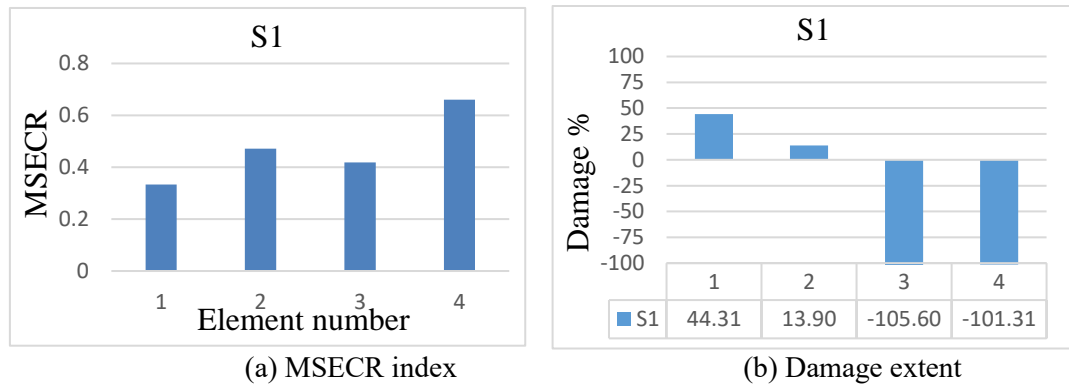
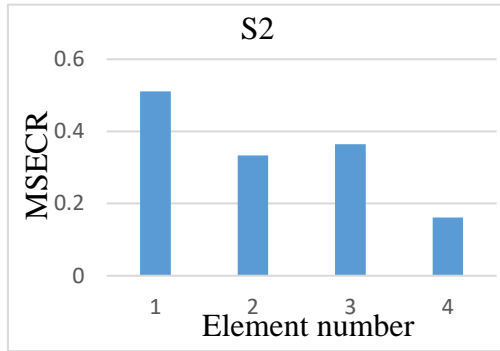
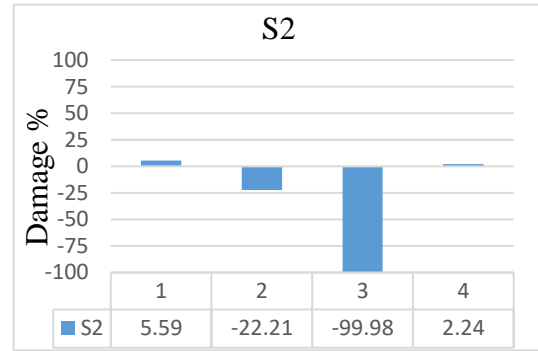


Figure 8.4 Damage state 1, mass on the 1st floor

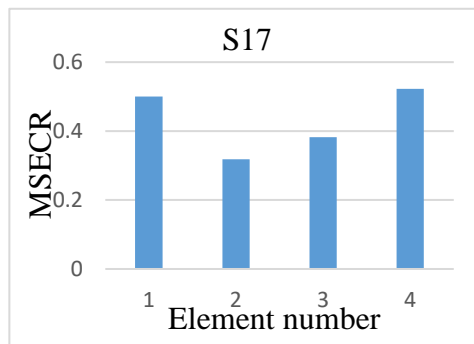


(a) MSECR index

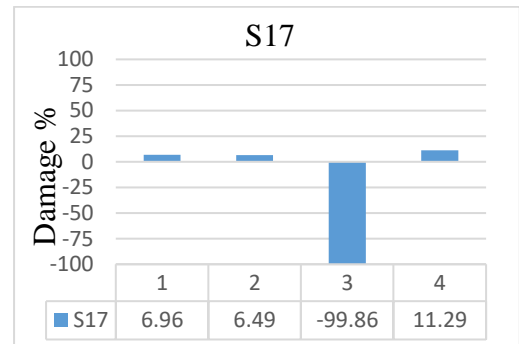


(b) Damage extent

Figure 8.5 Damage state 2, mass at the base

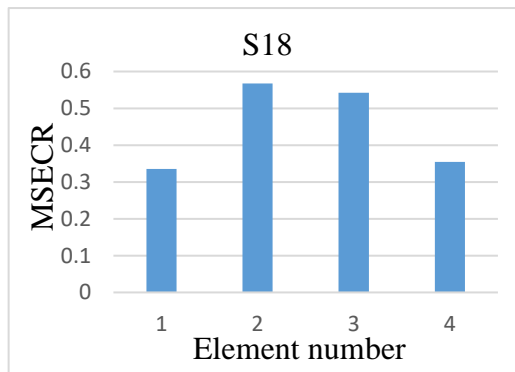


(a) MSECR index

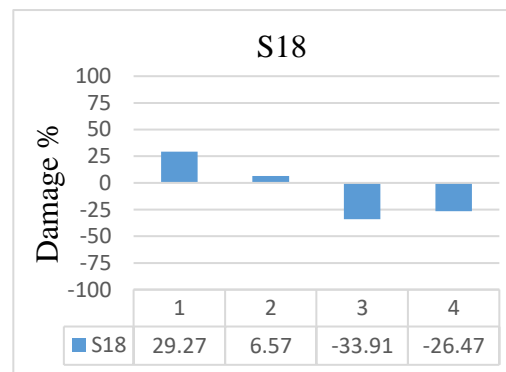


(b) Damage extent

Figure 8.6 Damage state 17, Column: 1BD – 50% stiffness reduction

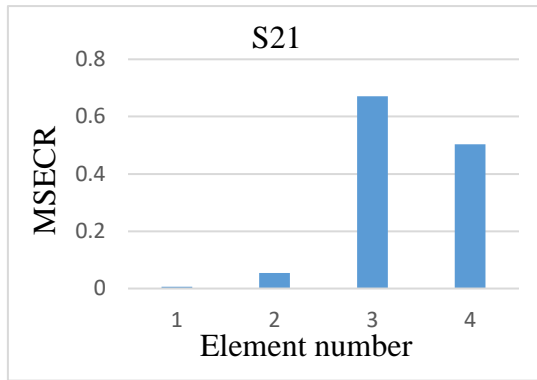


(a) MSECR index

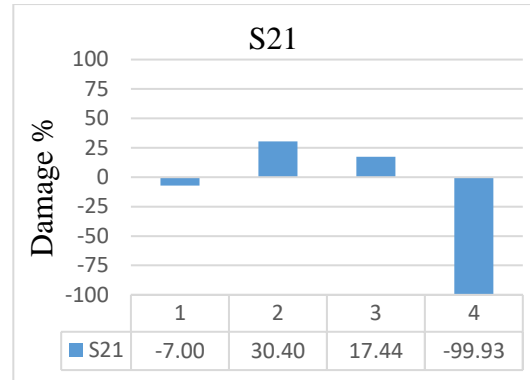


(b) Damage extent

Figure 8.7 Damage state 18, Column: 1AD + 1BD – 50% stiffness reduction

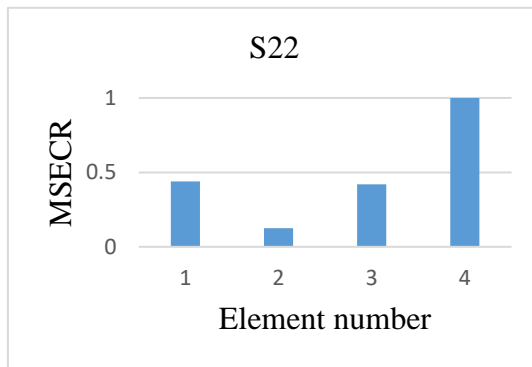


(a) MSECR index

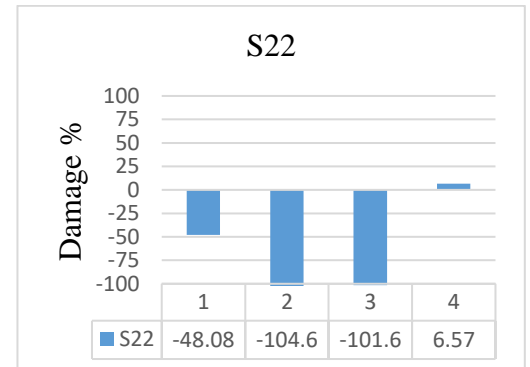


(b) Damage extent

Figure 8.8 Damage state 21, Column: 3BD – 50% stiffness reduction

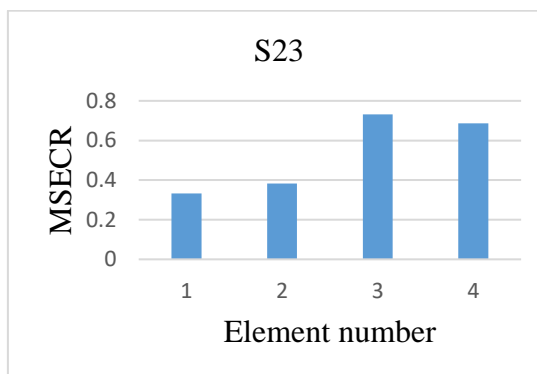


(a) MSECR index

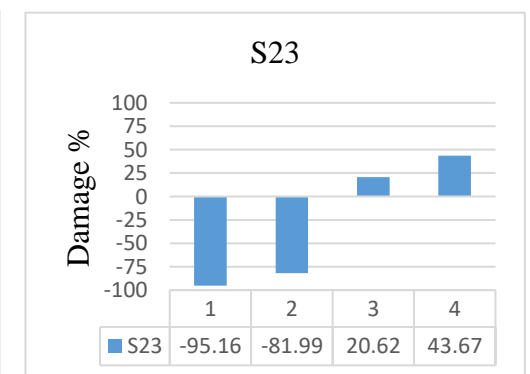


(b) Damage extent

Figure 8.9 Damage state 22, Column: 3AD + 3BD – 50% stiffness reduction



(a) MSECR index



(b) Damage extent

Figure 8.10 Damage state 23, Column: 2AD + 2BD – 50% stiffness reduction

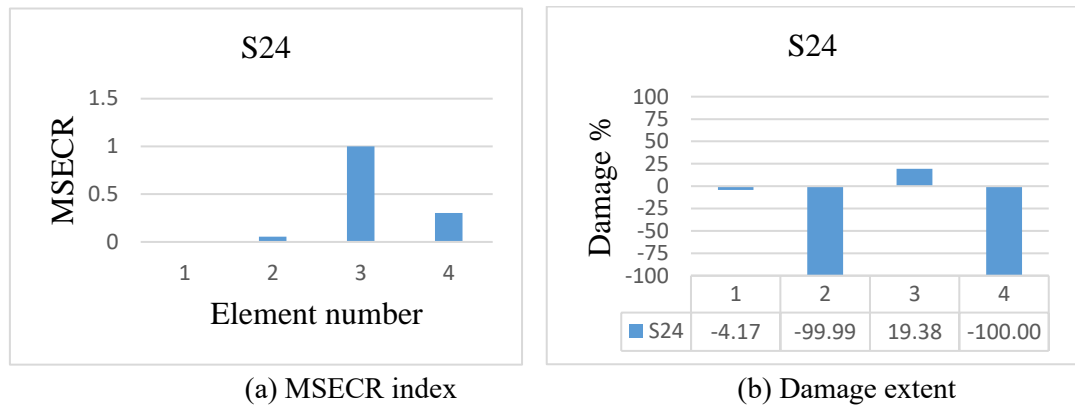


Figure 8.11 Damage state 24, Column: 2BD – 50% stiffness reduction

8.1.2 Discussion

Adding any mass at level 1 is associated with damage at any of the columns at lower level, the base level. In other words. According to Figure 8.3, damage state 1 is associated with damage at element 2. Figure 8.4(b) shows this with damage extent of 13.9 percent at element 2. However, there is also false damage of 44.31 percent at element 1. Similarly, when the mass is added to the base floor, it equals to occurring the damage at element 1 in Figure 8.3. Figure 8.5(b) shows the damage of 5.59 percent at element 1. However, there is a 2.24 percent damage at element 4 also that can be ignored.

According to Figure 8.6, 6.49 percent damage occurred at element 2 is true. However, its actual amount is 12.5 percent. Damages at elements 1 and 4 are also false. In Figure 8.7, damage at element 2 is 6.57 percent that is true and should be greater, 25 percent. Damage at element 1 is false.

In Figure 8.8, damage at element 2 is true. However, the actual damage is 12.5 percent. Damage at element 3 is also false. Moreover, Figure 8.9 shows 6.57 percent damage at element 4, which is a true damage. Damage at other elements is zero. However, the actual damage at element 4 is 12.5 percent.

In Figure 8.10, elements 3 and 4 have damaged with the amount of 20.62 and 43.67 percent, respectively. However, the true damaged element is element 3 with actual damage of 12.5 percent. In the last figure, element 3 has shown damaged with the extent of 19.38 percent, which is the only true damaged element. However, its actual amount of damage is 25 percent. The damage at other elements is also zero.

All in all, in the most states, although the improved method can recognize the location and approximate extent of the damage, there are some false damages, as well. As it was previously mentioned, it is because of that the structure does not provide the minimum mode number and natural frequency required for the proposed method. Since the structure has only 4 DOFs, consequently, the maximum number of mode shapes and natural frequencies is 4 which is less than the required number for the improved method that is at least five for stage 1 and more for stage 2 to quantify the damage. Anyhow, the improved method in most states has almost recognized the damages in terms of locating and quantifying.

8.2 Case study 2: I-40 Bridge, New Mexico, USA

The damage identification on the I-40 Bridge over the Rio Grande River in Albuquerque, the U.S. state of New Mexico shown in Figure 8.12, has been studied by many researchers (Alvin, 1995, James *et al.*, 1994, Mayes, 1994, Zimmerman, 1995) using the experimental data sets provided by Farrar *et al.* (1994). The data sets are still one of the most useful data of a real bridge in vibration-based damage identification. The data was acquired from a series of modal tests of a section of a highway bridge. Before destruction in 1993, a series of modal tests has been performed on this bridge after closing to traffic. Later on, a comprehensive study was performed by Farrar *et al.* (1999) on the Alamosa Canyon and I-40 Bridge with respect to examine the statistical significance of the damage identification results.



Figure 8.12 I-40 Bridges over the Rio Grande River in Albuquerque, New Mexico (Farrar *et al.*, 1999)

The concrete deck of bridge was approximately 13.3 m wide and 17.8 cm thick, supported by two steel plate girders, each 3.05 m high, and three steel stringers. For performing the modal tests, a section of the bridge including three continuous spans with the total length of about 130 m was considered and instrumented as Figures 8.13 and 8.14.

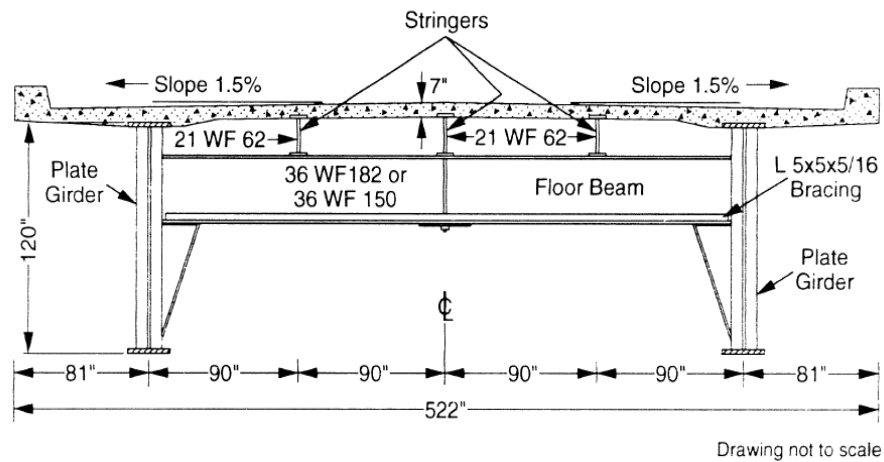


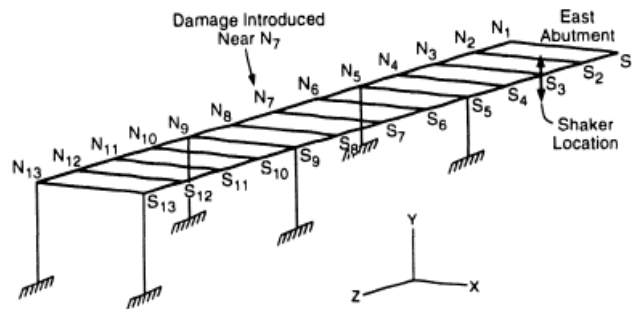
Figure 8.13 Typical cross section geometry of the bridge (Farrar *et al.*, 1994)



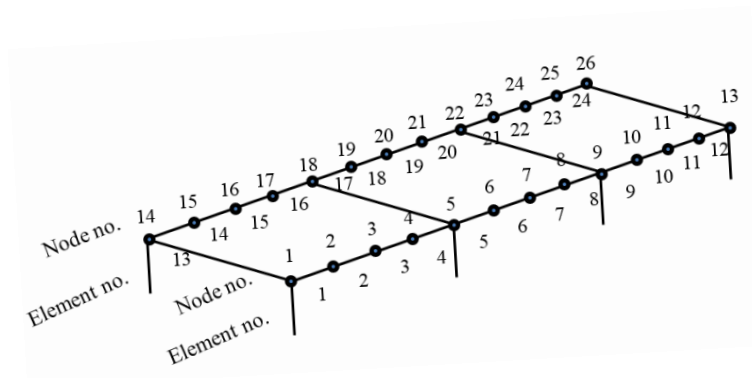
Figure 8.14 Bridge substructure (Farrar, 1994)

8.2.1 Instrumentation

The instrumentation consisted of 13 accelerometers installed on each of the two main plate girders along the length of the three spans, for measuring the total of 26 responses as shown in Figure 8.15. A 9863 kg reaction mass supported by three air springs moved by a 9.79 kN hydraulic actuator provided the excitation system. The actuator system was located on the deck right over one of the plate girders in the middle of the span closest to the abutment (Farrar *et al.*, 1999) as detailed in (Farrar *et al.*, 1994).



(a) Accelerometer locations



(b) Node and element numbering

Figure 8.15 Instrumentation and DoF numbering

8.2.2 Damage cases created

The created damage was intended to simulate fatigue cracking that has been observed in plate-girder bridges. The damage location was at near node 7 in Figure 8.15.a or at DoF number 20 either in the modal data sets or in Figure 8.15.b. Four damage cases were created by making various torch cuts in the web and flange of the girder, as shown in Figure 8.16.

- Case 1, cutting the web from mid-height toward the bottom of the section with a 61-cm-long (2 ft) and 10-mm-wide (3/8-in.) nominated as C1.
- Case 2, continuing this cut to the bottom of the web to create the second case of damage nominated as C2.
- Case 3, cutting the flange also halfway in from either side directly below the cut in the web nominated as C3.
- Case 4, the flange was completely cut through the whole flange nominated as C4.

In this way, only the top flange and the top 1.22 m of the web were left to carry the load at this location.

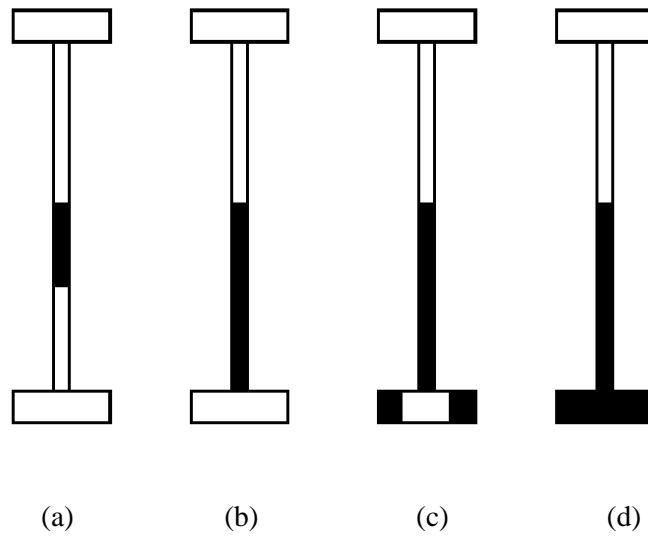


Figure 8.16 The four damage cases created in the I-40 plate girder

8.2.3 Mode shape comparison

To obtain the numerical Eigen parameters of the bridge, the mass and stiffness matrices given are used. The first six experimental mode shapes and natural frequencies are also given. Therefore, the first six numerical and experimental mode shapes of the bridge at undamaged case are primarily compared in the following Figures.

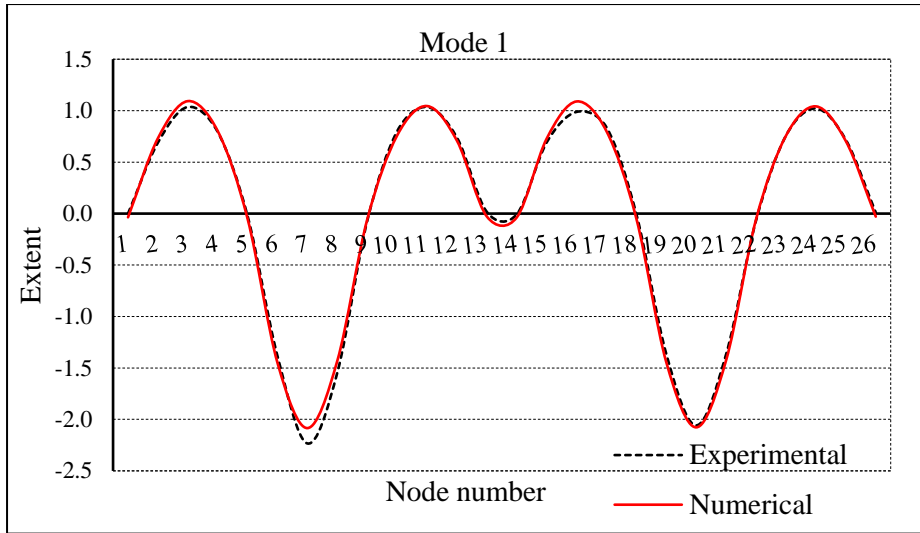


Figure 8.17 Comparison of numerical and experimental mode shape - Mode 1

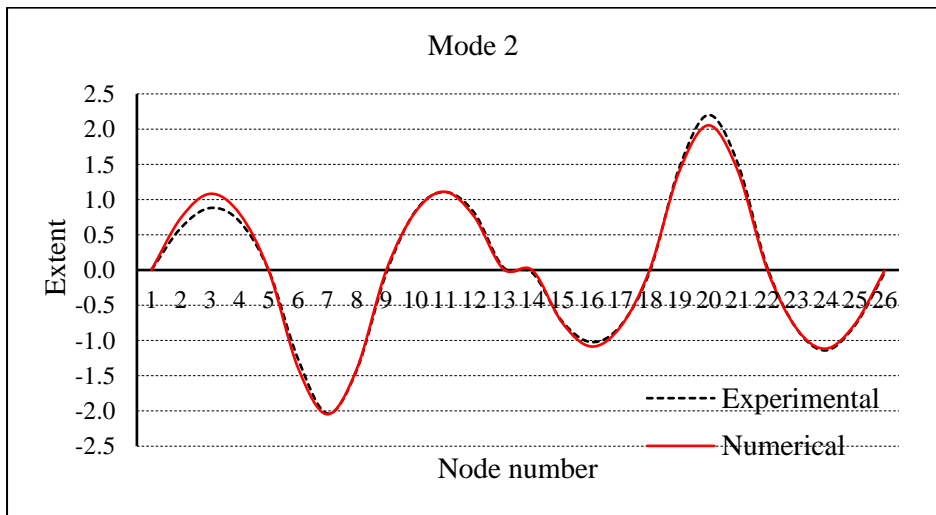


Figure 8.18 Comparison of numerical and experimental mode shape – Mode 2

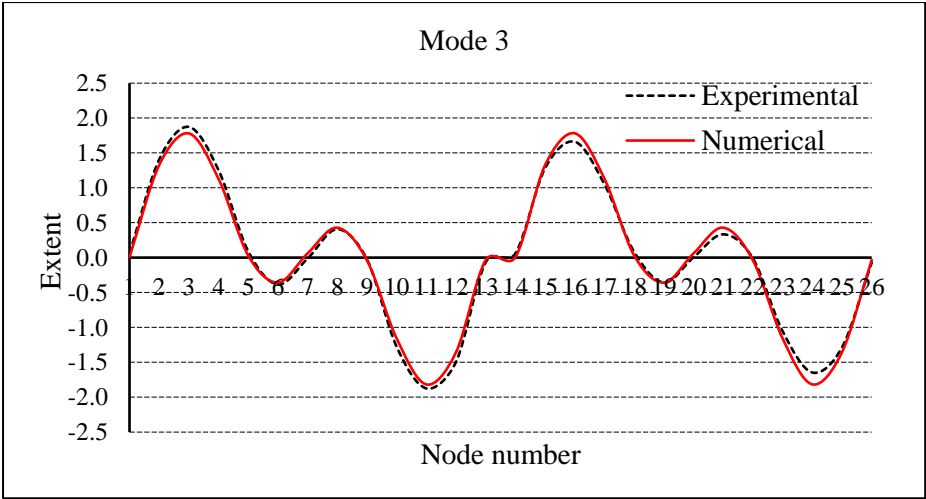


Figure 8.19 Comparison of numerical and experimental mode shape – Mode 3

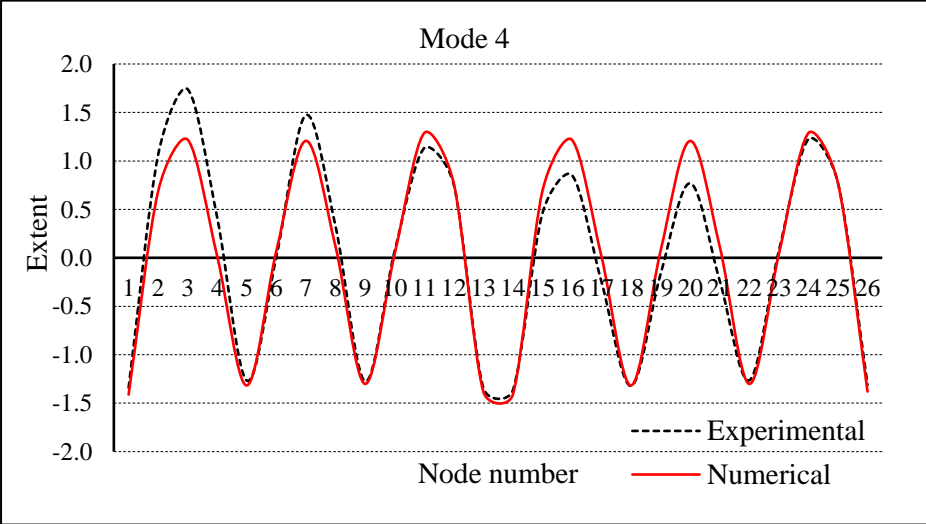


Figure 8.20 Comparison of numerical and experimental mode shape – Mode 4

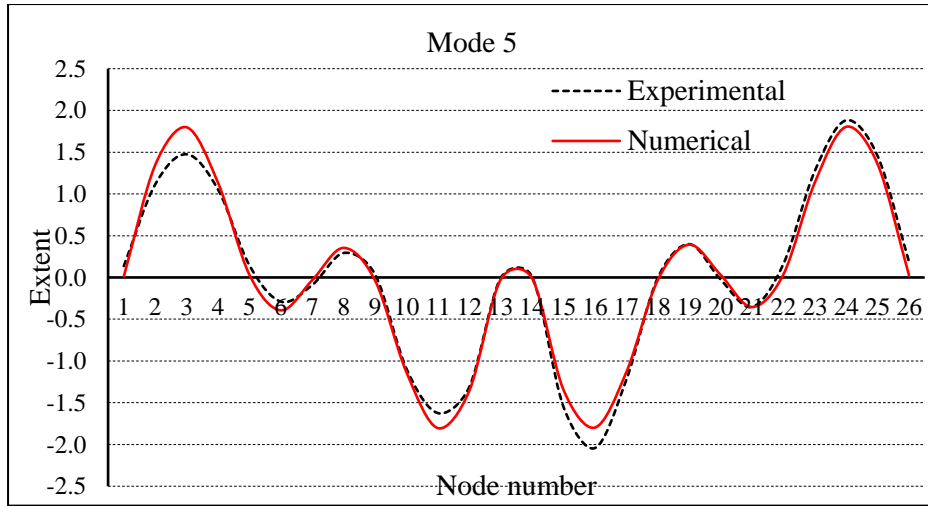


Figure 8.21 Comparison of numerical and experimental mode shape – Mode 5

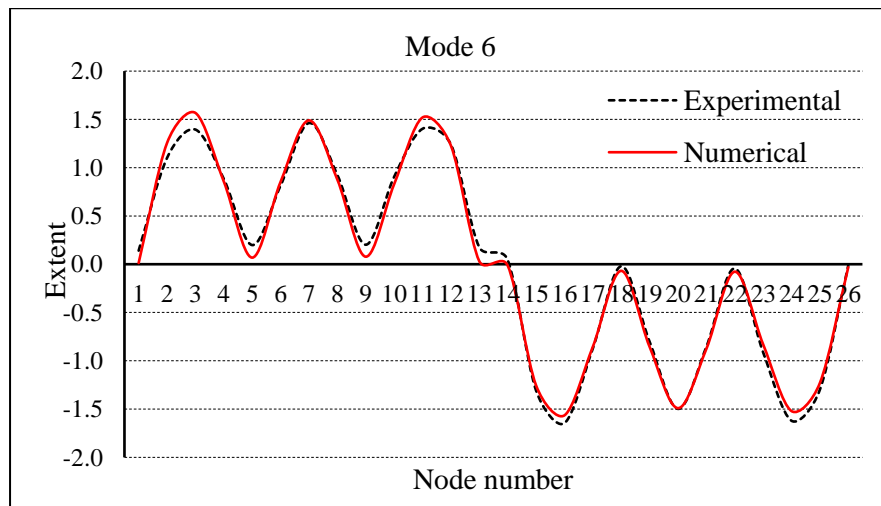


Figure 8.22 Comparison of numerical and experimental mode shape – Mode 6

As it is seen from the Figures 8.17-8.22, there is not much differences between numerical and experimental mode shapes. Even though, as the final assurance check, for each damage scenario, the MAC values will also be calculated and checked using numerical and experimental datasets of those damage cases.

8.2.4 Application of the improved MSE method

The proposed methodology of the improved MSE method is applied to the available data of the I-40 Bridge, as a real bridge, in different damage cases introduced in section 8.2.2. In the first stage, in order to identify the location of the damage, the first five mode shapes of damaged and undamaged of each damage case are used applying Eq. (4.11) using a MATLAB code. The results of cases 1-4 are shown in Figures 8.23, 8.25, 8.27 and 8.30, respectively.

In these figures, the MSECR index is versus the 12 elements of the bridge section under consideration. However, the damage has occurred in a node (node 20). Therefore, in the second stage, Eq. (4.44) is used for quantifying the damage using the mode expansion method (Shi *et al.*, 1995). For this purpose, the number of nodes to be examined are 13, which are the total number of nodes under consideration and measurement stated in section 8.2.1. However, to decrease the computational cycles, in each case, some suspected elements (and finally nodes) are selected. The results of the second stage for cases 1-4 are also shown in Figures 8.24, 8.26, 8.28-29 and 8.31, respectively.

8.2.5 Results and discussion

8.2.5.1 Damage case 1:

The MSECR index versus elements for the case 1 using the first five modes and Eq. (4.11) are shown in Figure 8.23. The suspected elements to damage are elements 16, 19, 20 and 21. However, in stage 2, quantifying, the damage is performed using Eq. (4.44). The results shown in Figure 8.24 indicate that the element 19 has damaged with the extent of 3.43% which is a true element. Elements 16 and 20 have negative or zero and the last element has received less than 1% damage.

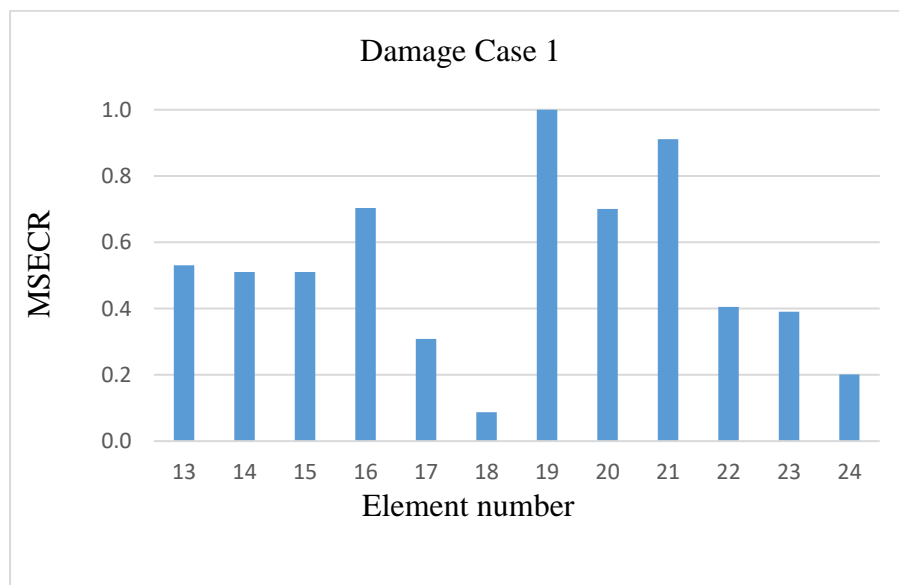


Figure 8.23 MSECR vs element number of I-40 Bridge, Case 1

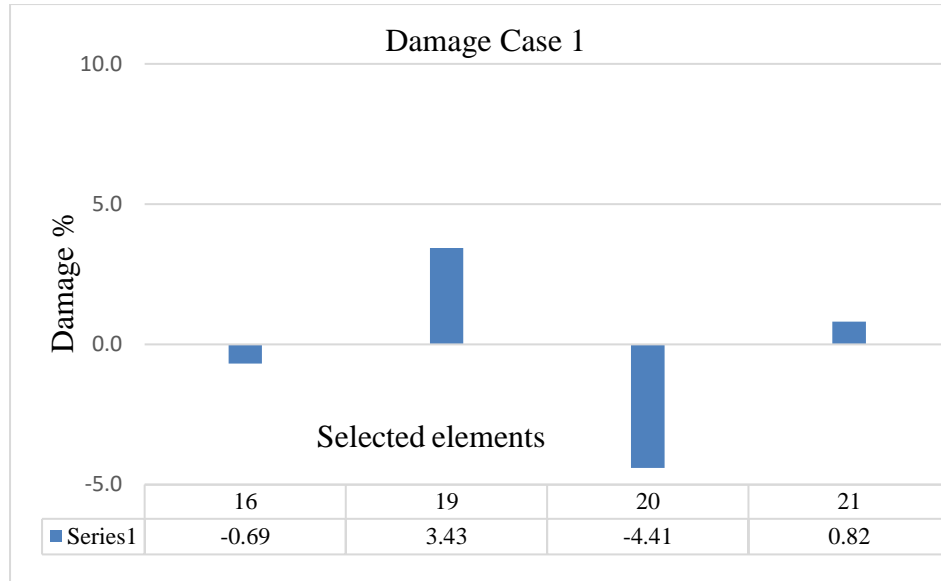


Figure 8.24 Damage extent vs element number of I-40 Bridge, Case 1

8.2.5.2 Damage case 2

Similarly, the MSECR index versus elements for the case 2 using the first five modes and Eq. (4.11) are shown in Figure 8.25. The suspected elements to damage are elements 18, 19, 20 and 21. In the second stage, to quantify the damage, element 20 has got 10.59% damage which is false and other elements have got negative or zero damage. It means, in this case, the proposed method does not identify the extent of the damage, however, the location (element 19) is among the suspected elements.

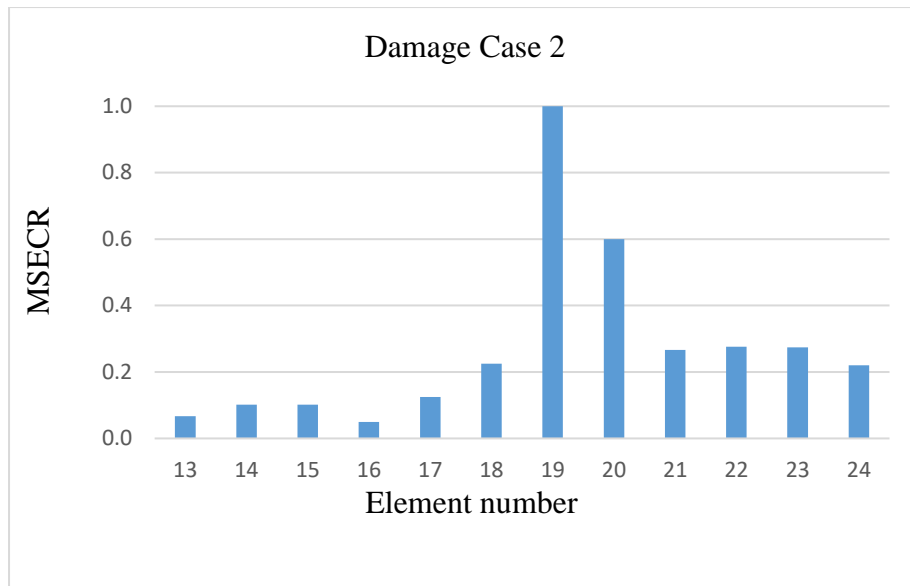


Figure 8.25 MSECR vs element number of I-40 Bridge, Case 2

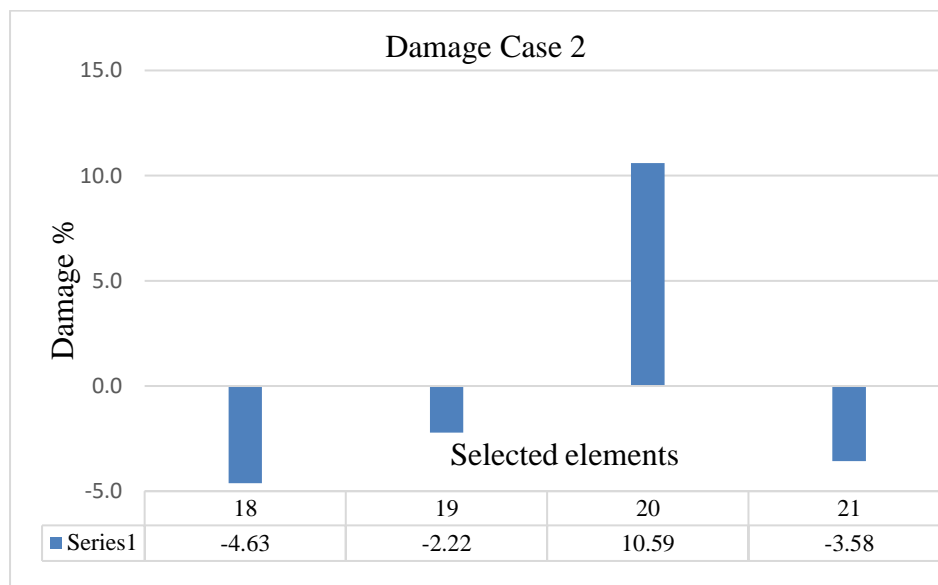


Figure 8.26 Damage extent vs element number of I-40 Bridge, Case 2

8.2.5.3 Damage case 3

For case 3, the MSECR index versus elements using the first five modes and Eq. (4.11) are shown in Figure 8.27. The suspected elements to damage are elements 17, 19, 20, 22, 23 and 24. The suspected elements is divided into two set and the results are shown

in Figures 8.28-8.29. The results show that the damage is occurred at element 19 with amount of 3.79 percent which is true and also at element 23 with amount of 3.79 percent which is false. Other elements show negative damage or zero. It means the proposed method shows the proper results at this case also.

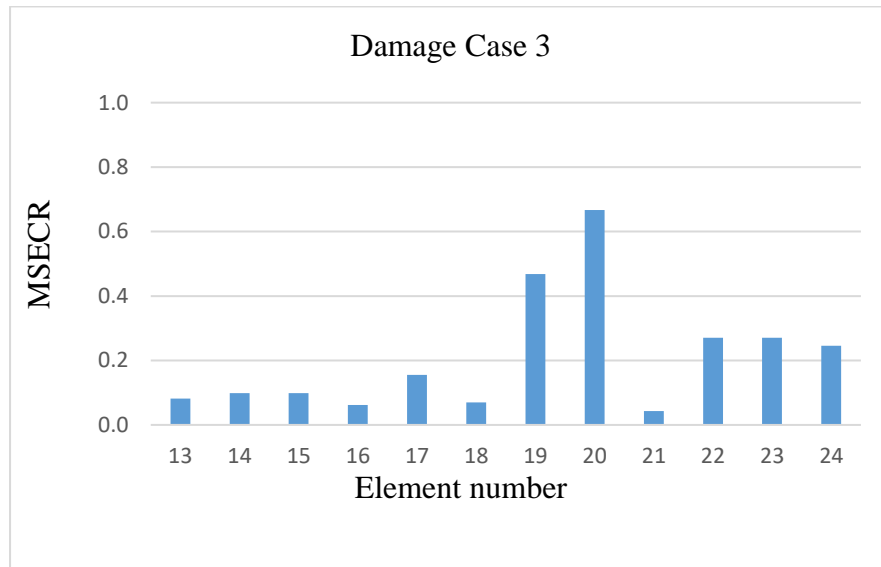


Figure 8.27 MSECR vs element number of I-40 Bridge, Case 3

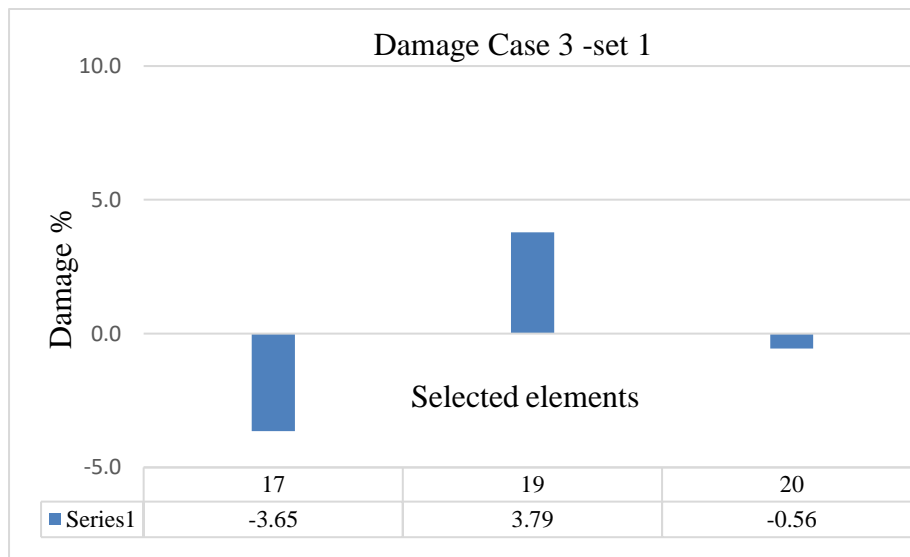


Figure 8.28 Damage extent vs element number of I-40 Bridge, Case 3, set 1

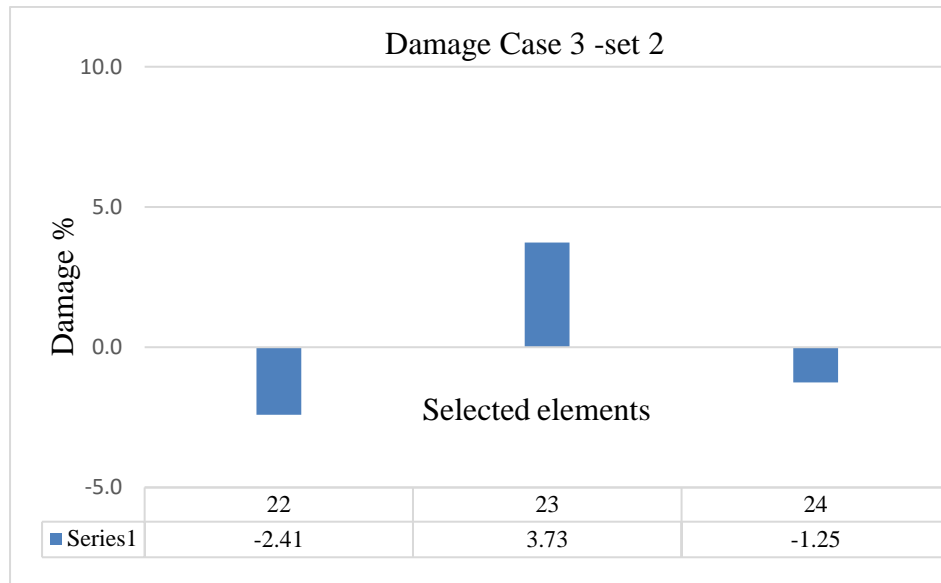


Figure 8.29 Damage extent vs element number of I-40 Bridge, Case 3, set 2

8.2.5.4 Damage case 4

For the last case, the MSECR index versus elements using the first five modes and Eq. (4.11) are shown in Figure 8.30. The suspected elements to damage are elements 17, 18, 19 and 20. In the second stage, to quantify the damage as shown in Figure 8.31, the method perfectly shows the both true damaged elements of 18 and 19 with a high amount of 33.14 and 30.93%, respectively. Showing an almost close amount for both elements is another good reason of the capability of the proposed method of capturing the damage in the bridge. Also, in this case, the bridge has critically damaged, and the proposed method properly has identified this.

Overall, the method is able to detect and quantify the damage in this real bridge in three cases 1, 3 and 4 with high certainty.

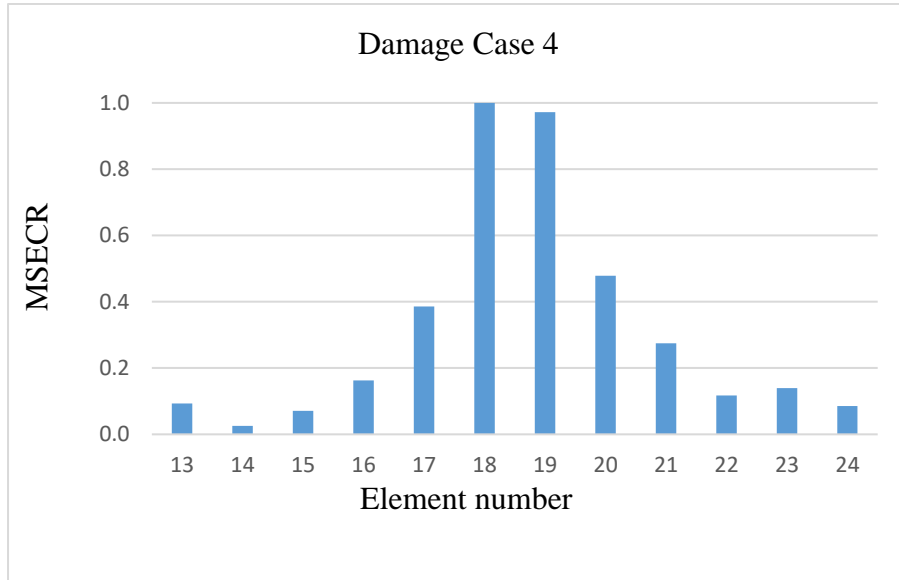


Figure 8.30 MSECR vs element number of I-40 Bridge, Case 4

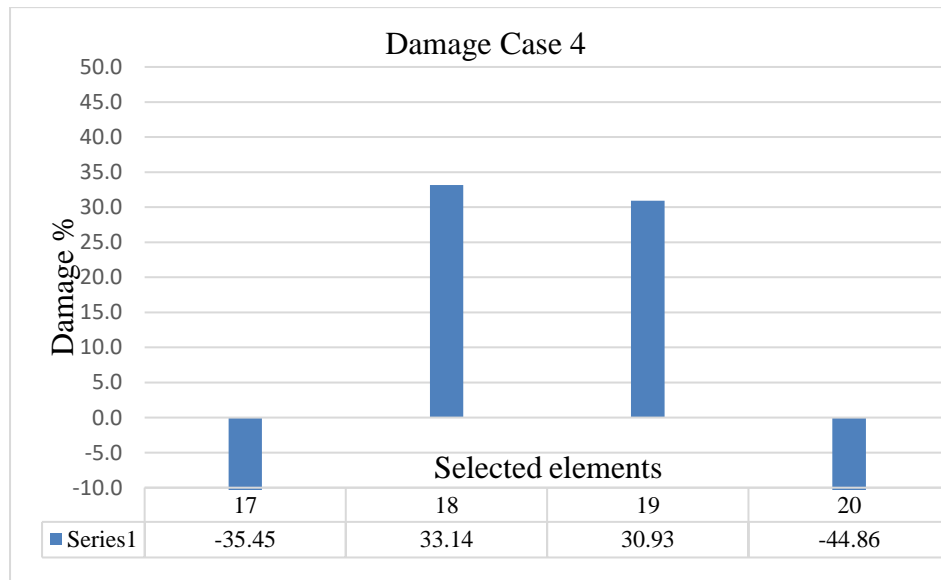


Figure 8.31 Damage extent vs element number of I-40 Bridge, Case 4

8.2.6 MAC value comparison

The MAC or modal correlation coefficient is used to determine the level of correlation between mode shapes obtained from the tests and the finite element method (FEM) through the Eq. (7.1) (Farrar *et al.*, 2000, Sinou, 2009).

The MAC values for the first six mode shapes identified from FEM are compared with those mode shapes acquired from experiments for different cases in Tables 8.2 to 8.6. Table 8.2 compares MAC values of the undamaged case of the bridge nominated as C0 while Tables 8.3 to 8.6 characterize the MAC values of damaged cases 1 to 4 presented in section 8.2.2.

Table 8.2 MAC values for comparison mode shapes identified from FEM compared with mode shapes acquired from experiments-Case C0

Mode/Test	1/Exp	2/Exp	3/Exp	4/Exp	5/Exp	6/Exp
1/FEM	0.9968	0.0015	0.0001	0.0126	0.0004	0.0011
2/FEM	0.0007	0.9945	0.0000	0.0002	0.0000	0.0089
3/FEM	0.0008	0.0004	0.9930	0.0003	0.0111	0.0001
4/FEM	0.0038	0.0001	0.0010	0.9830	0.0113	0.0139
5/FEM	0.0000	0.0017	0.0046	0.0055	0.9755	0.0002
6/FEM	0.0001	0.0032	0.0000	0.0084	0.0000	0.9832

Table 8.3 MAC values for mode shapes identified from FEM compared with mode shapes acquired from experiments-Case C1

Mode/Test	1/Exp	2/Exp	3/Exp	4/Exp	5/Exp	6/Exp
1/FEM	0.9956	0.0010	0.0002	0.0149	0.0000	0.0008
2/FEM	0.0004	0.9942	0.0000	0.0000	0.0002	0.0165
3/FEM	0.0011	0.0006	0.9969	0.0000	0.0086	0.0000
4/FEM	0.0019	0.0000	0.0003	0.9917	0.0007	0.0109
5/FEM	0.0000	0.0007	0.0010	0.0001	0.9835	0.0002
6/FEM	0.0005	0.0015	0.0000	0.0053	0.0053	0.9846

Table 8.4 MAC values for mode shapes identified from FEM compared with Mode Shapes acquired from Experiments-Case C2

Mode/Test	1/Exp	2/Exp	3/Exp	4/Exp	5/Exp	6/Exp
1/FEM	0.9921	0.0003	0.0001	0.0133	0.0001	0.0015
2/FEM	0.0000	0.9952	0.0000	0.0003	0.0000	0.0113
3/FEM	0.0018	0.0000	0.9946	0.0016	0.0131	0.0000
4/FEM	0.0019	0.0000	0.0012	0.9839	0.0003	0.0118
5/FEM	0.0001	0.0002	0.0025	0.0007	0.9840	0.0003
6/FEM	0.0000	0.0012	0.0000	0.0101	0.0007	0.9846

Table 8.5 MAC values for Mode Shapes Identified from FEM Compared with Mode Shapes acquired from Experiments-Case C3

Mode/Test	1/Exp	2/Exp	3/Exp	4/Exp	5/Exp	6/Exp
1/FEM	0.9964	0.0001	0.0003	0.0132	0.0000	0.0014
2/FEM	0.0000	0.9949	0.0002	0.0004	0.0001	0.0045
3/FEM	0.0013	0.0008	0.9937	0.0024	0.0092	0.0001
4/FEM	0.0021	0.0001	0.0016	0.9863	0.0021	0.0126
5/FEM	0.0000	0.0002	0.0021	0.0003	0.9852	0.0013
6/FEM	0.0000	0.0014	0.0001	0.0073	0.0015	0.9821

Table 8.6 MAC values for Mode Shapes Identified from FEM Compared with Mode Shapes acquired from Experiments-Case C4

Mode/Test	1/Exp	2/Exp	3/Exp	4/Exp	5/Exp	6/Exp
1/FEM	0.8726	0.0741	0.0006	0.0258	0.0000	0.0026
2/FEM	0.0874	0.9073	0.0001	0.0096	0.0001	0.0142
3/FEM	0.0022	0.0007	0.9946	0.0023	0.0091	0.0000
4/FEM	0.0039	0.0071	0.0014	0.9709	0.0091	0.0009
5/FEM	0.0003	0.0003	0.0007	0.0069	0.9617	0.0067
6/FEM	0.0033	0.0003	0.0001	0.0019	0.0189	0.9834

The MAC index operates based on orthogonality properties of mode shapes to compare the analytical and experimental mode shapes. When the modes are identical, the MAC index becomes a scalar value of one. If the modes are orthogonal and dissimilar, a value of zero is achieved. According to Ewins (1984) that indicates practically correlated modes will yield a value greater than 0.9, the MAC values of all cases in Tables 8.2-8.6 are well correlated. As shown it is seen, using the mode shape expansion method, the proposed method is able to detect the location of the damage in all four cases and properly quantify the damage in three cases including cases 1, 2 and 4. While, in the reference research by Farrar *et al.* (2000), only locating the damage at the first three cases has been reported.

However, there is an error because of the difference between physical structure and the FEM model in the case studies. In addition, creating an exact amount of damage in the model is difficult. The actual material properties may also be slightly different with the assumed ones. Another difficulty is the incomplete and limited measurements corrupted by environmental effects and noise pollution. For example, the rotational

DoF measurements are misplaced and are not included. Likewise, some errors occur during the processing of the experimental data using different software. There is also a big issue in acquiring the favourite and required mode shapes and natural frequencies from the experimental data.

8.3 Conclusion

Following the numerical and experimental verifications at Chapters 6 and 7 of the improved MSE method presented in Chapter 4, further corroboration is performed to perceive the application of the proposed method to a real-world model and a real bridge. For this purpose, the LANL steel truss bridge model was chosen as a real model that has been noticed by many researchers. Also, the I-40 Bridge in the US, with available data and compatible with the proposed methodology, was also selected as a real bridge for examining the proposed method. The improved method was successfully applied to these structures in a different case and situation of damages.

The results indicate that the improved method is able to mostly detect the damage in both structures studied, including perfect diagnosis of the damage location and extent through two consequent stages. It also shows that the method can easily detect the damage either in elements or nodes of the model and bridge having the first few modes and natural frequencies. Moreover, it is capable of capturing any single or multiple damage at any part of the system.

There are many reasons that numerical simulations show more accuracy compared to the experimental results in this study. First of all, structural modelling in the numerical simulations has less error. Besides, using the available FEM software allows to easily derive as many as numerical mode shapes and natural frequencies required for the proposed MSE method. These data are used as the input to the improved MSE method for identifying the assumed damage in the models. Moreover, mode shapes of transitional and rotational DoFs can be easily derived using the FEM package available. Damage simulation in the model can also be readily imposed and implemented. Considering all of these matters provides a very accurate data of the system as the input for the improved MSE method. Therefore, the accumulated error during the two-stage computation of the improved method is less and almost zero.

However, for the experimental cases the situation is different. The error can be accumulated from some sources such as, an error because of the difference between physical structure and the FEM model in the case studies, the error in creating the exact amount of damage in the model, difference between the assumed and actual material properties, incomplete and limited measurements corrupted by environmental effects and noise pollution, error during the processing of the experimental data using different software, and effect of unknown factors and uncertainties on any experimental studies.

In conclusion, all of the above-mentioned errors accumulated during the application of the improved MSE method rise to the false results in some cases. Definitely, by

minimizing any of these errors the results of the improved MSE method in the experimental studies can be improved and become more accurate.

CHAPTER 9

CONCLUSION AND FUTURE STUDIES

By increasing the importance of infrastructures especially bridges, the structural health monitoring has become more vital and challenging. Many literatures that indicate the global dynamic characteristics of the structure are affected by any damage in the structure or environmental temperature and humidity. Since the structures are always exposure to damage and environmental changes, there is more demand on a timely, safe, non-destructive and inexpensive structural monitoring. On the other hand, any structure or bridge requires its own especial method for monitoring. Besides, there is no unique solution to recognize the damage in structures and most of the studies performed are on some simple structure such as beam, plate and so on. Therefore, this study has focused on an MSE method for detecting the damage in bridges. The main features of the improved method are as follows.

- The improved MSE method has mathematically been established to increase the sensitivity to damage recognition and accuracy of the damage detected, reduce the computational cycles and number of iterations.
- The extent of elemental or nodal damage is expressed as a fractional reduction/increment of the elemental stiffness/mass matrix or rotational stiffness

matrix. The current study mainly uses the structural damaged stiffness matrix which is primarily unknown to establish a more accurate MSE change equation and, consequently, leads to a delicate sensitivity matrix. For the case of incremental mass matrix, primarily, a process is used to convert the case to an equivalent stiffness matrix reduction problem.

- Initially, an accurate MSE equation is formulated using damaged elemental stiffness which is an unknown variable. The MSE equation derived is then used for deriving an accurate sensitivity matrix that can perfectly quantify the damage.
- The improved MSE method identifies the damage in two stages, stage one, locating the damage and stage two, quantifying the damage through a cycle of mathematical process.
- The improved MSE method is able to identify both elemental and nodal damages in any structure.
- The improved MSE method is able to identify different damage scenarios including single or multiple damage scenarios.
- The improved MSE method is able to identify the aimed damages in contamination with up to 7 percent noise.

- The improved MSE method requires the following number of mode shapes and natural frequencies to identify the damage in the structure.

For stage 1, locating the damage requires only a pair of the first five (or more) modes of both damaged and undamaged cases of the structure.

For stage 2, quantifying the damage involves with all analytical mode shapes and natural frequencies or as many as analytical or experimental mode shapes and natural frequencies that are available or can be derived.

9.1 Conclusions

A new improved MSE method has been well numerically and experimentally improved and verified for some models and real structures. The findings of this research can be drawn as follows.

1. An MSE equation is established considering damaged elemental stiffness as a core improvement of an MSE method in Chapter 4. The MSE equation is then used for derivation of a new sensitivity matrix which is directly improved the accuracy of the damage extent and makes the method capable of recognizing the small damages in the system.

2. The improved method is numerically applied to different structural models such as a beam, a frame and a truss models with different material properties and element type, size, and structural type. As stated in Chapter 6, different damage scenarios including single and multiple damage are also considered for each model. Additionally, all simulations data are contaminated with up to seven percent noise to pretend the actual situation of noise pollution in the environment. In the last two case studies, the improved method is further verified for two different models representing medium span bridges. The results show the proficiency of the proposed method in all cases and, also, a well agreement with the numerical damages assumed in the models and closed form solution.
3. A case study of adding mass as a damage has also been successfully performed in Chapter 7. For this purpose, the case study is converted to an equivalent case of change/ damage in the structural stiffness and then the improved method is applied.
4. Experimental verifications on some laboratory models are also show that the improved method is able to recognize the damage in most cases in the continuation of Chapter The results indicate that the performance of the improved method is in a good agreement with the damages implemented and also with the FEM simulations.
5. In Chapter 8, the application of the improved method has been performed on the Los Alamos National Laboratory (LANL) bookshelf with several cases of single

and multiple damage at nodes. The results show the satisfactory performance of the improved method, although the structure does not provide the minimum mode number requirement for the proposed method.

6. Application of the proposed method to I-40 Bridge, in the USA, as a real bridge using the available data is the most important achievement of this research. Using available incomplete data, the proposed method is able to detect the damage in most cases.

However, the error and false results occurred in the experimental and real case studies in this dissertation, can be created from some sources including, effect of a high level of noise, difference between the physical model of the structure and its FEM model, limited sensors to simultaneously measure the required DoFs, error in creating the actual damage in the model, difference between the assumed and actual material properties of the model, difference between the assumed and actual boundary conditions, data processing and unknown parameters and uncertainties.

9.2 Significance and contributions

This study focuses on a sensitivity matrix based MSE technique for structural damage detection in bridges. The improved MSE method with a very sensitive matrix is able

to be applied to any structure/ bridge to evaluate its health condition in a different state and time. The improved MSE is characterized as follows.

1. The improved method is more accurate than previous methods because it calculates the actual MSE stored in the structure using an accurate MSE equation established. Also, the sensitivity matrix derived from the MSE equation is more accurate than similar methods.
2. The improved method converges very fast using few numbers of analytical modes.
3. The improved method is very sensitive to small damages and is able to simply recognize the small size damages with an amount of 1% or less.
4. The improved method is able to recognize the damage in both elements and nodes. However, the damage indicator is always stated in terms of elemental change.
5. The improved method can be applied to any structure including building or bridges regardless of type of the structure or material properties. However, in this study it has been applied to some numerical and laboratory models, a real structure and a real bridge using available data.

The findings of this study can be numerically extended to 2D and 3D infrastructures, particularly bridges to more accurately detect and quantify the damage. The method is capable of providing a proper SHM that facilitates timely maintenance of bridges to

minimize the loss of lives and property by identifying the unforeseen structural damages.

9.3 Recommendations for Further Researches

According to the above conclusions, the following recommendations can be suggested for the future studies.

1. The improved MSE method can be more extended and improved by developing the MSE equation and consequently sensitivity matrix or either MSE equation or sensitivity matrix using mathematical tools of the GA and ANN. However, it is expected to be more noise sensitive. If so, another approach is also required to overcome the issue.
2. In a similar way, the current study can be numerically extended for any 2D and 3D structure and observe the results regardless of type of the structure and material properties.
3. Also, the improved method can practically be tested for any laboratory model or real structure regardless of the type of the structure or material properties by measuring the first five mode shapes of the model or prototype.

4. More efforts can be put into using the improved method of having incomplete measurements to make it compatible with having fewer data available from the structure to use for detecting the damage in the structure.

REFERENCES

- Adams, R. and Coppendale, J. (1976). Measurement of the elastic moduli of structural adhesives by a resonant bar technique. *Journal of Mechanical Engineering Science*, 18(3): 149-158.
- Allemang, R.J. (2003). The modal assurance criterion—twenty years of use and abuse. *Sound and vibration*, 37(8): 14-23.
- Alvin, K.F. Robust model error localization for damage detection and finite element model update. Proc. of the 1995 International Adaptive Structures Conference, 1995.
- Asgarian, B., Amiri, M. and Ghafooripour, A. (2009). Damage detection in jacket type offshore platforms using modal strain energy. *Structural Engineering and Mechanics*, 33(3): 325-337.
- Bandara, R.P., Chan, T.H. and Thambiratnam, D.P. (2014). Structural damage detection method using frequency response functions. *Structural Health Monitoring*, 13(4): 418-429.
- Board, N. (2008). Collapse of I-35W Highway Bridge Minneapolis, Minnesota August 1, 2007. 2008. *National Transportation Safety Board: Washington DC*: 1.
- Brehm, M., Zabel, V. and Bucher, C. (2010). An automatic mode pairing strategy using an enhanced modal assurance criterion based on modal strain energies. *Journal of Sound and Vibration*, 329(25): 5375-5392.
- Carrasco, C.J., Osegueda, R.A., Ferregut, C.M. and Grygier, M. Damage localization in a space truss model using modal strain energy. Proceedings-SPIE the international society for optical engineering, 1997. SPIE International Society For Optical, 1786-1792.
- Cha, Y.J. and Buyukozturk, O. (2015). Structural damage detection using modal strain energy and hybrid multiobjective optimization. *Computer-Aided Civil and Infrastructure Engineering*, 30(5): 347-358.
- Chen, H.-P. and Ni, Y.-Q. (2018). *Structural health monitoring of large civil engineering structures*, John Wiley & Sons.

- Choi, S., Park, S., Yoon, S. and Stubbs, N. (2005). Nondestructive damage identification in plate structures using changes in modal compliance. *Ndt & E International*, 38(7): 529-540.
- Doebbling, S.W., Farrar, C.R. and Cornwell, P.J. (1997a). DIAMOND: A graphical interface toolbox for comparative modal analysis and damage identification. Los Alamos National Lab., NM (United States).
- Doebbling, S.W., Hemez, F.M., Peterson, L.D. and Farhat, C. (1997b). Improved damage location accuracy using strain energy-based mode selection criteria. *AIAA journal*, 35(4): 693-699.
- Dowling, L. and Rummey, G. (2004). *Guidelines for bridge management: structure information*.
- Dutta, A. and Talukdar, S. (2004). Damage detection in bridges using accurate modal parameters. *Finite Elements in Analysis and Design*, 40(3): 287-304.
- Efron, B. and Tibshirani, R.J. (1994). *An introduction to the bootstrap*, CRC press.
- Engineering, D.O.C.S. (1998). Washms Task 7.12: State-Of-The-Art In Vibration-Based Structural Damage Detection: Literature Review. *Washms Task 7.12*. Hong Kong The Hong Kong Polytechnic University, .
- Ewins, D.J. (1984). *Modal testing: theory and practice*, Research studies press Letchworth.
- Farrar, C.R., Baker, W., Bell, T., Cone, K., Darling, T., Duffey, T., Eklund, A. and Migliori, A. (1994). Dynamic characterization and damage detection in the I-40 bridge over the Rio Grande. Los Alamos National Lab., NM (United States).
- Farrar, C.R., Cornwell, P.J., Doebbling, S.W. and Prime, M.B. (2000). Structural health monitoring studies of the Alamosa Canyon and I-40 bridges. Los Alamos National Lab., NM (US).
- Farrar, C.R., Duffey, T.A., Doebbling, S.W. and Nix, D.A. (1999). A statistical pattern recognition paradigm for vibration-based structural health monitoring. *Structural Health Monitoring*, 2000(764-773).
- Farrar, C.R. and Worden, K. (2012). *Structural health monitoring: a machine learning perspective*, John Wiley & Sons.

- Fu, Z.-F. and He, J. (2001). *Modal analysis*, Butterworth-Heinemann.
- Furukawa, A., Otsuka, H. and Kiyono, J. (2006). Structural damage detection method using uncertain frequency response functions. *Computer-Aided Civil and Infrastructure Engineering*, 21(4): 292-305.
- Gopalakrishnan, S., Ruzzene, M. and Hanagud, S. (2011). *Computational techniques for structural health monitoring*, Springer Science & Business Media.
- Gudmundson, P. (1982). Eigenfrequency changes of structures due to cracks, notches or other geometrical changes. *Journal of the Mechanics and Physics of Solids*, 30(5): 339-353.
- Guo, H. and Li, Z. (2009). A two-stage method to identify structural damage sites and extents by using evidence theory and micro-search genetic algorithm. *Mechanical Systems and Signal Processing*, 23(3): 769-782.
- Hejll, A. (2004). *Structural health of bridges: monitor, assess and retrofit*. Luleå tekniska universitet.
- Hsu, T., Huang, S., Lu, K. and Loh, C. A damage detection algorithm integrated with a wireless sensing system. *Journal of Physics: Conference Series*, 2011. IOP Publishing, 012042.
- Hu, H. (1987). *Vibration theory of multiple degree of freedom systems*. Science Press, Beijing.
- Hu, H., Wu, C. and Lu, W.-J. (2011). Damage detection of circular hollow cylinder using modal strain energy and scanning damage index methods. *Computers & structures*, 89(1): 149-160.
- Hwang, H. and Kim, C. (2004). Damage detection in structures using a few frequency response measurements. *Journal of Sound and Vibration*, 270(1): 1-14.
- James, G., Mayes, R., Carne, T. and Reese, G. (1994). *Damage detection and health monitoring of operational structures*. Sandia National Labs., Albuquerque, NM (United States).
- James Hu, S.-L., Wang, S. and Li, H. (2006). Cross-modal strain energy method for estimating damage severity. *Journal of engineering mechanics*, 132(4): 429-437.

- Jiang, S.-F., Zhang, C.-M. and Zhang, S. (2011). Two-stage structural damage detection using fuzzy neural networks and data fusion techniques. *Expert systems with applications*, 38(1): 511-519.
- Kattan, P.I. (2010). *MATLAB guide to finite elements: an interactive approach*, Springer Science & Business Media.
- Kim, B.H., Park, T. and Voyiadjis, G.Z. (2006). Damage estimation on beam-like structures using the multi-resolution analysis. *International Journal of Solids and Structures*, 43(14): 4238-4257.
- Kim, C.-W., Morita, T., Oshima, Y. and Sugiura, K. (2015). A Bayesian approach for vibration-based long-term bridge monitoring to consider environmental and operational changes. *Smart Structures and Systems*, 15(2): 395-408.
- Kisa, M. and Arif, G. (2005). Modal analysis of cracked cantilever composite beams. *Structural Engineering and Mechanics*, 20(2): 143-160.
- Krishnan Nair, K. and Kiremidjian, A.S. (2007). Time Series Based Structural Damage Detection Algorithm Using Gaussian Mixtures Modeling. *Journal of Dynamic Systems, Measurement, and Control*, 129(3): 285.
- Law, S., Shi, Z. and Zhang, L. (1998). Structural damage detection from incomplete and noisy modal test data. *Journal of Engineering Mechanics*, 124(11): 1280-1288.
- Lei, Y., Kiremidjian, A., Nair, K., Lynch, J., Law, K., Kenny, T., Carryer, E. and Kottapalli, A. Statistical damage detection using time series analysis on a structural health monitoring benchmark problem. Proceedings of the 9th International Conference on Applications of Statistics and Probability in Civil Engineering, 2003. 6-9.
- Li, H., Yang, H. and Hu, S.-L.J. (2006). Modal strain energy decomposition method for damage localization in 3D frame structures. *Journal of engineering mechanics*, 132(9): 941-951.
- Li, L., Hu, Y. and Wang, X. (2013). Numerical methods for evaluating the sensitivity of element modal strain energy. *Finite Elements in Analysis and Design*, 64(13-23).
- Lu, Y. and Gao, F. (2005). A novel time-domain auto-regressive model for structural damage diagnosis. *Journal of Sound and Vibration*, 283(3-5): 1031-1049.

- Maeck, J. and De Roeck, G. Damage assessment of a gradually damaged RC beam using dynamic system identification. Proceedings of the 20th International Modal Analysis Conference (IMAC-XX)–CD-ROM, Los Angeles, California, 2002.
- Mayes, R.L. (1994). An experimental algorithm for detecting damage applied to the I-40 bridge over the Rio Grande. Sandia National Labs., Albuquerque, NM (United States).
- Messina, A., Williams, E. and Contursi, T. (1998). Structural damage detection by a sensitivity and statistical-based method. *Journal of sound and vibration*, 216(5): 791-808.
- Moradipour, P., Chan, T.H.T. and Gallage, C. Health monitoring of short-and medium-span bridges using an improved modal strain energy method. *In: Miyamoto, A., Hakola, I., Yabe, A. and Emoto, H., eds. Proceedings of the 5th International Workshop on Civil Structural Health Monitoring, 24-26 Oct. 2013 Ube, Yamaguchi, Japan. International Society for Structural Health Monitoring of Intelligent Infrastructure, 166-181.*
- Moradipour, P., Chan, T.H.T. and Gallage, C. (2015). An improved modal strain energy method for structural damage detection, 2D simulation. *Structural Engineering and Mechanics*, 54(1): 105-119.
- Nair, K., Kiremidjian, A., Lei, Y., Lynch, J. and Law, K. Application of time series analysis in structural damage evaluation. Proceedings of the international conference on structural health monitoring, 2003. 14-16.
- Nair, K.K., Kiremidjian, A.S. and Law, K.H. (2006a). Time series-based damage detection and localization algorithm with application to the ASCE benchmark structure. *Journal of Sound and Vibration*, 291(1–2): 349-368.
- Nair, K.K., Kiremidjian, A.S. and Law, K.H. (2006b). Time series-based damage detection and localization algorithm with application to the ASCE benchmark structure. *Journal of Sound and Vibration*, 291(1): 349-368.
- Ni, Y., Jiang, S. and Ko, J. (2001). Application of adaptive probabilistic neural network to damage detection of Tsing Ma suspension bridge. SPIE.
- Osegueda, R.A., Carrasco, C. and Meza, R. A modal strain energy distribution method to localize and quantify damage. Proceedings-SPIE The International Society For Optical Engineering, 1997. SPIE International Society For Optical, 1298-1304.

- Osegueda, R.A., Revilla, A., Pereyra, L. and Moguel, O. (1999). Fusion of modal strain energy differences for localization of damage. *Nondestructive Evaluation of Aging Aircraft, Airports, and Aerospace Hardware III, Proceedings of SPIE*, 3586(3586-28).
- Pandey, A. and Biswas, M. (1994). Damage detection in structures using changes in flexibility. *Journal of sound and vibration*, 169(1): 3-17.
- Pandey, A. and Biswas, M. (1995). Experimental verification of flexibility difference method for locating damage in structures. *Journal of sound and vibration*, 184(2): 311-328.
- Pandey, A., Biswas, M. and Samman, M. (1991). Damage detection from changes in curvature mode shapes. *Journal of sound and vibration*, 145(2): 321-332.
- Park, S., Stubbs, N., Bolton, R., Choi, S. and Sikorsky, C. (2001). Field Verification of the Damage Index Method in a Concrete Box-Girder Bridge via Visual Inspection. *Computer-Aided Civil and Infrastructure Engineering*, 16(1): 58-70.
- Pradeep, K., Rao, B.N., Srinivasan, S. and Balasubramaniand, K. (2014). Modal strain energy change ratio for damage identification in honeycomb sandwich structures. *Canadian Journal of Basic and Applied Sciences*, 2(01).
- Purkiss, J., Bailey, M., Friswell, M., Penny, J. and Wood, M. (1994). Analysis of the Effect of Ambient Conditions on the Dynamic Response of Prestressed Concrete Bridge Decks. *Institute of Structural Engineers Library*.
- Rytter, A. (1993). *Vibrational based inspection of civil engineering structures*. Aalborg University, Denmark
- Salawu, O. (1997). Detection of structural damage through changes in frequency: a review. *Engineering structures*, 19(9): 718-723.
- Sazonov, E. and Klinkhachorn, P. (2005). Optimal spatial sampling interval for damage detection by curvature or strain energy mode shapes. *Journal of sound and vibration*, 285(4): 783-801.
- Segerlind, L.J. and Saunders, H. (1987). Applied finite element analysis. American Society of Mechanical Engineers.
- Seyedpoor, S. (2012). A two stage method for structural damage detection using a modal strain energy based index and particle swarm optimization. *International Journal of Non-Linear Mechanics*, 47(1): 1-8.

- Shi, Z., Ding, X. and Gu, H. A new model reduction and expansion method. SDVNC'95- International Conference on Structural Dynamics, Vibration, Noise and Control, Hong Kong, 1995. 847-852.
- Shi, Z., Law, S. and Zhang, L. (1998). Structural damage localization from modal strain energy change. *Journal of Sound and Vibration*, 218(5): 825-844.
- Shi, Z., Law, S. and Zhang, L.M. (2000). Structural damage detection from modal strain energy change. *Journal of engineering mechanics*, 126(12): 1216-1223.
- Shih, H.W., Thambiratnam, D. and Chan, T.H. (2011). Damage detection in truss bridges using vibration based multi-criteria approach. *Structural Engineering and Mechanics*, 39(2): 187.
- Shih, H.W., Thambiratnam, D.P. and Chan, T.H. (2009). Vibration based structural damage detection in flexural members using multi-criteria approach. *Journal of sound and vibration*, 323(3): 645-661.
- Sinou, J.-J. (2009). A review of damage detection and health monitoring of mechanical systems from changes in the measurement of linear and non-linear vibrations. Nova Science Publishers, Inc.
- Smith, D.M. (2008). *Engineering computation with MATLAB*, Pearson/Addison Wesley.
- Smith, D.M. and Pournami, P. (2013). *Engineering computation with MATLAB*, Pearson.
- Solís, M., Algaba, M. and Galvín, P. (2013). Continuous wavelet analysis of mode shapes differences for damage detection. *Mechanical Systems and Signal Processing*, 40(2): 645-666.
- Srinivas, V., Ramanjaneyulu, K. and Jeyasehar, C.A. (2011). Multi-stage approach for structural damage identification using modal strain energy and evolutionary optimization techniques. *Structural Health Monitoring*, 10(2): 219-230.
- Strand7_Manual, B. (2010). Introduction to the Strand7 Finite Element Analysis System. Strand7 Pty Ltd.
- Stubbs, N., Kim, J. and Topole, K. An efficient and robust algorithm for damage localization in offshore platforms. Proceedings of the ASCE Tenth Structures Congress, 1992. 543-546.

- Tomaszewska, A. (2010). Influence of statistical errors on damage detection based on structural flexibility and mode shape curvature. *Computers & structures*, 88(3): 154-164.
- Wahalathantri, B.L., Thambiratnam, D., Chan, T. and Fawzia, S. (2012). An improved method to detect damage using modal strain energy based damage index. *Advances in Structural Engineering*, 15(5): 727-742.
- Wang, F.L., Chan, T.H., Thambiratnam, D.P., Tan, A.C. and Cowled, C.J. (2012). Correlation-Based Damage Detection for Complicated Truss Bridges Using Multi-Layer Genetic Algorithm. *Advances in Structural Engineering*, 15(5): 693-706.
- Wang, J.-Y., Ko, J.M. and Ni, Y.-Q. Modal sensitivity analysis of Tsing Ma Bridge for structural damage detection. Proceedings of the SPIE's 5th Annual International Symposium on Nondestructive Evaluation and Health Monitoring of Aging Infrastructure, International Society for Optics and Photonics, 2000. 5-9.
- Wang, L. (2012). *Innovative Damage Assessment Of Steel Truss Bridges Using Modal Strain Energy Correlation*. Queensland University of Technology
- Wang, L., Chan, T.H., Thambiratnam, D.P. and Tan, A.C. Damage detection for truss bridge structures using correlation-based structural modal strain energy. Proceedings of the 8th International Conference on Short and Medium Span Bridges, Niagara Falls, Ontario, Canada, 2010.
- Wang, S. (2013). Iterative modal strain energy method for damage severity estimation using frequency measurements. *Structural Control and Health Monitoring*, 20(2): 230-240.
- Wang, S., Zhang, M. and Liu, F. (2013). Estimation of semi-rigid joints by cross modal strain energy method. *Structural Engineering and Mechanics*, 47(6): 757-771.
- Wikipedia (2017). List of bridge failures. Wikipedia, The Free Encyclopedia.
- Wu, H. and Sun, L. Comparison and improvements of two damage identification methods based on modal strain energy. SPIE Smart Structures and Materials+ Nondestructive Evaluation and Health Monitoring, 2011. International Society for Optics and Photonics, 79813R-79813R-10.

- Yan, W.-J., Huang, T.-L. and Ren, W.-X. (2010a). Damage detection method based on element modal strain energy sensitivity. *Advances in Structural Engineering*, 13(6): 1075-1088.
- Yan, W.-J., Huang, T.-L. and Ren, W.-X. (2010b). Technical Papers: Damage Detection Method Based on Element Modal Strain Energy Sensitivity. *Advances in Structural Engineering*, 13(6): 1075-1088.
- Yan, Y., Yang, H., Wu, Z. and Ge, X. (2010c). Damage detection method for composite structures based on a combined technique of cross modal strain energy and niche genetic algorithms. *Journal of Vibration and Control*, 16(11): 1673-1683.
- Yuen, M.M.F. (1985). A numerical study of the eigenparameters of a damaged cantilever. *Journal of sound and vibration*, 103(3): 301-310.
- Zhong, S., Oyadiji, S.O. and Ding, K. (2008). Response-only method for damage detection of beam-like structures using high accuracy frequencies with auxiliary mass spatial probing. *Journal of Sound and Vibration*, 311(3): 1075-1099.
- Zhou, Z., Wegner, L. and Sparling, B. Assessing damage to a bridge deck using measured dynamic characteristics—Influence of the number of measurement points. Proceedings of the 6th International Conference on Short and Medium Span Bridges, Canadian Society for Civil Engineering, Vancouver, BC, 2002. 65-72.
- Zimmerman, D. (1995). The effects of finite element grid density on model correlation and damage detection of a bridge.